Exploration of state-space modeling techniques for transfer path analysis applications:

State-space substructuring

Rafael da Silva Oliveira Dias

Dissertation submitted to
Faculdade de Engenharia da Universidade do Porto
for the degree of:

Mestre em Engenharia Mecânica

Advisor at Faculdade de Engenharia da Universidade do Porto:
Prof. José Dias Rodrigues
(Associate Professor)
Advisor at Siemens Industry Software NV:
Eng. Fabio Bianciardi
(Research Engineer)

Departamento de Engenharia Mecânica
Faculdade de Engenharia da Universidade do Porto

Porto, 2020

The work presented in this dissertation was performed at
Siemens Industry Software NV
Leuven, Belgium.

Rafael da Silva Oliveira Dias
E-mail: up201504459@fe.up.pt

Faculdade de Engenharia da Universidade do Porto
Departamento de Engenharia Mecânica
Rua Dr. Roberto Frias s/n
4200-465 Porto
Portugal

Abstract

Substructuring assumes that a complex problem can be solved faster and with more accuracy, if decomposed in several simple problems. The application of this idea to evaluate the dynamic behaviour of a structure created a new research area named dynamic substructuring. This procedure brings up several advantages. Some of these advantages are the possibility of deeper analyze each substructure and perform a better optimization, a faster and less expensive problem resolution and the possibility of combine parts that were optimized by different work teams.

However, one of the nowadays difficulties of dynamic substructuring is the requirement of couple each of the analyzed substructures. Since $60s$ several coupling methods have been proposed, for example, component mode synthesis methods (CMS) or frequency based substructuring ones (FBS). The CMS methods are mainly used to couple analytical models, while FBS methods have been proposed to overcome the limitations of CMS method when coupling measured data (experimental dynamic substructuring). Even thought the appearance of FBS method, it has been observed that this method suffers of numerical ill-conditioning problems due to noisy data. These facts are the motivation for the exploration of state-space coupling techniques.

In this dissertation, an exploration from the scratch on these techniques has been performed with the aim to find the best technique to perform experimental substructuring. Two techniques have been found in the analyzed literature, one developed by Su and Juang [Su and Juang, 1994], another developed by Sjövall [Sjövall, 2004]. An exhaustive analysis of both was performed to fully understand each approach. Numerical models have been coupled with each technique, in order to full understand how these methods work and to evaluate the accuracy of the results.

At the final of this exhaustive analysis to both it was found that Su and Juang technique [Su and Juang, 1994] would be the best choice for its simplicity. Furthermore, this technique showed to be simple to apply to the estimated state-space models by polyreference least-squares complex frequency-domain method (PolyMAX) and maximum likelihood modal parameter identification method (ML-MM). By the use of this method two experimental couplings have been performed. For each of these experimental couplings the coupled frequency response functions (FRFs) have also been obtained by the use of FBS method applied to both synthetized FRFs and measured FRFs.

It has been observed a perfect match for both experimental couplings between the coupled FRFs computed with Su and Juang technique [Su and Juang, 1994] and FBS method when applied to the synthetized FRFs. The measured FRFs of the assembled structure were just available for the first experimental coupling. It was found that the measured coupled FRFs and the obtained by Su and Juang technique [Su and Juang, 1994] were different, however at some frequencies they were extremely close. It was found that the differences were mainly justified by experimental measurement errors.

Keywords: Dynamic Substructuring, Experimental Dynamic Substructuring, Modal Analysis, Frequency Based Substructuring, State-Space Models, State-Space Coupling

Resumo

A subestruturação assume que um problema complexo pode ser resolvido de uma forma mais rápida e obtendo melhores resultados, caso o mesmo seja dividido em vários problemas simples. A aplicação deste conceito para a avaliação do comportamento dinâmico de estruturas criou uma nova área de investigação denominada de subestructuração dinâmica. A utilização deste procedimento apresenta várias vantagens. Entre estas, permite a possibilidade de realizar uma análise mais profunda e detalhada a cada substrutura, permitindo uma melhor otimização de cada uma das mesmas.

No entanto, uma das dificuldades na aplicação da subestructuração dinâmica é a necessidade de após analisar cada uma das substruturas proceder ao seu acoplamento. Desde a década de 60 que vários métodos de acoplamento foram desenvolvidos. Entre eles, os métodos *component mode synthesis* (CMS) e *frequency based substructuring* (FBS). O método CMS é mais utilizado no acoplamento de modelos analíticos, enquanto que o FBS foi desenvolvido de modo a ultrapassar as dificuldades do método CMS no acoplamento de substruturas reais. Porém, o método FBS sofre de problemas numéricos, quando as *funções de resposta em frequência* (FRF) medidas apresentam ruído. Estes motivos são a motivação para a exploração de técnicas de acoplamento baseadas no espaço de estados.

Nesta dissertação, a exploração destas técnicas foi realizada de uma forma exaustiva, com o objetivo de compreender qual a melhor para realizar acoplamento entre substruturas reais. Duas técnicas foram descobertas na bibliografia analisada. Uma proposta por Su e Juang [Su and Juang, 1994], e outra por Sjövall [Sjövall, 2004]. Uma análise aprofundada a cada uma das mesmas, assim como vários acoplamentos de modelos numéricos foram realizados. Verificou-se que a técnica proposta por Su e Juang [Su and Juang, 1994] seria a mais adequada para realizar acoplamento entre substruturas reais. Por outro lado, este método revelou permitir acoplar de forma simples os espaços de estados estimados através dos métodos *polyreference least-squares complex frequency-domain method* (PolyMAX) and *maximum likelihood modal parameter identification method* (ML-MM). Pelo uso deste método, dois acoplamentos experimentais foram realizados. Sendo que, para cada um dos mesmos as FRFs acopladas foram estimadas pelo uso do método FBS aplicado às FRFs medidas e às FRFs sintetizadas de cada uma das subestruturas.

Verificou-se que as FRFs acopladas obtidas pelo recurso ao método proposto por Su e Juang [Su and Juang, 1994] e as obtidas pela aplicação do método FBS às FRFs sintetizadas eram, exatamente, iguais. Apenas para o primeiro acoplamento eram conhecidas as FRFs medidas da estrutura acoplada. A comparação das mesmas com as FRFs acopladas estimadas pelo método proposto por Su e Juang [Su and Juang, 1994], revelou que estas não coincidiam. Porém, para certas frequências ambas as soluções apresentaram-se bastante próximas, sugerindo que as diferenças encontradas seriam, maioritariamente, justificadas por erros de medição.

Palavras-Chave: Subestruturação Dinâmica, Subestruturação Dinâmica Experimental, Análise Modal, Acoplamento Baseado em Frequência, Modelos espaço de estados, Acoplamento espaço de estados

To my family, in special to my grandparents

Albina and Miguel

‘The future belongs to the competent. Get good, get better, be the best!’

Brian Tracy

Acknowledgements

Firstly, I would like to thank my university advisor, Prof. José Dias Rodrigues, for with his lessons make me have interest in mechanical vibrations topics and also for his suggestions to better this dissertation. I am also grateful to him for accept to be my advisor and to allow me to have this wonderful experience.

I would like to thank Siemens Industry Software NV for provide me the opportunity of working in a challenging and interesting subject. Definitely, the realization of this internship permitted me to have an out standard opportunity, which permitted me to grow not only as an engineer, but also as a team worker.

A special thanks goes to Eng. Fabio Bianciardi for his supervision and for our discussions about the work, which were fundamental for this dissertation. I would like to show my gratitude to Eng. Mahmoud El-Kafafy for his support over this dissertation, special in the state-space model estimation from measured data and for let me use his $MATLAB^{®}$ code to perform such estimations from the estimated modal model. I also would like to thanks both for always encourage me to expose my suggestions and for them constantly availability to clarify my doubts.

A special thanks goes to my university colleagues Marcos, Gil, Pedro and Bruno for them friendship and for our discussions. The more serious ones about the university lessons and works and for the more relaxed and funny ones.

Lastly, I would like to express my gratitude for my family and to my girlfriend Inês for all the patient, support and encouragement during the last five years.

Contents

List of Figures

List of Tables

Nomenclature

Subscripts

α, β relative to a substructure

b relative to internal degrees of freedom

c relative to interface degrees of freedom

D relative to the uncoupled diagonal state-space model

i, j relative to degrees of freedom

r relative to the number of the vibration mode

Superscripts

1,2, ... relative to degrees of freedom numeration

A, B, C, D, E relative to a substructure

$accel$ relative to acceleration state-space model

d relative to displacement

$disp$ relative to displacement state-space model

E variables related to the eletric engine

I relative to internal degrees of freedom

II relative to internal output and input

IJ relative to internal output and interface input

int relative to the intended variable arrangement

J relative to interface degrees of freedom

JI relative to interface output and internal input

JJ relative to interface output and input

obt relative to the obtained variable arrangement

SF variables related to the support frame

v relative to velocity

vel relative to velocity state-space model

x, y relative to different vectors

Acronyms

CMS Component Mode Synthesis

DOF Degree of Freedom

FBS Frequency Based Substructuring

FRF Frequency Response Function

LSCF Least-Squares Complex Frequency-Domain Estimation Method

MAC Modal Assurance Criterion

ML-MM Maximum Likelihood Modal Model-Based Method

PolyMAX Polyreference Least-Squares Complex Frequency-Domain Method

SVD Singular Value Decomposition

Operators

$|\bullet|$ Absolute value of a number

$\bullet^*$ complex conjugate of a number

$[\ \ ]^{-1}$ inverse of a matrix

$[\ \ ]^T$ transpose of a matrix

$[\bullet]^*$ complex conjugate of a matrix

$[\ \ ]^H$ transpose complex conjugate of a matrix

$\{\ \ \}^T$ transpose of a vector

$\{\bullet\}^*$ complex conjugate of a vector

$(\dot{\bullet})$ first order time derivative

$(\ddot{\bullet})$ second order time derivative

$L(\bullet)$ Laplace transform

Scalar Variables $(\bullet)$

$\bar{\bullet}$ relative to coupled variables

δ auxiliary variable

λ pole

ω frequency $/rads^{-1}$

ω_d damped natural frequency $/rads^{-1}$

ω_n undamped natural frequency $/rads^{-1}$

ϕ auxiliary variable

σ singular value

ξ damping ratio

a acceleration $/ms^{-2}$

C relative to the degrees pf freedom of the eletric engine, support frame and respective assembled structure

F load $/N$

j complex operator $\left(j = \sqrt{-1}\right)$

m mass $/Kg$

N_m number of modes

Q generalized force $/N$

q degree of freedom

R variables related to the receiver substructure

S variables related to the source substructure

s Laplace variable

SR variables related to the assembled source and receiver substructures

T kinetic energy $/j$

t time variable $/s$

u input

V potential elastic energy $/j$

x state

y output

Vector Variables $\{\quad\}$

$\{\bar{\bullet}\}$ relative to coupled vector variables

$\{\bar{A}(j\omega)\}$ acceleration response phasor vector

$\{\bar{X}(j\omega)\}$ displacement response phasor vector

$\{\gamma\}$ generic vector

$\{\Psi\}$ mode shape vector

$\{\widetilde{\bullet}\}$ relative to the coupling form of vector variables

$\{F(s)\}$ dynamic load vector in Laplace domain

$\{F\}$ dynamic load vector

$\{L\}$ modal participation factor vector

$\{r(t)\}$ dynamic response vector

$\{U(s)\}$ input vector in Laplace domain

$\{u(t)\}$ input vector in time domain

$\{X(s)\}$ state vector in Laplace domain

$\{x(t)\}$ state vector in time domain

$\{Y(s)\}$ output vector in Laplace domain

$\{y(t)\}$ output vector in time domain

$\{z(t)\}$ transformed state vector in time domain

Matrix Variables [ ]

$[\alpha(j\omega)]$ receptance FRF matrix

$[\bar{\bullet}]$ relative to coupled matrix variables

$[\Lambda]$ diagonal matrix of systems poles

$[\Psi]$ mode shapes matrix

$[\Sigma]$ diagonal singular values matrix

$[\tilde{\bullet}]$ relative to the coupling form of matrix variables

$[A(j\omega)]$ accelerance FRF matrix

$[A]$ state matrix

$[B]$ input matrix

$[C]$ output matrix

$[D]$ feed-through matrix

$[G]$ generic matrix

$[H(\omega)]$ FRF matrix

$[I]$ identity matrix

$[K]$ stiffness matrix

$[L]$ modal participation factors matrix

$[LR]$ lower residue matrix

$[M]$ mass matrix

$[N]$ projection of null-spaces $[N_B]$ and $[N_C]$

$[N_B]$ null-space of matrix $[B]$

$[N_C]$ null-space of the matrix composed by the first 2 rows of matrix $[T_{Sj}]$

$[Q]$ auxiliary variable matrix

$[R]$ residue matrix

$[S]$ auxiliary variable matrix

$[T]$ coupling matrix

$[T_{Sj}]$ Sjövall transformation matrix

$[U]$ left singular matrix

$[UR]$ upper residue matrix

$[V]$ damping matrix

$[W]$ right singular matrix

$[Z]$ dynamic stiffness matrix

Referential

x, y, z cartesian coordinate referential

Chapter 1

Introduction

1.1 Introduction

The substructuring idea was firstly developed in the $60s$. This development was motivated with the aim of solving a complex problem by decompose it in several and simpler ones. When this solving approach is used to evaluate the dynamic behaviour of a structure it is called dynamic substructuring.

The dynamic substructing permits the dynamic behaviour evaluation of one large complex structure in a faster and simpler way. It also permits a deeper analysis to each substructure, permitting a more effective modelling and optimization of each. In a industrial point of view, it allows the share and the combination of parts modeled from different project teams. On other hand, dynamic substructuring can be applied on models that are identified completely analytically, completely experimental or experimental-analytical models [de Klerk et al., 2008] [Konjerla, 2016].

After the analyze of each substructure dynamic behaviour, coupling must be performed to obtain the dynamic behaviour of the intended complex structure. To perform coupling, exists several techniques, from which two have been focus of intense research. Firstly, the component mode synthesis (CMS) methods, for which the substructures are reduced to a different domain (usually, modal domain) and then coupled. Secondly, the techniques which are based on directly couple experimental data. From these techniques it can be pointed the frequency based substructuring method (FBS) developed by Jetmundsen et al. [Jetmundsen et al., 1988].

The state-space coupling methods are based on the construction of a state-space model for each of substructures that coupling is intended. Afterwards, the coupling is performed between each of the computed state-space models. These methods have not been so much researched and are recent when comparing to the two other mentioned. However, two mainly contributions must be referred. Firstly, the state-space coupling method proposed by Su and Juang in paper [Su and Juang, 1994] and the proposed by Sjövall [Sjövall, 2004]. Both of these proposed approaches will be the starting point for the analyze to the state-space coupling techniques.

It is important to refer that, even though the aim of this dissertation is the exploration of state-space methods, the FBS method will be also analyzed. This is justified, because this dissertation is focused in experimental coupling and the FBS method is mainly used to this end. Thus, it is expected a comparison between the accuracy of the coupling results obtained from FBS and state-space coupling methods.

On other hand, the CMS methods are mostly used to couple analytical models. For analytical couplings, even though the substructures are in a reduced domain, the transformation matrix is known and can be tracked, permitting the establishment of coupling conditions (equilibrium and compatibility) in physical domain. In experimental substructuring, the coupling conditions cannot be made in a physical domain, but rather in a modal domain. The choice of the right modal coordinates to enforce coupling is not obvious, turning the establishment of the coupling conditions difficult [Gibanica, 2013]. For the pointed reasons, this method will not be analyzed in this dissertation. For the interested readers in CMS methods, the following reference is suggested [Craig and Kurdila, 2006].

1.2 Motivation

The interest in exploration of state-space coupling techniques is motivated for the difficulty to perform coupling of measured data. The reason for this difficulty is the fact of the most researched coupling methods are not totally suitable for this application. As stated at section 2.1, CMS methods are problematic for experimental substructuring and the FBS method suffer from numerical problems associated to ill conditioned matrices [Gibanica, 2013].

In the past, one of the mainly difficulties of the state-space coupling methods were the requirement of high quality estimations of the substructure state-space models from measured data. Fortunately, developments have been made (see [Peeters et al., 2004] and [El-Kafafy et al., 2015]) permitting a high quality estimation of these models. Therefore, nowadays, the exploration of the state-space coupling techniques reveals promising in experimental substructuring field.

1.3 State of the art

The state-space coupling techniques are recent comparing to others methods, for example, the CMS or the FBS method. Therefore, these methods have not been so deeply studied as the CMS or the FBS for which several developments could be pointed.

Two relevant studies in the field of statae-space coupling methods are given by Su and Juand [Su and Juang, 1994] and Sjövall [Sjövall, 2004]. Some theoretical developments in the approach proposed by Sjövall [Sjövall, 2004] have been performed, being the last reference to this method, known by the author, performed in book [Allen et al., 2020].

The experimental coupling results presented in literature by the use of state-space methods are rare. Gibanica et al. in paper [Gibanica et al., 2014], presents an experimental coupling between different blades and brackets of a wind turbine. Another example of experimental coupling is given in book [Allen et al., 2020], where was performed an experimental coupling between two major SUV components connected by four rubber bushings. In this reference, the coupling was also enforced considering rotational and translation motion.

Even though the state-space models estimation from measured data (system identification) are not the aim of this dissertation, in order to obtain high quality coupling results, high quality identifications are fundamental. Therefore, some references will be here presented for the interested readers.

Several developments in system identification methods have been performed in the last years. Some of these developments based on subspace methods can be found in [Overschee and de Moor, 1994], [Tomas McKelvey and Ljung, 1996], [Gibanica et al., 2018] and [Gumussoy et al., 2018]. The system identification method which will be used in this dissertation, is based on PolyMAX method and in an iterative method (ML-MM).

These methods have been developed and analyzed in papers [Peeters et al., 2004] and [El-Kafafy et al., 2015].

1.4 Objectives

The main objective of this dissertation is the exploration from scratch of state-space coupling techniques, in order to find the best technique to perform experimental substructuring. The main aim is also to perform a comparison between the accuracy of the obtained coupled results by the state-space techniques and the results obtained by the use of FBS method. To achieve this aim several objectives must be fulfilled, as the ones listed bellow:

- Perform a deep analysis of the existent state-space techniques;
- Apply each of the analyzed state-space coupling methods to couple numerical models;
- Understand in a superficial manner the modal parameter estimation by the use of PolyMAX and ML-MM methods and the state-space models estimation from the estimated modal parameters;
- Apply each of the analyzed state-space techniques to couple numerical models, however now with state-space models expressed in modal coordinates;
- Understand which state-space technique would be the best to couple state-space models expressed in modal coordinates;
- Perform coupling of real substructures by the use of the more suitable technique and compare the obtained results with the measured ones and with the obtained by the FBS method.

1.5 Layout

This document starts for present an introduction chapter, chapter 1, where is performed an introduction to the substructuring idea. Afterwards, the motivation, the state of the art, the objectives and the layout of this dissertation are presented.

In chapter 2, the theory used to perform this paper is presented. Starting for the presentation of the first order form and the computation of the FRFs from this formulation, followed by the modal assurance criterion (MAC) and the singular value decomposition (SVD) in sections 2.2, 2.3, 2.4 and 2.5, respectively. Then, the frequency based substructuring method (FBS) is presented, followed by the presentation of two state-space coupling methods and a discussion pointing some advantages and disadvantages of each presented state-space coupling techniques, sections 2.6, 2.7.1, 2.7.2 and 2.7.3, respectively. In section 2.8 an overview of the used system identification method and the computation of the estimated state-space models is presented. After, the section 2.9 performs a practical analyze to the coupling procedure with the method proposed by Su and Juang [Su and Juang, 1994], when coupling estimated state-space models from measured data. Finally, it is performed a discussion about the faced difficulties, when coupling non-rigidly connected substrutures, at section 2.10.1. Then, two different approaches are presented to perform this kind of couplings, at sections 2.10.2 and 2.10.3.

The chapter 3, presents in section 3.1 two numerical couplings. These couplings are performed with state-space models defined with states related to degrees of freedom (DOFs) (theoretical state-space models). Afterwards, in section 3.2 another two numerical couplings will be performed, however these state-space models are defined in modal coordinates (experimental state-space models).

The chapter 4, includes the coupling of real measured data. This chapter includes three sections. In the first and second sections, sections 4.1 and 4.2, two different mechanical systems composed by two substructures are analyzed and coupled. Each of these sections comprise three different subsections. The first performs a description of the mechanical system in analyze, the second explains how the state-space model estimation for each part was performed and the last explains in detail the coupling procedure. In the last section of the chapter 4, in section 4.3, a discussion about the accuracy of the obtained coupling results with the method developed by Su and Juang [Su and Juang, 1994] is performed.

Lastly, in chapter 5, the conclusion of this dissertation is performed and some possible future works are proposed, sections 5.1 and 5.2, respectively.

Chapter 2

Background Theory

2.1 Introduction

The aim of this chapter is to present the theory behind this dissertation. Firstly, it will be done a brief overview about the first order form (section 2.2). It will be explained how this first order form can be obtained from the general second order form and the procedure to compute FRFs from it (section 2.3). The modal assurance criterion (MAC) parameter and the singular value decomposition (SVD) of a matrix will be also analyzed at sections 2.4 and 2.5, respectively.

Secondly, three dynamic coupling methods will be analyzed. The frequency based substructuring (section 2.6) and two different state-space coupling methods (section 2.9). The first one proposed by Su and Juang in paper [Su and Juang, 1994] and the second one presented by Sjövall [Sjövall, 2004]. These coupling methods will be presented focusing rigid coupling.

Afterwards, it will be presented the utilized method to estimate state-space models from measured data, in section 2.8. Then, the coupling of estimated state-space models from measured data will be analyzed at section 2.9.1. Lastly, two different strategies to perform non-rigid coupling by the use of state-space coupling methods will be presented and discussed at section 2.10.

2.2 First Order Form

In dynamic experiments is common to express the differential equation of motion by a first order form, instead by a second order form, which is very used in analytical analysis. The reason for this choice is the fact that in dynamic experiments, the systems are analyzed by measuring the response in different locals (outputs) induced by exciting different system location points (inputs).

The first order form, directly, gives the relation between each of the inputs and the outputs, justifying its preference for dynamic experiments. The state-space model of a system can be easily obtained from its second order form. In order to illustrate the procedure, let consider the following generic differential equation of motion (2.1) expressed by a second order form

$$[M]\{\ddot{r}(t)\} + [V]\{\dot{r}(t)\} + [K]\{r(t)\} = \{F(t)\} \tag{2.1}$$

where matrices $[M] \in R^{n\times n}$, $[V] \in R^{n\times n}$ and $[K] \in R^{n\times n}$ are, respectively, the mass, the damping and the stiffness matrices. The vectors $\{r(t)\} \in R^{n\times 1}$ and $\{F(t)\} \in R^{n\times 1}$

represents the dynamic response vector and the dynamic load vector in time domain, respectively. Note that, the value of variable n is equal to the number of DOFs.

A generic first order form is written as follows

$$\begin{cases} \{\dot{x}(t)\} = [A]\{x(t)\} + [B]\{u(t)\} \\ \{y(t)\} = [C]\{x(t)\} + [D]\{u(t)\} \end{cases} \tag{2.2}$$

where $\{x(t)\} \in R^{2n\times 1}$ represents the state vector, $\{u(t)\} \in R^{n\times 1}$ represents the input vector and $\{y(t)\} \in R^{n\times 1}$ represents the output vector, which can be composed by displacement, velocity or acceleration outputs. The state vector includes both displacement and velocity states and is given as follows

$$\{x(t)\} = \begin{Bmatrix} x(t) \\ \dot{x}(t) \end{Bmatrix} \tag{2.3}$$

The matrices $[A] \in R^{2n\times 2n}$, $[B] \in R^{2n\times n}$, $[C] \in R^{n\times 2n}$ and $[D] \in R^{n\times n}$ have the following physical meanings:

- Matrix [A] is the state matrix;
- Matrix [B] is the input matrix;
- Matrix [C] is the output matrix;
- Matrix [D] is the feed-through matrix and it is not a null matrix only when the output is acceleration.

Note that, the following mathematical expressions are true

$$F_i = u_i, \quad i = 1, ..., n \tag{2.4a}$$

$$r_i = y_i, \quad i = 1, ..., n \tag{2.4b}$$

where,

- i is the i^{th} DOF;
- n is the number of DOFs;

Expressing in a explicit way the first block row of the generic state-space model presented at expression (2.2).

$$\begin{Bmatrix} \dot{x}(t) \\ \ddot{x}(t) \end{Bmatrix} = [A] \begin{Bmatrix} x(t) \\ \dot{x}(t) \end{Bmatrix} + [B]\{u(t)\} \tag{2.5}$$

Since the state vector includes both of displacement and velocity states, the matrices $[A]$ and $[B]$ will be composed by two block rows. The first block row of the expression (2.5) represents a dummy equation, which states that each velocity state is equal to itself. To obtain the second block row, it is needed to solve the equation (2.1) in order to acceleration as follows

$$\{\ddot{r}(t)\} = [M]^{-1}\left(\{F(t)\} - [V]\{\dot{r}(t)\} - [K]\{r(t)\}\right) \tag{2.6}$$

The state-space models here analyzed are defined directly by the stiffness, damping and mass matrices. In experimental analysis these matrices are not known, hence these models are theoretical ones. For theoretical models, the states are directly related to the considered DOFs to analyze the mechanical system under test. Therefore, the displacement states will provide in time domain the displacement associated to each DOF relatively to the reference position, the velocity and acceleration states will provide in time domain the velocity and the acceleration associated to each DOF, respectively. Thus, for these theoretical state-space models the states express the DOFs dynamic response and, therefore states and outputs will present the same physical meaning. So that, the following mathematical expressions are true

$$x_i = r_i, \quad i = 1, ..., n \tag{2.7a}$$

$$x_i = y_i, \quad i = 1, ..., n \tag{2.7b}$$

where,

- i is the i^{th} DOF;
- n is the number of DOFs;

Since the mathematical expressions (2.7a) and (2.4a) are true, the equation (2.6) can be directly inserted in the second block row of matrices $[A]$ and $[B]$ as follows

$$\begin{Bmatrix} \dot{x}(t) \\ \ddot{x}(t) \end{Bmatrix} = \begin{bmatrix} 0 & I \\ -M^{-1}K & -M^{-1}V \end{bmatrix} \begin{Bmatrix} x(t) \\ \dot{x}(t) \end{Bmatrix} + \begin{bmatrix} 0 \\ M^{-1} \end{bmatrix} \{u(t)\} \tag{2.8}$$

Where $[I] \in R^{n \times n}$ represents the identity matrix.

Since the expression (2.7b) is true for theoretical state-space models, the matrices $[C]$ and $[D]$ can be deduced by the use of a similar approach as used for the deduction of matrices $[A]$ and $[B]$. However, firstly the choice of the outputs should be made. In experimental mechanics the use of accelerometers to measure the dynamic response is common. Hence, the usual output is acceleration, for that reason the considered output in the deduction of $[C]$ and $[D]$ matrices will be acceleration. Since the considered output will be acceleration and because of the presented relation at equation (2.7b), the matrix $[C]$ will be given by the second block row of matrix $[A]$ and the matrix $[D]$ will be given by the second block row of matrix $[B]$, as follows

$$\{\ddot{y}(t)\} = \begin{bmatrix} -M^{-1}K & -M^{-1}V \end{bmatrix} \begin{Bmatrix} x(t) \\ \dot{x}(t) \end{Bmatrix} + \begin{bmatrix} M^{-1} \end{bmatrix} \{u\,(t)\} \tag{2.9}$$

The matrices deduced in the equations (2.8) and (2.9) are following presented

$$\begin{gathered} [A] = \begin{bmatrix} 0 & I \\ -M^{-1}K & -M^{-1}V \end{bmatrix}, \quad [B] = \begin{bmatrix} 0 \\ M^{-1} \end{bmatrix} \\ [C] = [-M^{-1}K \quad -M^{-1}V], \quad [D] = \begin{bmatrix} M^{-1} \end{bmatrix} \end{gathered} \tag{2.10}$$

If the considered output is velocity the matrices $[C]$ and $[D]$ are included in the first block row of the matrices $[A]$ and $[B]$, respectively, and would be given as follows

$$\{\dot{y}(t)\} = \begin{bmatrix} 0 & I \end{bmatrix} \begin{Bmatrix} x(t) \\ \dot{x}(t) \end{Bmatrix} + \begin{bmatrix} 0 \end{bmatrix} \{u\,(t)\} \tag{2.11}$$

Whereas, if the output is displacement the matrices $[C]$ and $[D]$ would be given as follows

$$\{y(t)\} = \begin{bmatrix} I & 0 \end{bmatrix} \begin{Bmatrix} x(t) \\ \dot{x}(t) \end{Bmatrix} + \begin{bmatrix} 0 \end{bmatrix} \{u(t)\} \tag{2.12}$$

Note that, the performed demonstrations and affirmations in this section are just valid for theoretical state-space models.

2.3 Frequency Response Functions

By the first order differential equations it is possible to obtain the frequency response functions (FRF) of the mechanical system in analyse. For such determination, the first order form should be written in frequency domain, instead of in time domain, as it was presented in equation (2.2). In order to rewrite the state-space model in frequency domain, a Laplace transformation must be applied. The Laplace transformation of a generic function $f(t)$ is given as follows

$$F(s) = L[f(t)] = \int_0^{\infty} f(t)e^{-st}dt \tag{2.13}$$

Note that capital letters represents frequency domain variables and small letters represents time domain variables.

Applying a Laplace transformation to the state-space model presented at expression (2.2) and using the following Laplace transformation property

$$L\left[\frac{d}{dt}f(t)\right] = sF(s) - f(0) \tag{2.14}$$

The state-space model (see expression (2.2)) rewritten in frequency domain is given as follows

$$\begin{cases} sX(s) - x(0) = [A]X(s) + [B]U(s) \\ Y(s) = [C]X(s) + [D]U(s) \end{cases} \tag{2.15}$$

Rewriting the first block row of the state-space model (2.15) in order to variable $X(s)$

$$X(s)(s[I] - [A]) = x(0) + [B]U(s) \tag{2.16}$$

Dividing equation (2.16) by $(s[I] - [A])$ and assuming null initial conditions, $x(0) = 0$, $\dot{x}(0) = 0$

$$X(s) = (s[I] - [A])^{-1}[B]U(s) \tag{2.17}$$

Substituting the value of $X(s)$, given in equation (2.17), in the second block row of the state-space model presented at expression (2.15)

$$Y(s) = ([C](s[I] - [A])^{-1}[B] + [D])U(s) \tag{2.18}$$

The frequency response function receptance (FRF), $\alpha_{ij}(j\omega)$ is given by the response (displacement) phasor in the degree of freedom i caused by the application of an harmonic force, which amplitude is unitary, in the degree of freedom j. The FRF mobility and accelerance have a similar definition. However, instead of the displacement response it is calculated by the velocity and acceleration response, respectively. Thus, is simple to get the frequency response functions with the equation (2.18). For that purpose, the ratio $\frac{Y(s)}{U(s)}$ should be calculated as follows

$$\frac{Y(s)}{U(s)} = [C](s[I] - [A])^{-1}[B] + [D] \tag{2.19}$$

The FRF that is obtained by the equation (2.19) depends on the considered input and output. In general, the considered input is force. The chosen output can be displacement, velocity or acceleration. Thus, the FRF that would be obtained is receptance, mobility or accelerance, respectively.

2.4 Modal Assurance Criterion

The modal assurance criterion (MAC) parameter is defined as the squared correlation coefficient between two vectors. This parameter is calculated as follows

$$MAC_{y,x} = \frac{\left| \{\gamma_x\}^T \{\gamma_y\} \right|^2}{(\{\gamma_x\}^T \{\gamma_x\})(\{\gamma_y\}^T \{\gamma_y\})} \tag{2.20}$$

where,

- $|\bullet|$ denotes the absolute value of a number;
- $\{\gamma_y\}$ and $\{\gamma_x\}$ are two different vectors, which a measure of its correlation is intended;
- $\{\bullet\}^T$ denotes the transpose of a vector.

In mechanical dynamics applications, the MAC parameter is mainly used to quantify the degree of correlation between two sets of mode shape data. Therefore, if the MAC parameter value is close to 0 it signifies that both of evaluated mode shapes are not from the same mode, whereas if the value is close to 1 the both evaluated mode shapes are in fact from the same mode. However, this parameter continues to be valid to evaluate the correlation between two vectors, whatever its physical meaning [Ewins, 2000].

2.5 Singular Value Decomposition

The singular value decomposition assumes that for a real matrix $[G]$ of dimensions $p \times q$, exists a $p \times p$ orthogonal matrix $[U]$, a $q \times q$ orthogonal matrix $[W]$ and a $p \times q$ diagonal matrix $[\Sigma]$ (possibly a diagonal square matrix augmented with zero rows and columns). The $[G]$ matrix decomposition is given as follows

$$[G] = [U]\,[\Sigma]\,[W]^T \tag{2.21}$$

where, $[\bullet]^T$ denotes the transpose of a matrix. The $[U]$ and $[W]$ matrices consists of left and right singular vectors of $[G]$ and $[\Sigma]$ is the diagonal singular value matrix of matrix $[G]$.

In the case of matrix $[G]$ is complex, the expression (2.21) becomes

$$[G] = [U]\,[\Sigma]\,[W]^H \tag{2.22}$$

where, superscript $[\bullet]^H$ denotes the complex conjugate transpose of a matrix [He and Fu, 2001][Ewins, 2000].

If the singular value decomposition is applied to a FRF matrix, the matrices $[U]$, $[\Sigma]$ and $[W]$ will have the following meaning [Siemens, 2018]:

- $[U]$ is the left singular matrix corresponding to the mode shape matrix;
- $[\Sigma]$ is a diagonal matrix composed by the FRF singular values;
- $[W]$ is the right singular matrix corresponding to the matrix of modal participation factors.

The singular values are usually extracted and presented in descending order. The rank of a matrix is a measure of the independence of the rows and columns and directly reflects its non-singularity. If all the singular values (σ) of a matrix are non-zero, the matrix is of full rank, is non-singular and is essentially well-conditioned from a numerical processing point of view. Otherwise, if one of the singular values is zero or close to zero, the matrix is rank-deficient, presenting a very high condition number and is singular.

An important measure that reflects the singularity of a matrix is the condition number. The condition number is the ratio between the greater and the lower singular value. If this number is very high the matrix is singular. In this situations, a usual practice is to replace any element of the matrix $[\Sigma]$, which would become infinite if defined by $(\frac{1}{\sigma})$ with a zero. In fact, the obtained solution will be an approximation, however the matrix inversion will be possible.

In mechanical dynamical applications, when the SVD is applied to an FRF and it is realized that one singular value of the diagonal singular value matrix is very small when compared to others or is zero, this means that the system have been analyzed supposing that it presents more degrees of freedom than it really presents. Therefore, the fact of the FRF matrix be singular is due of the problem not being well posed. This means that the SVD has the power to determinate the true order of the system under testing [Ewins, 2000].

2.6 Frequency Based Substructuring

The frequency based substructuring (FBS) is a well-known method used to enforce mechanical coupling between substructures. This method enforce coupling, directly, with the measured FRFs. Many formulations of FBS method are available in literature. In this section the formulation presented in paper [Su and Juang, 1994] will be exposed.

In order to understand how this method works let couple the substructures α and β presented in figure 2.1.

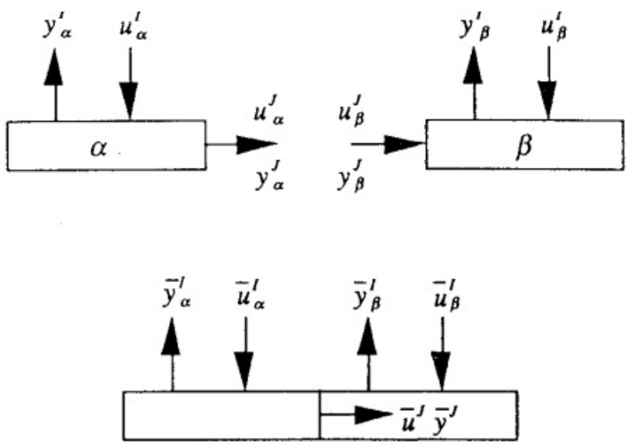

Figure 2.1: Mechanical System [Su and Juang, 1994]

The input-output transfer functions (FRFs) relations for both substructures are given as follows

$$\begin{bmatrix} y_\alpha^I \\ y_\alpha^J \end{bmatrix} = \begin{bmatrix} H_\alpha^{II} & H_\alpha^{IJ} \\ H_\alpha^{JI} & H_\alpha^{JJ} \end{bmatrix} \begin{bmatrix} u_\alpha^I \\ u_\alpha^J \end{bmatrix} \tag{2.23}$$

$$\begin{bmatrix} y_\beta^I \\ y_\beta^J \end{bmatrix} = \begin{bmatrix} H_\beta^{II} & H_\beta^{IJ} \\ H_\beta^{JI} & H_\beta^{JJ} \end{bmatrix} \begin{bmatrix} u_\beta^I \\ u_\beta^J \end{bmatrix} \tag{2.24}$$

where, the superscripts I and J are related to internal and interface degrees of freedom, respectively. The variable y is the output which can be displacement, velocity or acceleration, Lastly, the variable u is the input, which in general is a force.

For its turn the FRFs relations for the assembled structure are given as follows

$$\begin{bmatrix} \bar{y}_\alpha^I \\ \bar{y}_\beta^I \\ \bar{y}^J \end{bmatrix} = \begin{bmatrix} \bar{H}_{11} & \bar{H}_{12} & \bar{H}_{13} \\ \bar{H}_{21} & \bar{H}_{22} & \bar{H}_{23} \\ \bar{H}_{31} & \bar{H}_{32} & \bar{H}_{33} \end{bmatrix} \begin{bmatrix} \bar{u}_\alpha^I \\ \bar{u}_\beta^I \\ \bar{u}^J \end{bmatrix} \tag{2.25}$$

Note that, top bar variables are related to coupled variables.

In order to achieve the assembled structure FRFs from the uncoupled substructure FRFs, the compatibility and equilibrium conditions have to be enforced.

The compatibility condition states that the physical motion of the two substructures at the interface is the same. Thus, the compatibility equation is given as follows [Seijs, 2016]

$$\bar{y}^J = y_\alpha^J = y_\beta^J \tag{2.26}$$

On other hand, the equilibrium condition states that the sum of the internal forces has to be equal to the external applied forces. On other words, the applied force on the coupled DOF, must be equal to the sum of the applied force in each DOF that will be coupled. Thus, this condition can be written as follows

$$\bar{u}^J = u_\alpha^J + u_\beta^J \tag{2.27}$$

By the equation (2.26) and the bottom block rows of the system of equations presented at expressions (2.23) and (2.24)

$$u_\alpha^J = (H_\alpha^{JJ})^{-1}\bar{y}^J - (H_\alpha^{JJ})^{-1} H_\alpha^{JI} u_\alpha^I \tag{2.28}$$

$$u_\beta^J = (H_\beta^{JJ})^{-1}\bar{y}^J - (H_\beta^{JJ})^{-1} H_\beta^{JI} u_\beta^I \tag{2.29}$$

Adding both equations (2.28) and (2.29)

$$\bar{u}^J = (H_\alpha^{JJ})^{-1}\bar{y}^J - (H_\alpha^{JJ})^{-1} H_\alpha^{JI} u_\alpha^I + (H_\beta^{JJ})^{-1}\bar{y}^J - (H_\beta^{JJ})^{-1} H_\beta^{JI} u_\beta^I \tag{2.30}$$

Solving the equation (2.30), in order to $\bar{y}^J$

$$((H_\alpha^{JJ})^{-1} + (H_\beta^{JJ})^{-1})\bar{y}^J = (H_\alpha^{JJ})^{-1} H_\alpha^{JI} U_\alpha^I + (H_\beta^{JJ})^{-1} H_\beta^{JI} u_\beta^I + \bar{u}^J$$

$$<=> \bar{y}^J = ((H_\alpha^{JJ})^{-1} + (H_\beta^{JJ})^{-1})^{-1}((H_\alpha^{JJ})^{-1} H_\alpha^{JI} u_\alpha^I + (H_\beta^{JJ})^{-1} H_\beta^{JI} u_\beta^I + \bar{u}^J) \tag{2.31}$$

The following conditions can be stated

$$y_\alpha^I = \bar{y}_\alpha^I \qquad y_\beta^I = \bar{y}_\beta^I \qquad u_\alpha^I = \bar{u}_\alpha^I \qquad u_\beta^I = \bar{u}_\beta^I \tag{2.32}$$

Substituting the equations (2.28), (2.29), (2.31) and (2.32) into equations (2.23) and (2.24) the coupled structure FRFs are obtained as follows

$$\begin{aligned}
\bar{H}_{11} &= H_\alpha^{II} - H_\alpha^{IJ}(H_\alpha^{JJ} + H_\beta^{JJ})^{-1}H_\alpha^{JI} \\
\bar{H}_{12} &= H_\alpha^{IJ}(H_\alpha^{JJ} + H_\beta^{JJ})^{-1}H_\beta^{JI} \\
\bar{H}_{13} &= H_\alpha^{IJ}(H_\alpha^{JJ} + H_\beta^{JJ})^{-1}H_\beta^{JJ} \\
\bar{H}_{21} &= H_\beta^{IJ}(H_\alpha^{JJ} + H_\beta^{JJ})^{-1}H_\alpha^{JI} \\
\bar{H}_{22} &= H_\beta^{II} - H_\beta^{IJ}(H_\alpha^{JJ} + H_\beta^{JJ})^{-1}H_\beta^{JI} \\
\bar{H}_{23} &= H_\beta^{IJ}(H_\alpha^{JJ} + H_\beta^{JJ})^{-1}H_\alpha^{JJ} \\
\bar{H}_{31} &= H_\beta^{JJ}(H_\alpha^{JJ} + H_\beta^{JJ})^{-1}H_\alpha^{JI} \\
\bar{H}_{32} &= H_\alpha^{JJ}(H_\alpha^{JJ} + H_\beta^{JJ})^{-1}H_\beta^{JI} \\
\bar{H}_{33} &= H_\alpha^{JJ}(H_\alpha^{JJ} + H_\beta^{JJ})^{-1}H_\beta^{JJ}
\end{aligned} \tag{2.33}$$

Again, depending on the chosen output, displacement, velocity or acceleration, the obtained FRF will be receptance, mobility or accelerance, respectively. As this expressions were deduced it just permit the coupling of two substructures at same time. However, in some analyses it can be necessary the assembling of more than two substructures. Thus, this coupling should be generalized.

Considering the FRFs relation (for one generalized substructure composed by more than two substructures) as follows

$$\begin{bmatrix} y^I \\ y^J \end{bmatrix} = \begin{bmatrix} H^{II} & H^{IJ} \\ H^{JI} & H^{JJ} \end{bmatrix} \begin{bmatrix} u^I \\ u^J \end{bmatrix} \tag{2.34}$$

where,

$$\{u^I\} = \begin{bmatrix} u_\alpha^I \\ u_\beta^I \\ \vdots \end{bmatrix}, \quad \{y^J\} = \begin{bmatrix} y_\alpha^J \\ y_\beta^J \\ \vdots \end{bmatrix} \tag{2.35}$$

$$\{y^I\} = \begin{bmatrix} y_\alpha^I \\ y_\beta^I \\ \vdots \end{bmatrix}, \quad \{y^J\} = \begin{bmatrix} y_\alpha^J \\ y_\beta^J \\ \vdots \end{bmatrix} \tag{2.36}$$

Assuming, again, that the top bar variables are related to the assembled substructure, the FRF for the assembled structure will be

$$\begin{bmatrix} \bar{y}^I \\ \bar{y}^J \end{bmatrix} = \begin{bmatrix} \bar{H}^{II} & \bar{H}^{IJ} \\ \bar{H}^{JI} & \bar{H}^{JJ} \end{bmatrix} \begin{bmatrix} \bar{u}^I \\ \bar{u}^J \end{bmatrix} \tag{2.37}$$

Introducing the coupling matrix $[T]$, the compatibility and equilibrium conditions can be written as follows

$$y^J = T^T \bar{y}^J \tag{2.38}$$

$$\bar{u}^J = T u^J \tag{2.39}$$

Substituting the condition expressed by equation (2.38) in the bottom block row of the system of equations presented at expression (2.34)

$$y^J = H^{JI}u^I + H^{JJ}u^J$$

$$<=> T^T\bar{y}^J = H^{JI}u^I + H^{JJ}u^J$$

$$<=> (H^{JJ})^{-1}T^T\bar{y}^J = (H^{JJ})^{-1}H^{JI}u^I + u^J \tag{2.40}$$

Multiplying the equation (2.40) by the $[T]$ matrix and by the equilibrium equation (2.39)

$$T(H^{JJ})^{-1}T^T\bar{y}^J = T(H^{JJ})^{-1}H^{JI}u^I + Tu^J$$

$$<=> \bar{y}^J = [T(H^{JJ})^{-1}T^T]^{-1}[T(H^{JJ})^{-1}H^{JI}u^I + \bar{u}^J] \tag{2.41}$$

Lastly, by the substitution of the equations (2.40) and (2.41) in the system of equations (2.34), the assembled structure FRFs are obtained.

$$\begin{aligned}
\bar{H}^{JJ} &= [T(H^{JJ})^{-1}T^T]^{-1} \\
\bar{H}^{II} &= H^{II} - H^{IJ}(H^{JJ})^{-1}H^{JI} + H^{IJ}(H^{JJ})^{-1}T^T\bar{H}^{JJ}T(H^{JJ})^{-1}H^{JI} \\
\bar{H}^{IJ} &= H^{IJ}(H^{JJ})^{-1}T^T\bar{H}^{JJ} \\
\bar{H}^{JI} &= \bar{H}^{JJ}T(H^{JJ})^{-1}H^{JI}
\end{aligned} \tag{2.42}$$

In fact, the FBS method is much more used than the state-space coupling methods, which analyse is the objective of the presented paper. The choice for this method is justified for its simplicity and for being simpler applied.

Note that, with the measured FRFs of one component it is obtained the component FRFs. Thus, the FBS method can be directly applied to the obtained FRFs. On the other hand, by the use of state-space coupling methods, the obtained FRFs should be identified and transformed into a state-space model. This estimation should be almost perfect, in order to obtain high quality coupling results. However, this procedure is complex and is not always simple to obtain an high quality estimated state-space model from measured data (see section 2.8).

Even though the simple applicability of the FBS method compared to the state-space coupling methods, the FBS method reveals some numerical problems. These problems are due, for example, to noisy measured data and ill-conditioned matrix inversions (see equations (2.42)). Therefore, sometimes, the estimate of the coupled FRFs is poor, specially for more complex problems with a non-linear mechanical behaviour.

Thus, the exploration of another coupling techniques, in order to overcome these problems is the main reason for the research of state-space coupling methods.

2.7 State-space coupling: theoretical state-space models

In this section two state-space coupling methods will be discussed. The first one was proposed by Su and Juang [Su and Juang, 1994]. The another one was proposed by Sjövall [Sjövall, 2004]. The main objective is to understand the physical principles behind both methods and make a comparison between both, pointing some advantages and disadvantages.

In chapter 3 some numerical models will be coupled with each method and the results will be compared. The mathematical demonstration of the coupled state-space model will be also done for each method. However, it will be present in appendices of this dissertation.

The full demonstration of the coupled state-space model of the approach proposed by Su and Juang [Su and Juang, 1994] will be performed at appendix A, the deduction of coupling form and the coupled state-space model of the Sjövall approach [Sjövall, 2004] will be performed at appendices B and C, respectively.

2.7.1 State-space coupling method proposed by Su and Juang

In this subsection, the state-space coupling method proposed by Su and Juang [Su and Juang, 1994] will be explored. The basis conditions of the coupling is transverse to every coupling methods. As already performed for the FBS method (see section 2.6), the enforcement of the compatibility and equilibrium conditions along the interfaces of the substructures is the fundamental step.

The compatibility condition states that the matching pairs of degrees of freedom (DOF) must have the same output value and signal. Hence, the physical motion of the substructures at the interface have to be the same. The equilibrium condition states that the sum of the internal forces at the interface must be equal to the external force applied. Note that, the compatibility condition is responsible for the relation between outputs, while the equilibrium condition relates the inputs.

For a successful implementation of this method, it is fundamental to understand these simple conditions. Thus, it is of interest to analyze a simple mechanical system to demonstrate how the equilibrium and compatibility conditions must be established.

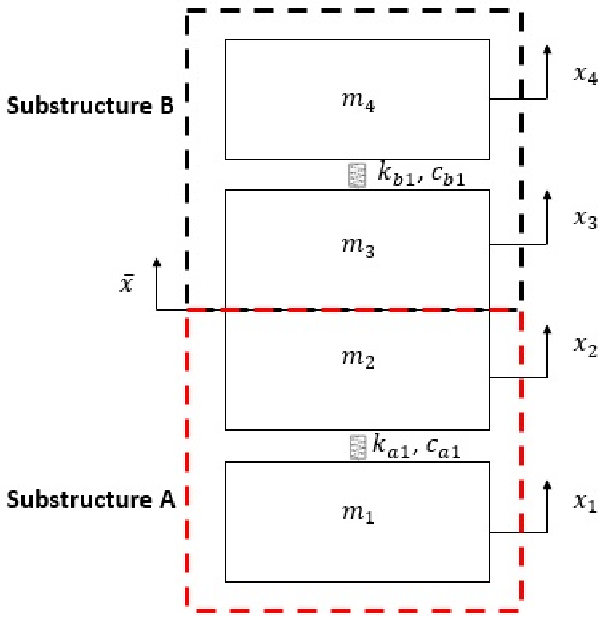

Figure 2.2: Mechanical System nº 1: Su and Juang method

For the mechanical system presented in figure 2.2 the DOFs that are going to be coupled are the number 2 and the number 3. Thus, the compatibility condition imposes that the outputs related to DOFs 2 and 3 has the same physical motion, which is equal to the physical motion of the coupled DOF. The following compatibility condition can be established

$$y_2 = y_3 = \bar{y} \tag{2.43}$$

Again, top bar variables will be related to the assembled structure.

On other hand, the equilibrium equation states that the sum of internal forces at the interface has to be equal to the external applied forces. On other words and applying to the presented mechanical system at figure 2.2, the applied force on the coupled DOF related to the sum of the masses m_2 and m_3 is equal to the sum of the forces applied on each DOF related to masses m_2 and m_3. Thus, the applied force in the coupled DOF will be

$$u_2 + u_3 = \bar{u} \tag{2.44}$$

In order to express these conditions in a simpler manner, a coupling matrix $[T]$ is introduced. By the use of this matrix the relationship between coupled DOFs and uncoupled ones is given as follows

$$\begin{bmatrix} y_2 \\ y_3 \end{bmatrix} = [T]^T \bar{y} \tag{2.45}$$

$$\bar{u} = [T] \begin{bmatrix} u_2 \\ u_3 \end{bmatrix} \tag{2.46}$$

Therefore, for the presented mechanical system the $[T]$ matrix is given as follows

$$[T] = \begin{bmatrix} 1 & 1 \end{bmatrix} \tag{2.47}$$

Note that $[T]$ matrix will always have a number of columns equal to the interface degrees of freedom. On other hand, the number of rows will be equal to the coupled DOFs, i.e, number of interface DOFs after coupling (in this example, will be just one).

The affirmations about the number of $[T]$ matrix rows and columns are explained by the observation of the mathematical expressions (2.45) and (2.46). For example, by the observation of expression (2.45) it can be observed that for the condition be respected the number of rows should be equal to the number of interface DOFs after coupling. Moreover, the affirmation about the number of $[T]$ matrix columns can be verified, for example, by the observation of equation (2.46), where the number of columns has to be equal to the number of the DOFs which will be coupled, in order to verify the expression.

After full understand the base conditions (compatibility and equilibrium) and how to construct the $[T]$ matrix, it is moment to start the coupling procedure. The first step is the computation of the uncoupled acceleration state-space models for each of substructures that will be coupled (see expression (2.8)). Secondly, a uncoupled diagonal acceleration state-space model from the uncoupled state-space models should be established as follows

$$\begin{aligned} \{\dot{x}\} &= [A_D]\{x\} + \begin{bmatrix} B_D^I & B_D^J \end{bmatrix} \begin{bmatrix} u^I \\ u^J \end{bmatrix} \\ \begin{bmatrix} y^I \\ y^J \end{bmatrix} &= \begin{bmatrix} C_D^I \\ C_D^J \end{bmatrix} \{x\} + \begin{bmatrix} D_D^{II} & D_D^{IJ} \\ D_D^{JI} & D_D^{JJ} \end{bmatrix} \begin{bmatrix} u^I \\ u^J \end{bmatrix} \end{aligned} \tag{2.48}$$

where the subscript D represents diagonal matrices and the superscripts I and J represents internal and interface degrees of freedom, respectively. The diagonal matrices are build as follows

$$
\begin{aligned}
[A_D] &= \begin{bmatrix} A_\alpha & & \\ & A_\beta & \\ & & \ddots \end{bmatrix}, \quad [B_D^I] = \begin{bmatrix} B_\alpha^I & & \\ & B_\beta^I & \\ & & \ddots \end{bmatrix} \\
[C_D^I] &= \begin{bmatrix} C_\alpha^I & & \\ & C_\beta^I & \\ & & \ddots \end{bmatrix}, \quad [D_D^{II}] = \begin{bmatrix} D_\alpha^{II} & & \\ & D_\beta^{II} & \\ & & \ddots \end{bmatrix}
\end{aligned}
\tag{2.49}
$$

Here, it is just present how to construct the diagonal matrices $[B_D]$, $[C_D]$ and $[D_D]$ related to the internal DOFs. However, the construction for the interface, for internal-interface and for interface-interface DOFs (as it succeeds for the matrix $[D_D]$) is equal. Note also, that the Greek letters subscripts represents the various substructures that are wanted to be coupled. The output and input vectors are given by

$$
\begin{aligned}
\{u^I\} &= \begin{bmatrix} u_\alpha^I \\ u_\beta^I \\ \vdots \end{bmatrix}, \quad \{u^J\} = \begin{bmatrix} u_\alpha^J \\ u_\beta^J \\ \vdots \end{bmatrix} \\
\{y^I\} &= \begin{bmatrix} y_\alpha^I \\ y_\beta^I \\ \vdots \end{bmatrix}, \quad \{y^J\} = \begin{bmatrix} y_\alpha^J \\ y_\beta^J \\ \vdots \end{bmatrix}
\end{aligned}
\tag{2.50}
$$

The coupled state-space model is achieved by the enforcement of the compatibility and equilibrium conditions at the interfaces between substructures. This enforcement is performed on the uncoupled diagonal acceleration state-space model (expression (2.48)). All the mathematical procedure is presented at appendix A, in this section the coupled state-space model will be just presented as follows

$$
\begin{aligned}
\{\dot{\bar{x}}\} &= [\bar{A}]\{\bar{x}\} + \begin{bmatrix} \bar{B}^I & \bar{B}^J \end{bmatrix} \begin{bmatrix} \bar{u}^I \\ \bar{u}^J \end{bmatrix} \\
\begin{bmatrix} \bar{y}^I \\ \bar{y}^J \end{bmatrix} &= \begin{bmatrix} \bar{C}^I \\ \bar{C}^J \end{bmatrix} \{\bar{x}\} + \begin{bmatrix} \bar{D}^{II} & \bar{D}^{IJ} \\ \bar{D}^{JI} & \bar{D}^{JJ} \end{bmatrix} \begin{bmatrix} \bar{u}^I \\ \bar{u}^J \end{bmatrix}
\end{aligned}
\tag{2.51}
$$

As it had been discussed the relationship between the interface uncoupled and coupled DOFs can be established by the $[T]$ matrix as follows

$$\{y^J\} = [T]^T \{\bar{y}^J\} \tag{2.52}$$

$$\{\bar{u}^J\} = [T]\{u^J\} \tag{2.53}$$

In its turn, the relationship between internal uncoupled and coupled outputs is a equality relation.

$$\{y^I\} = \{\bar{y}^I\} \tag{2.54}$$

The same can be pointed for the inputs.

$$\{u^I\} = \{\bar{u}^I\} \tag{2.55}$$

Since, in a theoretical state-space model the states are directly related to DOFs the following expression is also true.

$$x_i = y_i, \qquad i = 1, ..., n \tag{2.56}$$

where,

- i is the i^{th} DOF;
- n is the number of DOFs;

Assuming that, the number of states is equal to the number of outputs, the variable n will be equal to the number of considered DOFs.

In order to deduce how the coupled matrices $[\bar{A}]$, $[\bar{B}]$, $[\bar{C}]$ and $[\bar{D}]$ are constructed, the relations established in the equations (2.52), (2.53), (2.54) and (2.55) have to be introduced in the uncoupled acceleration diagonal state-space model (see equation (2.48)). This mathematical demonstration is presented in appendix A.

After the performance of the mathematical deduction, it can be concluded that the coupled matrices are build as follows

$$\begin{gathered}
[\bar{A}] = A_D + B_D^J Q C_D^J \\
[\bar{B}] = \begin{bmatrix} B_D^I + B_D^J Q D_D^{JI} & B_D^J (D_D^{JJ})^{-1} T^T S^{-1} \end{bmatrix} \\
[\bar{C}] = \begin{bmatrix} C_D^I + D_D^{IJ} Q C_D^J \\ S^{-1} T (D_D^{JJ})^{-1} C_D^J \end{bmatrix} \\
[\bar{D}] = \begin{bmatrix} D_D^{II} + D_D^{IJ} Q D_D^{JI} & D_D^{IJ} (D_D^{JJ})^{-1} T^T S^{-1} \\ S^{-1} T (D_D^{JJ})^{-1} D_D^{JI} & S^{-1} \end{bmatrix}
\end{gathered} \tag{2.57}$$

Where the auxiliary variables $[S]$ and $[Q]$ are given by

$$[S] = T (D_D^{JJ})^{-1} T^T \tag{2.58}$$

$$[Q] = (D_D^{JJ})^{-1} T^T S^{-1} T (D_D^{JJ})^{-1} - (D_D^{JJ})^{-1} \tag{2.59}$$

At this moment, the coupled matrices are deduced and can be obtained with the uncoupled state-space models of each substructure. However, the reader should be alerted for some details that one superficial observation could hide. Firstly, observe how the uncoupled diagonal state-space model is obtained (see equation (2.49)). Note that, because of matrix $[A_D]$ construction, the state vector will not have the usual arrangement. Thus, the coupled state vector will have the same arrangement as the state vector of the uncoupled diagonal state-space model. In expression (2.60) it can be observed the obtained coupled state vector and the intended one,

$$\{\bar{x}_{obt}\} = \begin{bmatrix} \{x_\alpha\} \\ \{x_\beta\} \\ \vdots \end{bmatrix}, \quad \{\bar{x}_{int}\} = \begin{bmatrix} x_1 \\ x_2 \\ \vdots \\ \dot{x}_1 \\ \dot{x}_2 \\ \vdots \end{bmatrix} \tag{2.60}$$

where, top bar variables are related to coupled variables. The subscripts *obt* and *int* represents obtained and intended state vectors, respectively.

The obtained state vector is, firstly, composed by all the states related to substructure α, displacement and velocity states. Then, all the states related to substructure β until the last substructure. In the usual state vector instead of organized by substructures, it is organized by the numeration of structure DOFs, coming firstly all the states related to the displacement and after the ones related to velocity. Therefore, a rearrangement of the state vector must be performed, which implies a rearrangement of $[\bar{A}]$ matrix rows and columns as well a rearrangement of the $[\bar{B}]$ matrix rows in accordance with state vector rearrangement,.

In its turn, the input vector has a different rearrangement than the usual one. Again, the construction of the diagonal uncoupled state-space matrices is the reason. As it can be observed in equation (2.50), the matrix $[B_D]$ is obtained firstly by the matrix $[B]$ columns of each uncoupled substructure related to internal DOFs and after by the columns related to the interface DOFs. Hence, the inputs arrangement of the obtained coupled input vector does not coincide with the intended one. The arrangement of the obtained coupled input vector and the intended one are presented as follows

$$\{\bar{u}_{obt}\} = \begin{bmatrix} \{u_\alpha^I\} \\ \{u_\beta^I\} \\ \vdots \\ \{u_\alpha^J\} \\ \{u_\beta^J\} \\ \vdots \end{bmatrix}, \quad \{\bar{u}_{int}\} = \begin{bmatrix} u_1 \\ u_2 \\ \vdots \end{bmatrix} \tag{2.61}$$

This fact implies a rearrangement of the $[\bar{B}]$ matrix columns in accordance with input vector rearrangement.

Note that, the rearrangement of $[\bar{A}]$ and $[\bar{B}]$ matrices is not related to the quality of the obtained results. However, this is essential to know the position of each state, input and output in the respective vector, specially when is intended to couple a large number of substructures.

Summarizing, it is needed two different rearrangements. Firstly, a rearrangement of $[\bar{A}]$ matrix rows and columns, and for the rows of $[\bar{B}]$ matrix in accordance with state vector rearrangement. Secondly, the rearrangement of the $[\bar{B}]$ matrix columns in accordance with input vector rearrangement.

Another relevant aspect is that the obtained coupled state-space model is not a minimal-order one. This means that it is considered an excess of states in the state-space model. In fact, the excess number of states will appear due the coupling procedure. For example, for the coupling of the two substructures presented in figure 2.2, instead of the presence in the state vector of the state related to the coupled DOF ($\bar{x}$) it will be present the both interface states (x_2 and x_3), which in reality has the same physical meaning (see equations (2.43) and (2.56)). Note that, the same will occur for the, respectively, velocity states.

Analyzing the generic state-space model (see equation (2.2)), it can be realized that each row of the $[A]$ matrix is multiplied by the state vector. By the compatibility condition (see equation (2.43)) and by the equality relation presented in equation (2.56), it is known that $\bar{x}=x_2=x_3$. Therefore, to achieve a minimal-order state-space vector the columns of the $[\bar{A}]$ matrix which will multiply by the states x_2 and x_3, and $\dot{x}_2$ and $\dot{x}_3$ must be added. After adding both columns, one of both should be kept, while the other should be removed, as well the correspondent row. This row elimination should be also performed for the matrix $[\bar{B}]$, however for this matrix no columns must be added neither eliminated. The four states (x_2, x_3, $\dot{x}_2$, $\dot{x}_3$) should be, therefore replaced by just two states, $\bar{x}$ and $\dot{\bar{x}}$.

Note that, the compatibility and equilibrium conditions (see equations (2.43) and (2.44)) will guarantee the achievement of minimal-order input and output vectors. These vectors will, instantly, contain the coupled inputs and outputs, while the uncoupled interface ones will not be present. This is the reason for not perform any sum neither any matrix $[\bar{B}]$ columns elimination.

The last step, is the matrices $[\bar{C}]$ and $[\bar{D}]$ computation. Assuming, acceleration outputs the matrix $[\bar{C}]$ will be equal to the second block row of the matrix $[\bar{A}]$, while the $[\bar{D}]$ will be equal to the second block row of matrix $[\bar{B}]$ (see section 2.2).

2.7.2 State-space coupling method proposed by Sjövall

The state-space coupling method proposed by Sjövall [Sjövall, 2004] is derived from the one proposed by Su and Juang [Su and Juang, 1994]. The aim for the development of this approach is, directly, obtain the coupled state-space model in a minimal-order form. Therefore, no states elimination is needed, eliminating some possible difficulties and mistakes that could occur in that process.

This method starts for the transformation of the substructures state-space model into a coupling form. In order to perform this transformation, a transformation matrix $[T_{Sj}]$ for the substructure is established as follows[Abrahamsson, 2018][Allen et al., 2020]

$$[T_{Sj}] = \begin{bmatrix} C \\ CA \\ N \end{bmatrix} \tag{2.62}$$

where, $[A]$ and $[C]$ matrices are taken from the substructure displacement state-space model. The matrix $[N]$ presented in the $[T_{Sj}]$ matrix is the projection of two different null-spaces, $[N_B]$ and $[N_C]$

$$N = N_C N_B^T (N_B N_B^T)^{-1} N_B \tag{2.63}$$

where,

$$N_B B = 0 \tag{2.64}$$

$$\begin{bmatrix} C \\ CA \end{bmatrix} N_C^T = 0 \tag{2.65}$$

The coupling form of the substructure state-space models, is achieved by transforming the state vector, as follows

$$z = T_{Sj} x \tag{2.66}$$

Remembering the generic state-space model (see expression (2.2))

$$\begin{cases} \{\dot{x}(t)\} = [A]\{x(t)\} + [B]\{u(t)\} \\ \{y(t)\} = [C]\{x(t)\} + [D]\{u(t)\} \end{cases} \tag{2.67}$$

By the equation (2.66)

$$x = T_{Sj}^{-1} z \tag{2.68}$$

Substituting the value of x (see equation (2.68)) in the generic state-space model (see equation (2.67)), the coupling form of the substructure state-space model is obtained as follows

$$\begin{cases} \{\dot{z}(t)\} = [T_{Sj}][A][T_{Sj}]^{-1}\{z(t)\} + [T_{Sj}][B]\{u(t)\} \\ \{y(t)\} = [C][T_{Sj}]^{-1}\{z(t)\} + [D]\{u(t)\} \end{cases} \tag{2.69}$$

The presented state-space model in equation (2.69) can be also expressed as follows

$$\begin{cases} \{\dot{z}(t)\} = [\widetilde{A}]\{z(t)\} + [\widetilde{B}]\{u(t)\} \\ \{y(t)\} = [\widetilde{C}]\{z(t)\} + [\widetilde{D}]\{u(t)\} \end{cases} \tag{2.70}$$

Since, the matrices $[\widetilde{C}]$ and $[\widetilde{D}]$ can be computed from the matrices $[\widetilde{A}]$ and $[\widetilde{B}]$, respectively (see section 2.2), from now on just the $[\widetilde{A}]$ and $[\widetilde{B}]$ matrices of this state-space model will be presented and analyzed.

Assuming that the coupling of two generic substructures A and B is intended to be performed, the first block row of the coupling form of the state-space model of a generic substructure A by explicit presenting the matrices $[\widetilde{A}]$ and $[\widetilde{B}]$ is given as follows

$$\begin{bmatrix} \dot{y}_c \\ \ddot{y}_c \\ \dot{x}_b^i \end{bmatrix} = \begin{bmatrix} 0 & I & 0 \\ A_{vd}^A & A_{vv}^A & A_{vb}^A \\ A_{bd}^A & A_{bv}^A & A_{bb}^A \end{bmatrix} \begin{bmatrix} y_c \\ \dot{y}_c \\ x_b^i \end{bmatrix} + \begin{bmatrix} 0 \\ B_{vv}^A \\ 0 \end{bmatrix} (u_c^A) \tag{2.71}$$

Note that, the proof for the structure of matrices $[\widetilde{A}]$ and $[\widetilde{B}]$ is given at appendix B.

In equation (2.71) the therm B_{vv}^A is the inverse of the interface inertia related to the interface DOF of the generic substructure A. The variables with subscripts b and c are related to internal and interface degrees of freedom, respectively. Variables d and v are related to displacement and velocity, respectively. Again, over bar variables are related to the assembled structure.

After the achievement of both substructure state-space models expressed in coupling form, the compatibility and equilibrium conditions must be enforced, in order to obtain the coupled structure state-space model. By the enforcement of both conditions, the following coupled matrices are obtained

$$[\bar{A}] = \begin{bmatrix} 0 & I & 0 & 0 \\ \bar{A}_{vd} & \bar{A}_{vv} & \bar{A}_{vb}^A & \bar{A}_{vb}^B \\ \bar{A}_{bd}^A & A_{bv}^A & \bar{A}_{bb}^A & 0 \\ \bar{A}_{bd}^B & \bar{A}_{bv}^B & 0 & A_{bb}^B \end{bmatrix}, \quad [\bar{B}] = \begin{bmatrix} 0 \\ \bar{B}_{vv} \\ 0 \\ 0 \end{bmatrix} \tag{2.72}$$

where,

- $\bar{B}_{vv} = ((B_{vv}^A)^{-1} + (B_{vv}^B)^{-1})^{-1}$;
- $\bar{A}_{vd} = \bar{B}_{vv}((B_{vv}^A)^{-1}A_{vd}^A + (B_{vv}^B)^{-1}A_{vd}^B)^{-1}$;
- $\bar{A}_{vv} = \bar{B}_{vv}((B_{vv}^A)^{-1}A_{vv}^A + (B_{vv}^B)^{-1}A_{vv}^B)^{-1}$;
- $\bar{A}_{vb}^A = \bar{B}_{vv}(B_{vv}^A)^{-1}A_{vd}^A$;
- $\bar{A}_{vb}^B = \bar{B}_{vv}(B_{vv}^B)^{-1}A_{vd}^B$;

The coupling form of the coupled state-space model is given as follows

$$\begin{bmatrix} \dot{\bar{y}} \\ \ddot{\bar{y}} \\ \dot{x}_b^A \\ \dot{x}_b^B \end{bmatrix} = \begin{bmatrix} 0 & I & 0 & 0 \\ \bar{A}_{vd} & \bar{A}_{vv} & \bar{A}_{vb}^A & \bar{A}_{vb}^B \\ A_{bd}^A & A_{bv}^A & A_{bb}^A & 0 \\ A_{bd}^B & A_{bv}^B & 0 & A_{bb}^B \end{bmatrix} \begin{bmatrix} \bar{y} \\ \dot{\bar{y}} \\ x_b^A \\ x_b^B \end{bmatrix} + \begin{bmatrix} 0 \\ \bar{B}_{vv} \\ 0 \\ 0 \end{bmatrix} (\bar{u}) \tag{2.73}$$

The mathematical proof for the achievement of the coupling form of the coupled state-space model is presented at appendix C. Note that, the presented variables x_b^A and x_b^B, in fact represents the displacement and velocity states as follows

$$\{x_b^A\} = \begin{bmatrix} x_b^A \\ \dot{x}_b^A \end{bmatrix}, \quad \{x_b^B\} = \begin{bmatrix} x_b^B \\ \dot{x}_b^B \end{bmatrix} \tag{2.74}$$

Analyzing the coupling form of the coupled state-space model (see equation (2.73)), it can be realized that the unique rows related to coupled outputs and inputs are the first and the second. The rest of the rows, are just directly taken from the substructure state-space models.

The construction of the coupled state-space model is needed. This construction has to be made manually. Starting for the $[\bar{A}]$ matrix construction and by taking as example the mechanical system presented at figure 2.2, the intended state vector for the coupled state-space model would be the following

$$\{\bar{x}\} = \begin{bmatrix} x_1 \\ \bar{x} \\ x_4 \\ \dot{x}_1 \\ \dot{\bar{x}} \\ \dot{x}_4 \end{bmatrix} \tag{2.75}$$

To perform such construction, firstly the rows related to the internal states of the substructure A state-space model should be inserted, then the coupled row obtained from the coupling form of the coupled state-space model (see expression (2.73)) and finally the rows related to the internal states of the substructure B state-space model. Note that, the described sequence should be done for the rows related to velocity states and then repeated for the rows related to acceleration ones. On other hand, for each of the inserted rows, a different column rearrangement has to be performed.

In its turn, let focus in construction of $[\bar{B}]$ matrix. The second Newton law establishes a relation between force and acceleration (see equation (2.76)). Thus, the mass related to each DOF will directly contribute for the acceleration state related to the same DOF.

$$F = m \times a \tag{2.76}$$

On other hand, there is no direct relation between velocity and force. Therefore, the first block row of the $[\bar{B}]$ matrix, which is related to velocity states should be composed by null terms. For the second block row, it should be composed by a diagonal matrix. This diagonal matrix must include the inverse of the mass related to each DOF.

2.7.3 Comparing the presented approaches

After analysing both of the methods, it will be of interest to point some advantages and disadvantages between both. The method proposed by Su and Juang [Su and Juang, 1994] is simple, permitting the coupling of several substructures at same time, and several interface DOFs, even if shared by more than two substructures. However, has the disadvantage of the coupled state-space model be obtained in a non minimal-order form.

On other hand, the Sjövall approach [Sjövall, 2004] permits the, instantly, achievement of a minimal order state-space model. Even though the presented advantage, this method also has some disadvantages. To start, the formulation is complex, specially for the transformation matrix $[T_{Sj}]$. Moreover, it does not allow the coupling of more than two system at same time. The coupling of multiple system has to be performed step by step. It is not possible to couple DOFs which are shared by more than two substructures. Another disadvantage is that instead of just needing one arrangement of rows and columns of $[\bar{A}]$ matrix, it will be need several ones. If it is expected to couple several DOFs even more arrangements will be needed. To finish, in order to achieve the coupled state-space model, it is, firstly, necessary the computation of the coupling form of the coupled state-space model to obtain the coupled rows. Secondly, it is necessary a manually construction of the coupled state-space model.

2.8 PolyMAX combined with ML-MM method

The aim of this section is the performance of a superficial description of the used method to estimate state-space models from measured FRFs. This is not the objective of the present dissertation, justifying the superficial analyse to it. For a detail exploration on PolyMAX method the readers are forwarded to [Peeters et al., 2004]. On other hand, for a detail exploration in the combined use of PolyMAX and ML-MM methods the readers are forwarded to [El-Kafafy et al., 2015].

2.8.1 PolyMAX method

The PolyMAX method is a polyreference version of the least-squares complex frequency-domain (LSCF) estimation method. In fact, the interest in LSCF method started because very clear stabilisation diagrams were obtained. This method estimates a common-denominator model, which closely fit the measured FRFs data. However, when this model is converted to a modal model by reducing residues using the singular value decomposition (see section 2.5) the quality of the fit decreases. On other hand, the stabilization diagram is constructed just with pole information (eigenfrequencies and damping ratios), no more information is available. This fact results that closely spaced poles will erroneously appear as just a single pole.

In order to overcome the two pointed limitations of LSCF method it was developed PolyMAX, which is a polyreference version of the LSCF method. Using PolyMAX, at the construction of the stabilization diagrams it is not only known the pole information, but also the modal participation factors. This fact, avoid the use of SVD (singular value decomposition) step and closely spaced poles can be separated.

In order to estimate the modal parameters with PolyMAX method it is common to over-specify the model order considerably, trying to fit high order models, which contains more modes than presented in the data. Afterwards, the physical and mathematical modes are identified from the stabilization diagram (see figure G.1). This chart is obtained by repeating the analysis for increasing model order, in each analyze the poles are calculated from the estimated denominator coefficients. The identification of the physical meaning poles (real poles of the system) and the mathematical poles can be done from this diagram. The physical poles tend to appear for each estimation order at nearly identical locations, while the mathematical ones tend to appear in different positions. Thus, if the differences observed in the different analyses are within pre-set limits, the pole is considered a physical one, if it is not the pole is neglected. By the use of PolyMAX method this identification is simpler since the non physical poles are estimated with a negative damping ratio.

The pre-sets limits, in order to identify real physical poles are established between two consecutive model orders, and are related to the following parameters:

- Maximum variation of MAC (see section 2.4) value for the modal participation vectors;
- Maximum frequency variation;
- Maximum damping ratio variation.

By the stabilization diagram interpretation it is identified a set of poles and the modal participation factors. The mode shapes can then be found by considering the modal model.

Assuming, that the system under testing presents a sub-critic damping, for all its vibration modes, which means that[Rodrigues, 2018]

$$0 < \xi_r < 1 \quad \forall\ r\ \epsilon\ \mathbb{N} \tag{2.77}$$

where, ξ_r is the damping ratio of the r^{th} system vibration mode. A generic displacement FRF can be expressed by the following modal model [International, 2000][Guillaume, n.d.][International, 2012]

$$[H(\omega)] = \sum_{r=1}^{N_m} \left(\frac{[R_r]}{j\omega - \lambda_r} + \frac{[R_r]^*}{j\omega - \lambda_r^*} \right) + \frac{[LR]}{s^2} + [UR] \tag{2.78}$$

where,

- N_m is the number of identified modes;
- s is the Laplace variable;
- subscript $[\bullet]^*$ denotes the complex conjugate of a matrix;
- $[R_r]$ is the r^{th} residue matrix;
- λ_r is the r^{th} pole:
- $[LR]$ and $[UR]$ are the lower and upper residuals matrices modelling respectively the influence of the lower and upper out-of-band modes in the considered frequency band.

The poles will appear in a complex conjugate pairs, as follows

$$\lambda_r, \lambda_r^* = -\xi_r \omega_{nr} \pm j\omega_{nr}\sqrt{1 - \xi_r^2} \tag{2.79}$$

where,

- ω_{nr} is the undamped natural frequency of the r^{th} vibration mode;
- j is the complex operator ($j = \sqrt{-1}$).

The residue matrix presented at equation (2.78) is given by the following expression

$$R_r = a_r \{\Psi_o\}_r \{\Psi_i\}_r \tag{2.80}$$

where,

- $\{\Psi_o\}_r$ is the mode shape vector (column) of the r^{th} vibration mode with mode shapes coefficients at the output DOFs;

- $\{\Psi_i\}_r$ is the mode shape vector (row) of the r^{th} vibration mode with mode shapes coefficients at the input DOFs;
- a_r is a complex scaling constant of the r^{th} mode shape, which value is determined by the scaling of the mode shapes.

The residue matrix can also be expressed as follows

$$[R_r] = \{\Psi_o\}_r\{L\}_r \tag{2.81}$$

where, vector $\{L\}_r$ is a row vector, its coefficients expresses the participation of the mode r in the response of each input DOF. The coefficients which composes this vector are called modal participation factors.

Remembering equation (2.80) the following relation can be established

$$a_k\{\Psi_i\}_r = \{L\}_r \tag{2.82}$$

Assuming that the structure under test has a proportional damping and, thus, will present real mode shapes, the scaling factor a_k is given as follows

$$a_k = -\frac{j}{2m_r\omega_{dr}} \tag{2.83}$$

where,

- j is the complex operator ($j = \sqrt{-1}$);
- m_r is the modal mass of mode r;
- ω_{dr} is the damped natural frequency.

Again, by assuming that the structure under testing presents a sub-critic damping, the damped natural frequency is related with the undamped one as follows

$$\omega_{dr} = \omega_{nr}\sqrt{1-\xi^2} \tag{2.84}$$

The generic displacement modal model of an FRF can be thus computed as follows

$$[H(\omega)] = \sum_{r=1}^{N_m}\left(\frac{\{\Psi_o\}_r\{L\}_r}{j\omega-\lambda_r} + \frac{\{\Psi_o\}_r^*\{L\}_r^*}{j\omega-\lambda_r^*}\right) + \frac{[LR]}{s^2} + [UR] \tag{2.85}$$

Observing the equation (2.85) the unique unknowns are the mode shapes, the lower and upper residuals, which can be obtained by solving that equation in a linear least-squares sense.

2.8.2 ML-MM: maximum likelihood modal model-based method

The ML-MM is an iterative method based on solving a non-linear optimization problem. Thus, initial values for the modal model parameters are needed to start the optimization process. These initial values are obtained with PolyMAX method. As it was referred this method estimates the poles and the participation modal factors of the physical modes within the frequency band of interest. Afterwards, the mode shapes, the lower and upper residuals are estimated by solving equation (2.85) in a linear least-square sense.

The optimization procedure has the aim to minimize a cost-function by the use of Gauss-Newton optimization. This procedure is done in two different stages. At each iteration, ML-MM solver consider the poles and the modal participation factors as the parameters to be updated, while the mode shapes and the lower and upper residuals are calculated in a linear least-squares formulation by the use of the updated poles and participation factors and with the measured FRFs.

The final of this optimization process is defined by an relative error between two consecutive calculated cost-functions or by reaching the maximum number of iterations.

2.8.3 Implementation of system identification method and estimation of state-space models

Summarizing the exposed steps, in order to implement the PolyMAX combined with ML-MM method:

1. Obtain with PolyMAX method a first estimation of poles and the participation modal factors of the physical modes;

2. Estimate the mode shapes, the lower and upper residuals in a linear least-squares sense.

3. Definition of a cost function and start the Gauss-Newton optimization, in order to minimize it;

    (a) Poles and modal participation factors update;

    (b) Update of mode shapes, the lower and upper residuals by a linear least-squares formulation using the updated poles, updated participation factors and measured FRFs;

4. The optimization procedure ends when the relative error between two consecutive calculated cost-functions reaches a predefined limit or the maximum number of iterations is reached.

The described method is already implemented in software *Simcenter Testlab*®, justifying the use of this software to estimate a modal model from measured FRFs at sections 4.1.2 and 4.2.2. Moreover, the implementation of this method on *Simcenter Testlab*® permits the estimation of the modal model by enforcing two different constraints, reciprocity or real mode constraint.

The first constraint permits the estimation of the modal model assuming that the system under test verifies the Maxwell-Betti reciprocity principle. This means that the response at DOF j caused by the application of a force in DOF i, would be equal to the response at DOF i caused by the application of the same force in DOF j. Therefore, it is assumed that the system FRFs under test verifies the following expression

$$H_{ij} = H_{ji} \quad \forall \ i, j \ \epsilon \ \mathbb{N} \tag{2.86}$$

The real mode constraint permits the estimation of the modal model assuming that the structure under test has a proportional damping. The reason for the introduction of this assumption is to lower the numerical complexity of the calculations [El-Kafafy et al., 2015]. On other hand, the estimation of a state-space model from the estimated modal model is simpler. In fact, this constraint will be enforced to perform the estimation of a modal model from measured data at sections 4.1.2 and 4.2.2.

After the modal model estimation, a $MATLAB^{\circledR}$ script provided by Siemens Industry Software NV was used to obtain the estimation of the displacement and acceleration state-space models from the estimated modal model. As these state-space models are estimated from experimental data, the physical meaning of each matrix is not the same as the previous presented (see section 2.2). In fact, the estimated state-space model will be expressed in modal coordinates.

The presented displacement modal model (see expression (2.85)) can be also expressed by the following expression (2.87)(for the complete demonstration see paper [Lembregts et al., 1988]).

$$[H(\omega)] = [\Psi \quad \Psi^*] \left[s[I] - \begin{bmatrix} \Lambda & 0 \\ 0 & \Lambda^* \end{bmatrix} \right]^{-1} \begin{bmatrix} L \\ L^* \end{bmatrix} + \frac{[LR]}{s^2} + [UR] \tag{2.87}$$

Resuming the generic expression of an FRF obtained from state-space matrices (equation (2.19)).

$$\frac{Y(s)}{U(s)} = [C](s[I] - [A])^{-1}[B] + [D] \tag{2.88}$$

Analysing the presented expression for the displacement modal model (equation (2.87)) and the generic expression (2.88), each of state-space matrices, $[A]$, $[B]$, $[C]$ and $[D]$ can be identified from equation (2.87). Thus, the displacement state-space matrices will be given by

$$[A^{disp}] = \begin{bmatrix} \Lambda & 0 \\ 0 & \Lambda^* \end{bmatrix}, \quad [B^{disp}] = \begin{bmatrix} L \\ L^* \end{bmatrix}, \quad [C^{disp}] = [\Psi \quad \Psi^*], \quad [D^{disp}] = \begin{bmatrix} UR \end{bmatrix} \tag{2.89}$$

where,

- $[\Lambda]$ is a diagonal matrix containing the systems poles;
- $[L]$ is a matrix containing the modal participation factors vectors;
- $[\Psi]$ is a matrix containing the mode shapes vectors;
- $[UR]$ is a matrix containing the upper residuals;
- superscript $[\bullet]^*$ denotes the complex conjugate of a matrix.

Therefore the obtained displacement state-space model can be expressed as follows

$$\begin{cases} \{\dot{x}(t)\} = [A^{disp}]\{x(t)\} + [B^{disp}]\{u(t)\} \\ \{y(t)\} = [C^{disp}]\{x(t)\} + [D^{disp}]\{u(t)\} \end{cases} \tag{2.90}$$

By the observation of the displacement state-space matrices it can be realised that the lower residuals are not included in none of them.

On other hand the acceleration state-space model can be obtained by performing a twice differentiation of the presented displacement modal model (see appendix E), the obtained acceleration state-space model is given by

$$\begin{cases} \{\dot{x}(t)\} = [A^{accel}]\{x(t)\} + [B^{accel}]\{u(t)\} \\ \{\ddot{y}(t)\} = [C^{accel}]\{x(t)\} + [D^{accel}]\{u(t)\} \end{cases} \tag{2.91}$$

The acceleration state-space matrices and displacement ones are related as follows

$$\begin{aligned} [A^{accel}] &= \left[A^{disp}\right], \quad [B^{accel}] = \left[B^{disp}\right] \\ [C^{accel}] &= [C^{disp}][A^{disp}][A^{disp}], \quad [D^{accel}] = [C^{disp}][A^{disp}][B^{disp}] + [LR] \end{aligned} \tag{2.92}$$

Observing the acceleration state-space matrices it can be realised that the lower residuals are now included in $[D^{accel}]$ matrix, however the upper residuals are not include in none of the matrices.

In order to take in account the upper residuals in the estimated acceleration state-space modal, this residues are converted into residual modes. The modal parameters of those residual modes are then used together with the modal parameters of the in-band flexible modes to construct the $[A^{accel}]$, $[B^{accel}]$, $[C^{accel}]$, and $[D^{accel}]$ matrices of the acceleration state-space model.

2.9 State-space coupling: synthesized state-space models

The used $MATLAB^{®}$ script to estimate state-space models from the estimated modal model was able to estimate the displacement and acceleration state-space models, therefore it has to be chosen which one will be used to perform coupling. However, firstly would be profitable to understand the importance of the lower and upper residuals, since for the acceleration state-space model (see expression (2.91)) both of them are included and for displacement state-space model (see expression (2.90)) just the upper residuals are included.

The lower and upper residuals are responsible to model the influence of the out-of-band modes in the considered frequency band. Thus, the lower residuals are responsible to model the influence of modes which are contained below the lower frequency of the frequency band. On other hand, the upper residuals are responsible to model the influence of modes contained in upper frequencies than the highest frequency of the frequency band.

Therefore, the inclusion of the lower and upper residuals in the identified state-space models and in the coupling procedure is of high importance. In fact, for the simple numerical mechanical systems, which will be analysed in section 3.2, these lower and upper residuals will not be important, since the localization of all poles is known and the systems can be analysed in the desired frequency range. However, for a real structure, the number of modes and the localization of the poles is unknown. On other hand, the frequency band is limited to the excitation bandwidth. Thus, to perform the best possible identification and to obtain the best possible estimation of the coupled FRFs it is primordial to take into account both of lower and upper residuals.

Due the importance of lower and upper residuals and since both are included in the estimated acceleration state-space model, the natural choice would be use the acceleration state-space model in order to perform coupling. On other hand, the coupled state-space matrices of the method proposed by Su and Juang [Su and Juang, 1994] are derived from the uncoupled diagonal acceleration state-space model (see appendix A), thus to perform coupling with this approach the computation of the coupled state-space model from the diagonal uncoupled acceleration state-space model is a fundamental request. The achievement of this diagonal uncoupled acceleration state-space model is simpler and more direct, when using substructure acceleration state-space models. However, it is also possible when using displacement substructure state-space models, as presented at appendix D. Since, the estimated acceleration state-space models take in account both lower and upper residuals and because of being simpler to achieve the diagonal uncoupled state-space models, the coupling must be performed by the use of acceleration substructure state-space models.

In fact, the Su and Juang method [Su and Juang, 1994] showed to be simpler and easier to apply when dealing with estimated state-space models from measured data. On other hand, it does not imposes a limit to the DOFs to couple, neither to the number of substructures to couple. Moreover, the fact of this method provide a non-minimal order coupled state-space model (see section 2.7.3), vanish when coupling estimated state-space models as it will be presented in section 2.9.1. This fact is justified, because the estimated state-space model from the estimated modal model will be obtained in modal coordinates. Thus, the states will be related to different vibration modes. Since, the used system identification procedure (PolyMAX and ML-MM methods, see section 2.8) determine the model order of each substructure, no redundant states will be taken into account and, therefore, no states elimination are needed. Moreover, compatibility and equilibrium conditions, continue to guarantee the achievement of a minimal-order input vector and output vector.

In fact, the achievement of a non-minimal order coupled state-space model, when coupling theoretical state-space models, is justified because in this models the states are related to DOFs and are equal to the correspondents DOFs outputs. Therefore, each of substructures that share a DOF will present a state in its state-space model that has the same physical meaning, justifying the appearance of redundant states in the coupled state-space model.

For these reasons, the Sjövall approach [Sjövall, 2004] was not explored for coupling state-space models expressed in modal coordinates. Furthermore, the obtained coupling results with the method proposed by Su and Juang [Su and Juang, 1994] are of high quality not only for numerical couplings but also for experimental ones (see section 3.2 and chapter 4).

2.9.1 State-space coupling method proposed by Su and Juang

The estimated state-space model from measured data is obtained in modal coordinates, therefore, the states are not related to DOFs, but are related to different vibration modes. Hence, the Su and Juang method [Su and Juang, 1994] has to be reformulated.

This fact do not invalidate the deduced equations neither the used coupling method presented at section 2.7.1. The only difference is that a minimal-order system is instantly obtained after coupling and no states elimination should be performed.

The justification behind this affirmation comes from the system identification procedure. Since the model order of each substructure is determined in the identification procedure (PolyMAX and ML-MM methods, see section 2.8), no redundant states will be taken in account. Therefore, no states elimination should be performed. On other hand the compatibility and equilibrium conditions will guarantee the achievement of a minimal-order input vector and output vector. Hence, the number of lines of matrices $[C]$ and $[D]$ and the number of columns of matrices $[B]$ and $[D]$ will be minimal as well. Thus, no elimination is needed.

In fact, the achievement of a non-minimal order coupled state-space model, when coupling theoretical state-space models, is justified because in this models the states are related to DOFs and are equal to the correspondents DOFs outputs. Therefore, each of substructures that share a DOF will present a state in its state-space model that has the same physical meaning, justifying the appearance of redundant states in the coupled state-space model.

Moreover, the rearrangement of the states as explained in section 2.7.1 is negligible since no states elimination will be performed. The rearrangements which should be performed are just the columns rearrangements of the matrices $[B]$ and $[D]$ in accordance with input vector rearrangement and rows rearrangement of matrices $[C]$ and $[D]$ in accordance with output vector rearrangement. In fact, the implementation of this method to couple the state-space models obtained from system identification method is even simpler than for coupling theoretical state-space models.

Note that, since the states are now related to different vibration modes, the states are no more equal to the outputs. Therefore, the $[C]$ and $[D]$ matrices cannot be directly obtained from the $[A]$ and $[B]$ matrices as exposed in section 2.2. This is just valid for theoretical state-space models.

Summarizing all the steps in order to do a practical implementation of the coupling method developed by Su and Juang [Su and Juang, 1994]:

1. Establishment of the uncoupled diagonal acceleration state-space model;
2. Establishment of compatibility and equilibrium conditions;
3. Construction of $[T]$ matrix;
4. Achievement of the coupled acceleration state-space model;
5. Rearrangement of the columns of the coupled acceleration state-space matrices $[\bar{B}]$ and $[\bar{D}]$ in accordance with input vector rearrangement and rearrangement of the rows of the coupled acceleration state-space matrices $[\bar{C}]$ and $[\bar{D}]$ in accordance with output vector rearrangement;
6. The minimal-order coupled state-space model is, instantly, achieved.

2.10 Coupling substructures non-rigidly connected

In this section, a discussion about the difficulties in the enforcement of non-rigid coupling will be performed (section 2.10.1). Afterwards, two possible procedures in order to perform coupling between non-rigidly connected substructures will be presented (sections 2.10.2 and 2.10.3, respectively).

2.10.1 Difficulties in the enforcement of non-rigid coupling

An immediate possibility to perform a non-rigid coupling would be the construction of a state-space model to define the connecting elements. Then, it would be possible to treat this connecting elements substructure as another substructure rigidly connected to the substructures that these elements connects. This approach would permit the use of the presented procedures at sections 2.7 and 2.9, in order to perform coupling.

However, when coupling theoretical state-space models this approach cannot be, directly, applied. The reason is that in theory is usual to consider that the connecting elements are massless elements. This consideration unable the construction of a state-space model for the connecting elements, since the construction of a state-space model to define a substructure requires that this substructure has mass. Moreover, it is needed to define inputs and outputs on the connecting elements at the interface locations with each of the others substructures, otherwise it is not possible to enforce the equilibrium and compatibility conditions (see equations (2.44) and (2.43)). This fact is justified because in theoretical state-space models the inputs and outputs are directly related to the mechanical system masses. Thus, it is not possible to define inputs and/or outputs for the connecting elements, because they are treated as massless elements.

In order to overcome the exposed difficulties one possibility is the insertion of small fictitious masses at the interface of the connecting elements with each of the others substructures [Su and Juang, 1994]. The value of the inserted masses must be negligible when compared to the mass of the others substructures, in order to guarantee that the inserted masses will present a negligible influence on the mechanical properties of the assembled structure. A practical rule for the value of these fictitious masses is to assume that they are 10^6 times lower than the mass of the others substructures.

These inserted masses will permit the computation of a state-space model for the connecting elements. Furthermore, each of these inserted masses will correspond to the insertion of inputs and outputs at the interface with each of the others substructures permitting the enforcement of equilibrium and compatibility conditions. Therefore, it is possible the performance of the non-rigid coupling supposing that the connecting elements can be considered as another substructure rigidly connected to the others substructures.

On other hand, when coupling estimated state-space models from measured data it is possible to perform a non-rigid coupling assuming that the connecting elements can be, directly, considered as another substructure rigidly coupled to the others substructures. This is justified, because in reality the connecting elements presents mass, even if it is very low compared to its stiffness. Moreover, for estimated state-space models from measured data the inputs are defined by the excitation locations, while the outputs are defined by the dynamic response measurement locations. Thus, if the excitation and the dynamic response measurement are performed at the interface with each of the others substructures, it will be possible to enforce the equilibrium and compatibility conditions.

However, this is not recommended since the mass of the connecting elements is extremely low when compared to its stiffness. Hence, the resonance frequencies of this connecting elements substructure would be localized at higher frequencies than the higher frequency of the measured frequency band. The estimation of the modal parameters by the use of the method presented at section 2.8 is recommended to be performed in a frequency band which includes system poles, otherwise the modal parameters estimation will not be of high quality. Therefore, it is not recommended the coupling of the connecting elements by, directly, considering it as another substructure, neither the insertion of small fictitious masses at the interface with each of the others substructures as it was recommended when coupling theoretical state-space models.

In order to overcome the pointed limitations, another solution was developed. This solution is based in the insertion of not negligible masses at the interface of the connecting elements with each of the others substructures. The insertion of these masses will decrease the system resonance frequencies. The mass values of the inserted masses must guarantee the presence of system poles in the measured frequency band, permitting the achievement of an high quality estimated modal model.

However, this excess of mass due the insertion of not negligible masses must be removed. For that purpose, another connecting elements substructure with the same inserted masses at the same locations and with wisely chosen stiffness and damping properties must be coupled in a negative way [Mahmoudi et al., 2020], which will guarantee the achievement of the coupled FRFs of the intended assembled structure.

Summarizing, the first described approach that will be analyzed at section 2.10.2 is just recommended to perform coupling of analytical substructures defined by theoretical state-space models. On other hand, the second described approach that will be further analyzed at section 2.10.3 is recommended for coupling analytical substructures defined by theoretical state-space models and for coupling real substructures defined by estimated state-space models from measured data. However, since the simplicity of the first presented approach it is recommended just the use of the second approach to couple real substructures non-rigidly connected.

2.10.2 Fictitious masses insertion

This approach is based in the insertion of small fictitious masses between the connecting elements and the substructures. This procedure can be easily understand by the observation of the figure 2.3.

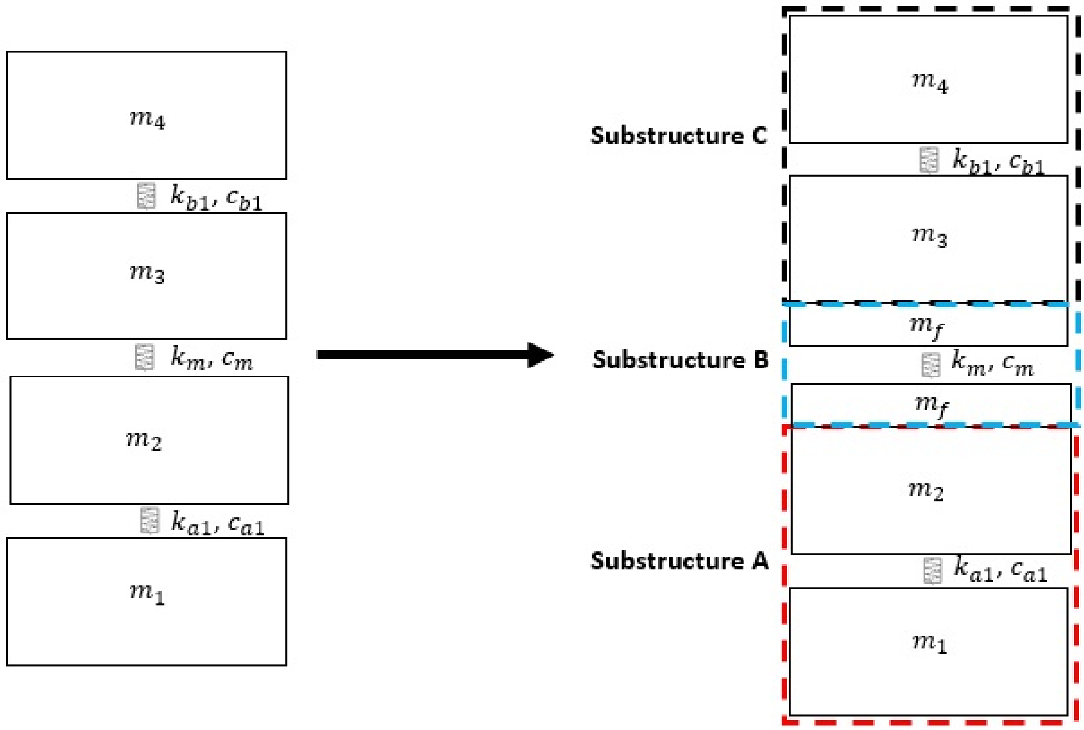

Figure 2.3: Insertion of fictitious masses and structure division

As it can be seen in figure 2.3 the mechanical system is divided in 3 different substructures, from which one is related to the inserted fictitious masses and the connecting elements (substructure B). In order to obtain the coupled state-space model of the mechanical system presented in figure 2.3 it is just needed to perform the coupling between the uncoupled state-space models of the substructures A, B and C considering that these substructures are rigidly connected [Mahmoudi et al., 2020][Su and Juang, 1994]. This coupling should be performed by following the same presented procedures at sections 2.7 and 2.9.

2.10.3 Coupling a positive and negative state-space model

The method here presented is based on the inclusion of fictitious masses between the substructures interface and the connecting elements. However, these inserted masses are not negligible, since its value must guarantee the presence of poles in the measured frequency band. The inserted masses and the connecting elements will be treated as another substructure.

The insertion of these non-negligible masses will change the mass properties of the analysed mechanical system, therefore, the obtained coupled state-space model will not correspond to the assembled structure state-space model. In order to achieve the required structure state-space model, the influence of the inserted masses should be removed.

A solution to remove the influence of the inserted masses is the construction of another substructure composed by the connecting elements and masses with the same value of the inserted ones, and then perform the coupling of this substructure in a negative form [Mahmoudi et al., 2020]. However, this procedure imposes that the first composed connecting elements substructure cannot have the same stiffness and damping properties of the real connecting elements. If it was the case, the negative coupling of the second connecting elements substructure would take the influence of the inserted masses, but also the influence of the connecting elements, which is not intended. This is justified because it is not possible to construct a state-space model of a substructure that just presents mass, it also has to present stiffness and/or damping.

Thus, a possible approach would be construct a first connecting elements substructure with twice the stiffness and damping of the real connecting elements and the second connecting elements substructure would be constructed with the real values of stiffness and damping. The coupling of the first connecting elements substructure would be performed in a regular way, and the second one in a negative way. This would remove the inserted masses and the excess of stiffness and damping inserted by the first coupling. This would guarantee the achievement of the intended coupled state-space model. Note that, other mechanical properties for both connecting elements substructures could be chosen, since the achievement of the intended coupled structure state-space model be guaranteed.

This procedure is, thus, composed by three steps. The first one is the definition of the real and connecting elements substructures, this procedure is schematically presented in figure 2.4. Secondly, perform the first coupling, which is a regular one (figure 2.5). Lastly, perform a negative coupling, in order to remove the influence of the inserted masses and the excess of damping and stiffness inserted by the first coupling (figure 2.6).

The regular state-space coupling should be performed as presented in sections 2.7 and 2.9. On other hand, the negative state-space coupling was not explored yet. In fact this coupling is similar and follows the same procedure of the regular one, the unique difference is that the state-space model which will be coupled should be defined in a negative way. The definition of a negative state-space model from a regular one is simple.

In order to illustrate this procedure, let assume that the states are related to degrees of freedom, thus the state-space matrices will be given by

$$\begin{gathered}[A] = \begin{bmatrix} 0 & I \\ -M^{-1}K & -M^{-1}V \end{bmatrix}, \quad [B] = \begin{bmatrix} 0 \\ M^{-1} \end{bmatrix} \\ [C] = [-M^{-1}K \quad -M^{-1}V], \quad [D] = \begin{bmatrix} M^{-1} \end{bmatrix}\end{gathered} \tag{2.93}$$

The definition of the negative state-space model is performed by multiply the mass, stiffness and damping matrices by -1, as follows

$$\begin{gathered}[A] = \begin{bmatrix} 0 & I \\ -(-M)^{-1}(-K) & -(-M)^{-1}(-V) \end{bmatrix}, \quad [B] = \begin{bmatrix} 0 \\ -M^{-1} \end{bmatrix} \\ [C] = [-(-M)^{-1}(-K) \quad -(-M)^{-1}(-V)], \quad [D] = \begin{bmatrix} -M^{-1} \end{bmatrix}\end{gathered} \tag{2.94}$$

Comparing the negative state-space model (equation (2.94)) and the regular one (equation (2.93)) it can be realized that the unique differences are in matrices $[B]$ and $[D]$, which in negative state-space model are multiplied by -1 [Scheel et al., 2019]. Even if, this was proved to theoretical state-space models, it continue to be true for state-space models defined in modal coordinates. The negative coupling is achieved by coupling the state-space model rewritten in a negative form using the exposed procedures.

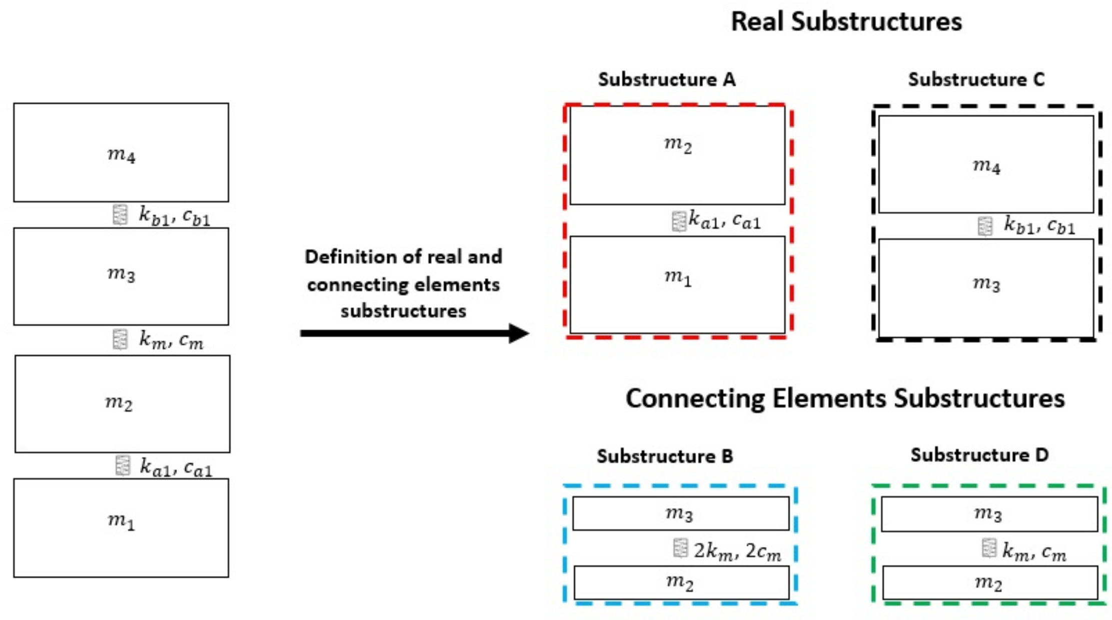

Figure 2.4: Coupling a positive and negative state-space model - substructures definition

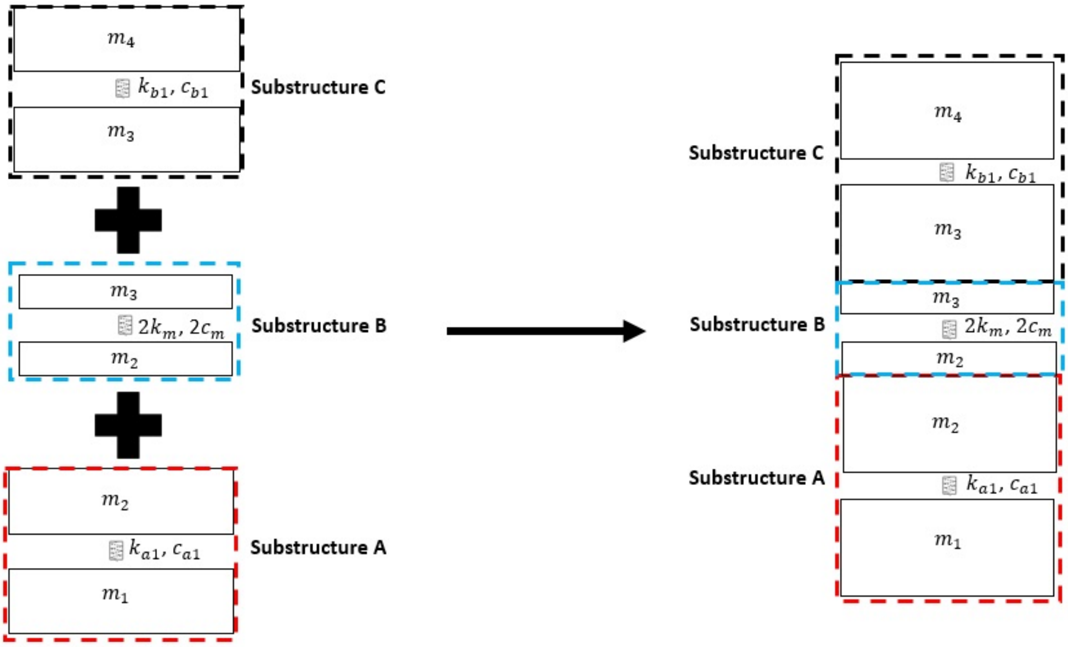

Figure 2.5: Coupling a positive and negative state-space model - first coupling

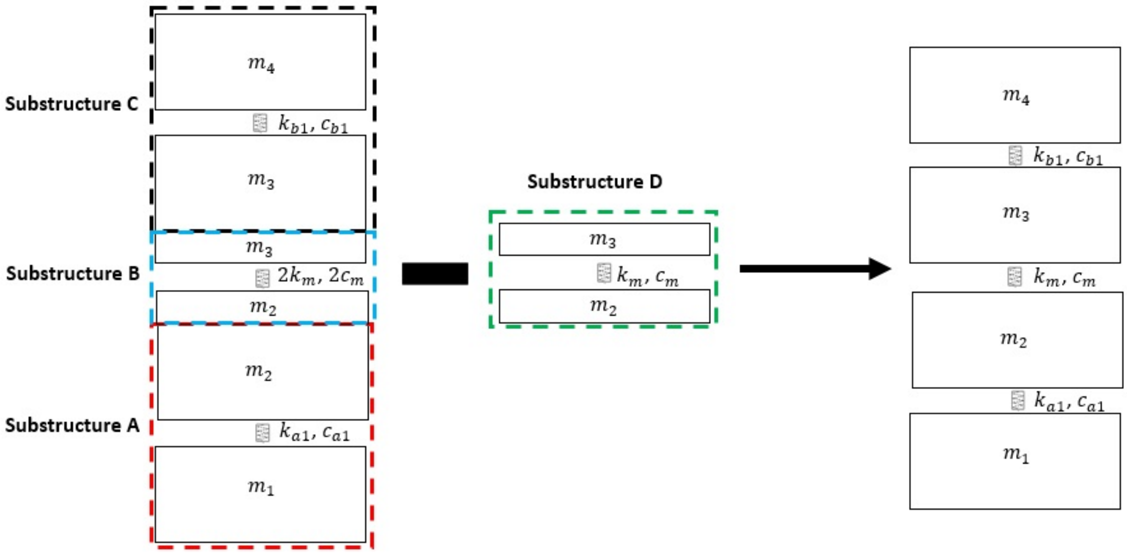

Figure 2.6: Coupling a positive and negative state-space model - second coupling

Chapter 3

Numerical Results

This chapter will be composed by two different sections. Firstly, a section where two mechanical systems will be divided in different substructures and then coupled by each of the presented state-space coupling methods (see section 2.7). This coupling will be performed with theoretical substructure state-space models (see section 2.2).

In the second section, two different mechanical systems will be divided in different substructures and then coupled. However, the coupling will be performed with state-space models expressed in modal coordinates (see section 2.9). These state-space models will be obtained in the following steps:

- Computation of the theoretical state-space models from the substructure mechanical properties;
- Achievement of accelerance FRFs from the computed state-space model;
- Modal parameters estimation from the computed accelerance FRFs by the use of the presented methods in section 2.8;
- Estimation of the state-space model expressed in modal coordinates from the estimated modal parameters.

The obtained coupled state-space models will be used to compute the coupled FRFs, which will be compared with the analytical ones, in order to evaluate the accuracy of both presented coupling methods.

3.1 Numerical Results - Coupling theoretical state-space models

3.1.1 Numerical example nº 1

The first mechanical system that will be analysed is presented at figure 3.1 and its mechanical properties are presented in table F.1.

To start, the mechanical properties matrices of each substructure and of the assembled structure should be obtained. In order to do that achievement the Lagrange equations will be applied for each part (substructures and assembled structure).

These Lagrange equations are deduced from the, well-known Hamilton Variational principle. The Lagrange equations are given by the mathematical expression (3.1) [Rodrigues, 2018].

$$\frac{d}{dt}\left(\frac{\partial T}{\partial \dot{q}_j}\right) - \left(\frac{\partial T}{\partial q_j}\right) + \left(\frac{\partial V}{\partial q_j}\right) = Q_j \qquad j = 1, ..., n \tag{3.1}$$

where,

- T is the kinetic energy;
- V is the potential elastic energy;
- q_j is the j^{th} degree of freedom (in this example $n = 2$ for each substructure and $n = 3$ for the assembled structure);
- Q_j are the generalized applied forces in the j^{th} degree of freedom;

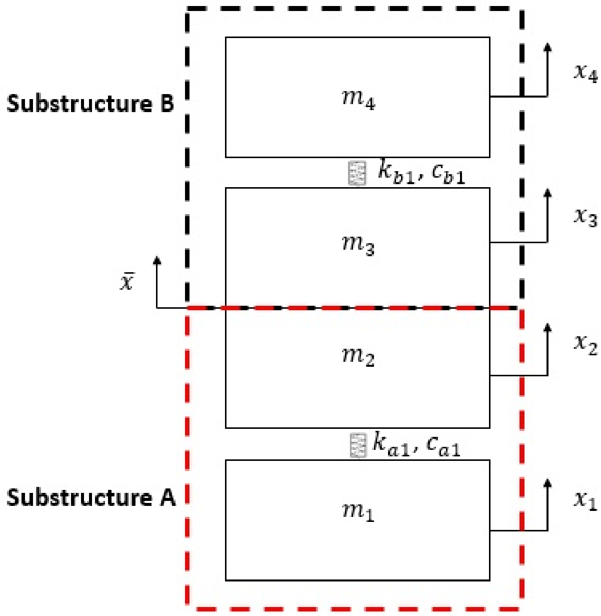

Figure 3.1: Mechanical System nº 1

The Lagrange equations permits the computation of stiffness, damping and mass matrices. Even though the equation (3.1) does not include the damping elements, a viscous dissipate Rayleigh function can be defined in order to include viscous damping generalized forces in the presented Lagrange formulation [Rodrigues, 2018]. However, for simplicity, in this and in the following analysed mechanical systems the damping matrix will be considered equal to the stiffness matrix, but instead of stiff therms it will contain damping ones.

In order to exemplify the achievement of stiffness, damping and mass matrices the Lagrange equations will be applied to the substructure A. This procedure was used to find out all mechanical properties matrices for all of analysed mechanical systems (substructures and assembled structures). However, in this dissertation it will just be presented this procedure for the achievement of the substructure A mechanical properties (see figure 3.1).

To start, the kinetic energy is given as follows

$$T = \frac{1}{2}m_1(\dot{x}_1(t))^2 + \frac{1}{2}m_2(\dot{x}_2(t))^2 \tag{3.2}$$

The potential energy is given by

$$V = \frac{1}{2}k_{a1}(x_1 - x_2)^2 = \frac{1}{2}k_{a1}(x_1^2 - 2x_1x_2 + x_2^2) \tag{3.3}$$

Calculating the derivatives presented in equation (3.1) for each degree of freedom

$$\begin{aligned}
\frac{d}{dt}\left(\frac{\partial T}{\partial \dot{q}_1}\right) &= \frac{d}{dt}\left(2 \times \frac{1}{2}m_1\dot{x}_1(t)\right) = m_1\ddot{x}_1(t)\\
\frac{d}{dt}\left(\frac{\partial T}{\partial \dot{q}_2}\right) &= \frac{d}{dt}\left(2 \times \frac{1}{2}m_2\dot{x}_2(t)\right) = m_2\ddot{x}_2(t)\\
\left(\frac{\partial T}{\partial q_1}\right) &= 0\\
\left(\frac{\partial T}{\partial q_2}\right) &= 0\\
\left(\frac{\partial V}{\partial q_1}\right) &= \frac{1}{2}k_{a1}(2x_1(t) - 2x_2(t)) = k_{a1}(x_1(t) - x_2(t))\\
\left(\frac{\partial V}{\partial q_2}\right) &= \frac{1}{2}k_{a1}(-2x_1(t) + 2x_2(t)) = k_{a1}(-x_1(t) + x_2(t))
\end{aligned} \tag{3.4}$$

By the use of equation (3.1), the Newtonian differential equations of motion of substructure A will be obtained in a matrix form. In fact, the presented equation (3.1) is just valid for non damped systems, thus it is not possible to obtain the system damping matrix. However, remember that for simplicity it will be supposed that the damping matrix is given by the stiffness matrix, but replacing stiff therms by damping ones. Therefore, the following Newtonian differential equations in matrix form are obtained

$$\begin{bmatrix} m_1 & 0 \\ 0 & m_2 \end{bmatrix}\begin{bmatrix} \ddot{x}_1(t) \\ \ddot{x}_2(t) \end{bmatrix} + \begin{bmatrix} k_{a1} & -k_{a1} \\ -k_{a1} & k_{a1} \end{bmatrix}\begin{bmatrix} x_1(t) \\ x_2(t) \end{bmatrix} + \begin{bmatrix} c_{a1} & -c_{a1} \\ -c_{a1} & c_{a1} \end{bmatrix}\begin{bmatrix} \dot{x}_1(t) \\ \dot{x}_2(t) \end{bmatrix} = \begin{bmatrix} Q_1(t) \\ Q_2(t) \end{bmatrix} \tag{3.5}$$

From the system of differential equations (3.5) the stiffness, damping and mass matrices can be identified as follows

$$[M] = \begin{bmatrix} m_1 & 0 \\ 0 & m_2 \end{bmatrix}, \quad [K] = \begin{bmatrix} k_{a1} & -k_{a1} \\ -k_{a1} & k_{a1} \end{bmatrix}, \quad [V] = \begin{bmatrix} c_{a1} & -c_{a1} \\ -c_{a1} & c_{a1} \end{bmatrix} \tag{3.6}$$

From the identification of these matrices, it is possible the computation of the substructure A state-space model. This procedure should be repeated for the substructure B and also for the assembled structure. The achievement of this state-space models was performed by a $MATLAB^{®}$ script (provided by Siemens Software Industry NV) in accordance with the presented procedure at section 2.2.

After the computation of the coupled structure state-space model, the coupled FRFs should be computed, in order to be a reference to evaluate the accuracy of both presented state-space coupling methods (see section 2.7). These FRFs computation were performed in accordance with the procedure presented at section 2.3, by the use of the $MATLAB^{®}$ function $freqresp$. However, in order to compute the assembled structure FRFs a more classical approach could be used with same accuracy. In fact, the receptance FRFs are the inverse of the dynamic stiffness matrix. This matrix is given as follows[Rodrigues, 2019]

$$[Z] = [[K] - \omega^2[M] + j\omega[V]] \tag{3.7}$$

Thus, the frequency response function receptance matrix $[\alpha]$ will be given as follows

$$[\alpha(j\omega)] = [Z]^{-1} = [[K] - \omega^2[M] + j\omega[V]]^{-1} \tag{3.8}$$

In numerical applications the inversion of matrices are the lowest efficient calculations and as it can be observed in section (3.8) it will be needed one inversion for each frequency for which the receptance FRFs are wanted to be known. Therefore, it should be preferable to solve it as a system of equations.

After the achievement of the receptance FRF the achievement of the accelerance FRF is simple. Remember that, the frequency response function receptance (FRF), $\alpha_{ij}(\omega)$ is given by the response (displacement) phasor in the degree of freedom i caused by the application of an harmonic force, which amplitude is unitary, in the degree of freedom j. The FRF accelerance has a similar definition. However, instead of be calculated by the displacement phasor response it is calculated with the acceleration phasor response. Therefore, the displacement phasor should be derived twice in frequency domain to obtain the acceleration phasor. Thus, the accelerance FRF must be computed as follows

$$[A(j\omega)] = \frac{\{\bar{A}(j\omega)\}}{\{F\}} = -\frac{\omega^2\{\bar{X}(j\omega)\}}{\{F\}} = -\omega^2[\alpha(j\omega)] \tag{3.9}$$

where $[A(j\omega)]$ is the matrix of accelerance FRFs, the $\{\bar{X}(j\omega)\}$ is the displacement response phasor vector and $\{\bar{A}(j\omega)\}$ is the acceleration response phasor vector.

After the computation of the analytical assembled structure FRFs, it is time to apply the two discussed state-space coupling methods. To start, the method proposed by Su and Juang [Su and Juang, 1994] will be used (see section 2.7.1).

The first step is the achievement of the uncoupled diagonal state-space model, as presented in equation (2.48). The second step, after obtaining the uncoupled diagonal state-space model is the achievement of the transformation matrix $[T]$. In fact, this step has been already done in section 2.7.1, resuming the transformation matrix $[T]$ from equation (2.47)

$$[T] = [1 \quad 1] \tag{3.10}$$

The third step is the achievement of the state-space model for the coupled structure as presented in expression (2.57). The fourth step is the state and input vector rearrangement. Starting for the coupled state vector, which is organized as follows

$$\{\bar{x}\} = \begin{bmatrix} x_1 \\ x_2 \\ \dot{x}_1 \\ \dot{x}_2 \\ x_3 \\ x_4 \\ \dot{x}_3 \\ \dot{x}_4 \end{bmatrix} \tag{3.11}$$

Note that, top bar variables are related to coupled variables. Remember that the coupled state vector is firstly composed by the states related to the first substructure (in this case substructure A) and after the states related to the second substructure (in this case substructure B). The usual form for the coupled state vector of this mechanical system would be the following

$$\{\bar{x}\} = \begin{bmatrix} x_1 \\ x_2 \\ x_3 \\ x_4 \\ \dot{x}_1 \\ \dot{x}_2 \\ \dot{x}_3 \\ \dot{x}_4 \end{bmatrix} \tag{3.12}$$

Thus, the rearrangement of the coupled state vector should be done. So that, the rows and columns of $[\bar{A}]$ matrix has to be rearranged in accordance with the state vector rearrangement, as well the rows of the matrix $[\bar{B}]$.

In its turn, the input coupled vector is organized as follows

$$\{\bar{u}\} = \begin{bmatrix} u_1 \\ u_4 \\ \bar{u} \end{bmatrix} \tag{3.13}$$

Remember that because of the equilibrium equation the $[\bar{B}]$ matrix columns are obtained in a minimal-order form, thus no redundant variables are present (that is why the input vector is just composed by three inputs). Remember also, that this vector is firstly composed by the inputs related to internal degrees of freedom and after by the related to the interface ones. The usual form for the coupled input vector of this mechanical system would be the following

$$\{\bar{u}\} = \begin{bmatrix} u_1 \\ \bar{u} \\ u_4 \end{bmatrix} \tag{3.14}$$

Thus, the columns of matrix $[\bar{B}]$ should be rearranged in accordance with the rearrangement of the input vector.

The last step is the elimination of the auxiliary states presented in the coupled state vector. As it can be observed on figure 3.1 and by the compatibility conditions the DOFs x_2 and x_3 are in fact the same DOF, thus $x_2 = x_3 = \bar{x}$ and $\dot{x}_2 = \dot{x}_3 = \dot{\bar{x}}$. Remember the equation (2.2), where it can be seen that each line of the matrix $[\bar{A}]$ is going to be multiplied by the state vector $\{x\}$. So that and because of $x_2 = x_3 = \bar{x}$ and $\dot{x}_2 = \dot{x}_3 = \dot{\bar{x}}$ the columns of matrix $[\bar{A}]$ related to x_2 and x_3, and the columns related to $\dot{x}_2$ and $\dot{x}_3$ has to be summed.

Therefore, in this example the columns 2 and 3, and columns 6 and 7 of the matrix $[\bar{A}]$ has to be summed. After this procedure the 2^{nd} row and 2^{nd} column or the 3^{rd} row and 3^{rd} column should be eliminated in order to achieve a minimal-order coupled state-space model. As well, the 6^{th} or 7^{th} row and respective columns, for the velocity states. The minimal-order coupled state vector will be

$$\{\bar{x}\} = \begin{bmatrix} x_1 \\ \bar{x} \\ x_4 \\ \dot{x}_1 \\ \dot{\bar{x}} \\ \dot{x}_4 \end{bmatrix} \tag{3.15}$$

The $[\bar{B}]$ matrix rows are not obtained in a minimal order form. Thus, just the elimination of rows should be computed in accordance with the elimination of $[\bar{A}]$ rows.

The steps for achieve minimal-order coupled matrices $[\bar{A}]$ and $[\bar{B}]$ are full explained. However the $[\bar{C}]$ and $[\bar{D}]$ are still missing. If the consider output is acceleration, which usually is in mechanical experiments, the minimal order output vector will be

$$\{\ddot{y}\} = \begin{bmatrix} \ddot{y}_1 \\ \ddot{y} \\ \ddot{y}_4 \end{bmatrix} \tag{3.16}$$

Obviously, for theoretical state-space models

$$\ddot{y}_i = \ddot{x}_i \quad i = 1, 2, 4 \tag{3.17}$$

Thus, the $[\bar{C}]$ and $[\bar{D}]$ are included in matrices $[\bar{A}]$ and $[\bar{B}]$, respectively. The matrix $[\bar{C}]$ will be equal to the last three rows of the matrix $[\bar{A}]$, while matrix $[\bar{D}]$ will be equal to the last three rows of the matrix $[\bar{B}]$.

After the achievement of the coupled state-space model by the method proposed by Su and Juang [Su and Juang, 1994], it is the moment to achieve the same model by the use of the technique proposed by Sjövall [Sjövall, 2004] (see section 2.7.2).

Resuming the coupling form of the substructure state-space model (2.71) and applying to the substructure A of this numerical example

$$\begin{bmatrix} \dot{y}_2 \\ \ddot{y}_2 \\ \dot{x}_1 \\ \ddot{x}_1 \end{bmatrix} = \begin{bmatrix} 0 & I & 0 \\ A^A_{vd} & A^A_{vv} & A^A_{vb} \\ A^A_{bd} & A^A_{bv} & A^A_{bb} \end{bmatrix} \begin{bmatrix} y_2 \\ \dot{y}_2 \\ x_1 \\ \dot{x}_1 \end{bmatrix} + \begin{bmatrix} 0 & 0 \\ B^A_{vv} & 0 \\ 0 & 0 \\ 0 & B^A_{bb} \end{bmatrix} \begin{bmatrix} u_2 \\ u_1 \end{bmatrix} \tag{3.18}$$

Note that here, the states related to the internal DOFs are explicitly presented (see section 2.7.2). This justifies the appearance of another column related to the uncoupled input for the matrix $[\widetilde{B}^A]$, since by the second law of Newton the force directly contributes for the acceleration (see equation (2.76)). The same is valid for the presented coupling form of the substructure B state-space model. This also justifies the appearance of two new columns related to the uncoupled inputs of each substructures, A and B, for the $[\widetilde{B}]$ of the coupling form of the coupled state-space model. From now and until the end of the resolution of this numerical coupling, superscript A and B are used for variables related to the substructure state-space models, A and B, respectively. Over tilde variables are variables associated to the coupling form of state-space models.

The unique degrees of freedom which are taking in account to achieve the coupled row are the interface DOFs of each substructure which are going to be coupled and the internal ones which are, directly, related to the referred interface DOFs. Thus, for the substructure A the coupling form of the state vector is given as follows

$$\{x^A\} = \begin{bmatrix} y_2 \\ \dot{y}_2 \\ x_1 \\ \dot{x}_1 \end{bmatrix} \tag{3.19}$$

The state-space model of the substructure A can be expressed as follows

$$\begin{bmatrix} \dot{x}_1 \\ \dot{x}_2 \\ \ddot{x}_1 \\ \ddot{x}_2 \end{bmatrix} = \begin{bmatrix} A^A_{11} & A^A_{12} & A^A_{13} & A^A_{14} \\ A^A_{21} & A^A_{22} & A^A_{23} & A^A_{24} \\ A^A_{31} & A^A_{32} & A^A_{33} & A^A_{34} \\ A^A_{41} & A^A_{42} & A^A_{43} & A^A_{44} \end{bmatrix} \begin{bmatrix} x_1 \\ x_2 \\ \dot{x}_1 \\ \dot{x}_2 \end{bmatrix} + \begin{bmatrix} B^A_{11} & B^A_{12} \\ B^A_{21} & B^A_{22} \\ B^A_{31} & B^A_{32} \\ B^A_{41} & B^A_{42} \end{bmatrix} \begin{bmatrix} u_1 \\ u_2 \end{bmatrix} \tag{3.20}$$

Therefore, from the substructure A state-space model (see equation (3.20)) it is possible to obtain the terms presented in the coupling form of the substructure A state-space model (see equation (3.18))

$$\begin{aligned} A^A_{vd} &= A^A_{42} \\ A^A_{vv} &= A^A_{44} \\ A^A_{vb} &= \begin{bmatrix} A^A_{41} & A^A_{43} \end{bmatrix} \\ A^A_{bd} &= \begin{bmatrix} A^A_{12} \\ A^A_{32} \end{bmatrix} \\ A^A_{bv} &= \begin{bmatrix} A^A_{14} \\ A^A_{34} \end{bmatrix} \\ A^A_{bb} &= \begin{bmatrix} A^A_{11} & A^A_{13} \\ A^A_{31} & A^A_{33} \end{bmatrix} \\ B^A_{vv} &= B^A_{42} \\ B^A_{bb} &= B^A_{31} \end{aligned} \tag{3.21}$$

Taking the same approach to compute the coupling form of the substructure B state-space model. The state-space model of the substructure B can be expressed as follows

$$\begin{bmatrix} \dot{x}_3 \\ \dot{x}_4 \\ \ddot{x}_3 \\ \ddot{x}_4 \end{bmatrix} = \begin{bmatrix} A^B_{11} & A^B_{12} & A^B_{13} & A^B_{14} \\ A^B_{21} & A^B_{22} & A^B_{23} & A^B_{24} \\ A^B_{31} & A^B_{32} & A^B_{33} & A^B_{34} \\ A^B_{41} & A^B_{42} & A^B_{43} & A^B_{44} \end{bmatrix} \begin{bmatrix} x_3 \\ x_4 \\ \dot{x}_3 \\ \dot{x}_4 \end{bmatrix} + \begin{bmatrix} B^B_{11} & B^B_{12} \\ B^B_{21} & B^B_{22} \\ B^B_{31} & B^B_{32} \\ B^B_{41} & B^B_{42} \end{bmatrix} \begin{bmatrix} u_3 \\ u_4 \end{bmatrix} \tag{3.22}$$

The coupling form of the substructure B state-space model is given as follows

$$\begin{bmatrix} \dot{y}_3 \\ \ddot{y}_3 \\ \dot{x}_4 \\ \ddot{x}_4 \end{bmatrix} = \begin{bmatrix} 0 & I & 0 \\ A^B_{vd} & A^B_{vv} & A^B_{vb} \\ A^B_{bd} & A^B_{bv} & A^B_{bb} \end{bmatrix} \begin{bmatrix} y_3 \\ \dot{y}_3 \\ x_4 \\ \dot{x}_4 \end{bmatrix} + \begin{bmatrix} 0 & 0 \\ B^B_{vv} & 0 \\ 0 & 0 \\ 0 & B^B_{bb} \end{bmatrix} \begin{bmatrix} u_3 \\ u_4 \end{bmatrix} \tag{3.23}$$

Therefore, from the substructure B state-space model (see equation (3.22)) it is possible to obtain the terms presented in the coupling form of the substructure B state-space model (see equation (3.23))

$$
\begin{aligned}
A^B_{vd} &= A^B_{31} \\
A^B_{vv} &= A^B_{33} \\
A^B_{vb} &= \begin{bmatrix} A^B_{32} & A^B_{34} \end{bmatrix} \\
A^B_{bd} &= \begin{bmatrix} A^B_{21} \\ B^B_{41} \end{bmatrix} \\
A^B_{bv} &= \begin{bmatrix} A^B_{23} \\ A^B_{43} \end{bmatrix} \\
A^B_{bb} &= \begin{bmatrix} A^B_{22} & A^B_{24} \\ A^B_{42} & A^B_{44} \end{bmatrix} \\
B^B_{vv} &= B^B_{31} \\
B^B_{bb} &= B^B_{42}
\end{aligned}
\tag{3.24}
$$

At this moment it is possible, to obtain the coupling form of the structure state-space model. Resuming the presented coupling form of the coupled state-space model 2.7.2

$$
\begin{bmatrix} \dot{\bar{y}} \\ \ddot{\bar{y}} \\ \dot{x}_1 \\ \ddot{x}_1 \\ \dot{x}_4 \\ \ddot{x}_4 \end{bmatrix} = \begin{bmatrix} 0 & I & 0 & 0 \\ \bar{A}_{vd} & \bar{A}_{vv} & \bar{A}^A_{vb} & \bar{A}^B_{vb} \\ \bar{A}^A_{bd} & \bar{A}^A_{bv} & A^A_{bb} & 0 \\ \bar{A}^B_{bd} & \bar{A}^B_{bv} & 0 & A^B_{bb} \end{bmatrix} \begin{bmatrix} \bar{x} \\ \dot{\bar{x}} \\ x_1 \\ \dot{x}_1 \\ x_4 \\ \dot{x}_4 \end{bmatrix} + \begin{bmatrix} 0 & 0 & 0 \\ \bar{B}_{vv} & 0 & 0 \\ 0 & 0 & 0 \\ 0 & B^A_{bb} & 0 \\ 0 & 0 & 0 \\ 0 & 0 & B^B_{bb} \end{bmatrix} \begin{bmatrix} \bar{u} \\ u_1 \\ u_4 \end{bmatrix}
\tag{3.25}
$$

where,

$$
\begin{aligned}
\bar{B}_{vv} &= ((B^A_{vv})^{-1} + (B^B_{vv})^{-1})^{-1} \\
\bar{A}_{vd} &= \bar{B}_{vv}((B^A_{vv})^{-1}A^A_{vd} + (B^B_{vv})^{-1}A^B_{vd})^{-1} \\
\bar{A}_{vv} &= \bar{B}_{vv}((B^A_{vv})^{-1}A^A_{vv} + (B^B_{vv})^{-1}A^B_{vv})^{-1} \\
\bar{A}^A_{vb} &= \bar{B}_{vv}(B^A_{vv})^{-1}A^A_{vd} = \bar{B}_{vv}(B^A_{vv})^{-1}\begin{bmatrix} A^A_{41} & A^A_{43} \end{bmatrix} \\
\bar{A}^B_{vb} &= \bar{B}_{vv}(B^B_{vv})^{-1}A^B_{vd} = \bar{B}_{vv}(B^B_{vv})^{-1}\begin{bmatrix} A^B_{32} & A^B_{34} \end{bmatrix}
\end{aligned}
\tag{3.26}
$$

It can be observed that all variables of the coupling form of the coupled state-space model can be computed from the variables of the coupling form of the substructure state-space models.

The variables $\{\bar{A}^A_{vb}\}$ and $\{\bar{A}^B_{vb}\}$ are vector variables, each of its therms will be named as follows

$$
\begin{aligned}
\bar{A}^{A1}_{vb} &= \bar{B}_{vv}(B^A_{vv})^{-1}A^A_{41} \\
\bar{A}^{A2}_{vb} &= \bar{B}_{vv}(B^A_{vv})^{-1}A^A_{43} \\
\bar{A}^{B1}_{vb} &= \bar{B}_{vv}(B^B_{vv})^{-1}A^B_{32} \\
\bar{A}^{B2}_{vb} &= \bar{B}_{vv}(B^B_{vv})^{-1}A^B_{34}
\end{aligned}
\tag{3.27}
$$

After the achievement of the coupling form of the assembled structure state-space model the regular form of this state-space model can be obtained. This model is achieved by the insertion of each uncoupled rows related to internal DOFs and the coupled rows from the coupling form of the coupled state-space model. Thus, several vectors rearrangement will be needed.

The usual state vector of the coupled state-space model is given as follows

$$\{\bar{x}\} = \begin{bmatrix} x_1 \\ \bar{x} \\ x_4 \\ \dot{x}_1 \\ \dot{\bar{x}} \\ \dot{x}_4 \end{bmatrix} \tag{3.28}$$

For each substructure state-space models the state vector is following presented

$$\{x^A\} = \begin{bmatrix} x_1 \\ x_2 \\ \dot{x}_1 \\ \dot{x}_2 \end{bmatrix}, \quad \{x^B\} = \begin{bmatrix} x_3 \\ x_4 \\ \dot{x}_3 \\ \dot{x}_4 \end{bmatrix} \tag{3.29}$$

The state vector for the coupled row is the following

$$\{\widetilde{x}\} = \begin{bmatrix} \bar{x} \\ \dot{\bar{x}} \\ x_1 \\ \dot{x}_1 \\ x_4 \\ \dot{x}_4 \end{bmatrix} \tag{3.30}$$

Starting for the computation of the $[\bar{A}]$ matrix. Since this matrix will be composed by uncoupled rows taken from each of substructure state-space models and for the coupled row taken from the coupling form of the coupled state-space model, several rearrangements will be needed. Observing the expressions (3.29) and (3.30), three different rearrangements will be needed, one for each of the substructure state-space model uncoupled row and for the coupled row of the coupling form of the coupled state-space model. Note that, both substructures just has four states and the intended one has six states. Therefore, two null coefficients must be added to the uncoupled row of each substructure.

The coupled matrix $[\bar{B}]$ is composed by the uncoupled rows of each substructures state-space model (expressions (3.20) and (3.22)) and by the coupled rows taken from the coupling form of the coupled state-space model (expression (3.25)). However, the columns must be rearranged in accordance with input vector.

The coupled input vector will be given by

$$\{\bar{u}\} = \begin{bmatrix} u_1 \\ \bar{u} \\ u_4 \end{bmatrix} \tag{3.31}$$

The input vector of each substructure is given as follows

$$\{u^A\} = \begin{bmatrix} u_1 \\ u_2 \end{bmatrix}, \quad \{u^B\} = \begin{bmatrix} u_3 \\ u_4 \end{bmatrix} \tag{3.32}$$

The input vector of the coupling form of the coupled state-space model is given as follows

$$\{\widetilde{u}\} = \begin{bmatrix} \bar{u} \\ u_1 \\ u_4 \end{bmatrix} \tag{3.33}$$

Observing the expressions (3.32) and (3.33), 3 different rearrangements will be needed, one for each of the state-space models uncoupled row and another for the coupled row taken from the coupling form of the coupled state-space model. After the computation of matrices $[\bar{A}]$ and $[\bar{B}]$ the first block row of the coupled state-space model is given as follows

$$\begin{bmatrix} \dot{x}_1 \\ \dot{\bar{x}} \\ \dot{x}_4 \\ \ddot{x}_1 \\ \ddot{\bar{x}} \\ \ddot{x}_4 \end{bmatrix} = \begin{bmatrix} 0 & 0 & 0 & 1 & 0 & 0 \\ 0 & 0 & 0 & 0 & 1 & 0 \\ 0 & 0 & 0 & 0 & 0 & 1 \\ A^A_{31} & A^A_{32} & 0 & A^A_{33} & A^A_{34} & 0 \\ A^{A1}_{vb} & \bar{A}_{vd} & A^{B1}_{vb} & A^{A2}_{vb} & \bar{A}_{vv} & A^{B2}_{vb} \\ 0 & A^B_{41} & A^B_{42} & 0 & A^B_{43} & A^B_{44} \end{bmatrix} \begin{bmatrix} x_1 \\ \bar{x} \\ x_4 \\ \dot{x}_1 \\ \dot{\bar{x}} \\ \dot{x}_4 \end{bmatrix} + \begin{bmatrix} 0 & 0 & 0 \\ 0 & 0 & 0 \\ 0 & 0 & 0 \\ B^A_{vv} & 0 & 0 \\ 0 & \bar{B}_{vv} & 0 \\ 0 & 0 & B^B_{vv} \end{bmatrix} \begin{bmatrix} u_1 \\ \bar{u} \\ u_4 \end{bmatrix} \tag{3.34}$$

Again, the matrix $[\bar{C}]$ will be equal to the last 3 rows of the matrix $[\bar{A}]$, while matrix $[\bar{D}]$ will be equal to the last 3 rows of the matrix $[\bar{B}]$.

The FRFs obtained from both of coupled state-space models deduced by the two methods were computed and compared with the analytical FRFs. It was observed a perfect fit between the three solutions for all of the FRFs. In figure 3.2 are represented 3 different curves, representative of the assembled structure FRF considering as output the DOF related to mass m_4 and as input the coupled DOF related to the sum of the masses m_2 and m_3 (y_4 and $\bar{u}$). The black curve represents the analytical accelerance FRF, the blue curve represents the same accelerance FRF computed from the coupled state-space model obtained with the method proposed by Su and Juang [Su and Juang, 1994] and the red curve represents the same FRF computed from the coupled state-space model obtained with the method proposed by Sjövall [Sjövall, 2004].

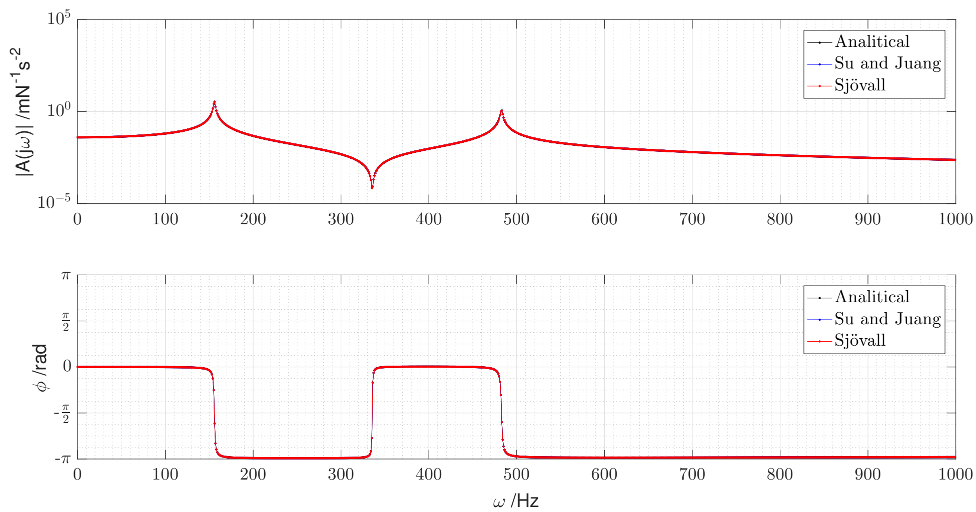

Figure 3.2: Mechanical System nº 1: Accelerance FRF considering as output the DOF related to the mass m_4 and as input the coupled DOF

3.1.2 Numerical example nº 2

The mechanical system which will be analyzed in this numerical example is composed by seven degrees of freedom, which are connected by soft connections. In order to show the applicability of both coupling analysed methods, this system is going to be divided in five different substructures as presented in figure 3.3.

This problem will be coupled by introducing small fictitious masses in the connections between the degrees of freedoms (see section 2.10.2). The resulting system after these masses insertion, can be observed in figure 3.4. The mechanical properties are given in table F.2.

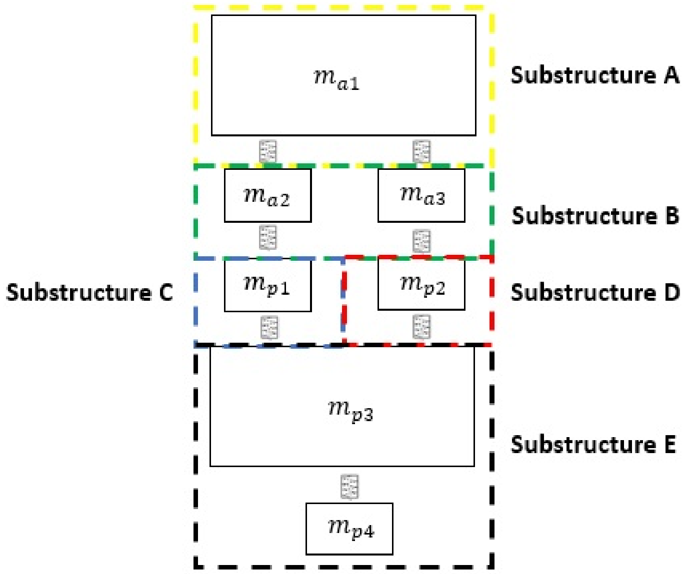

Figure 3.3: Mechanical System nº 2

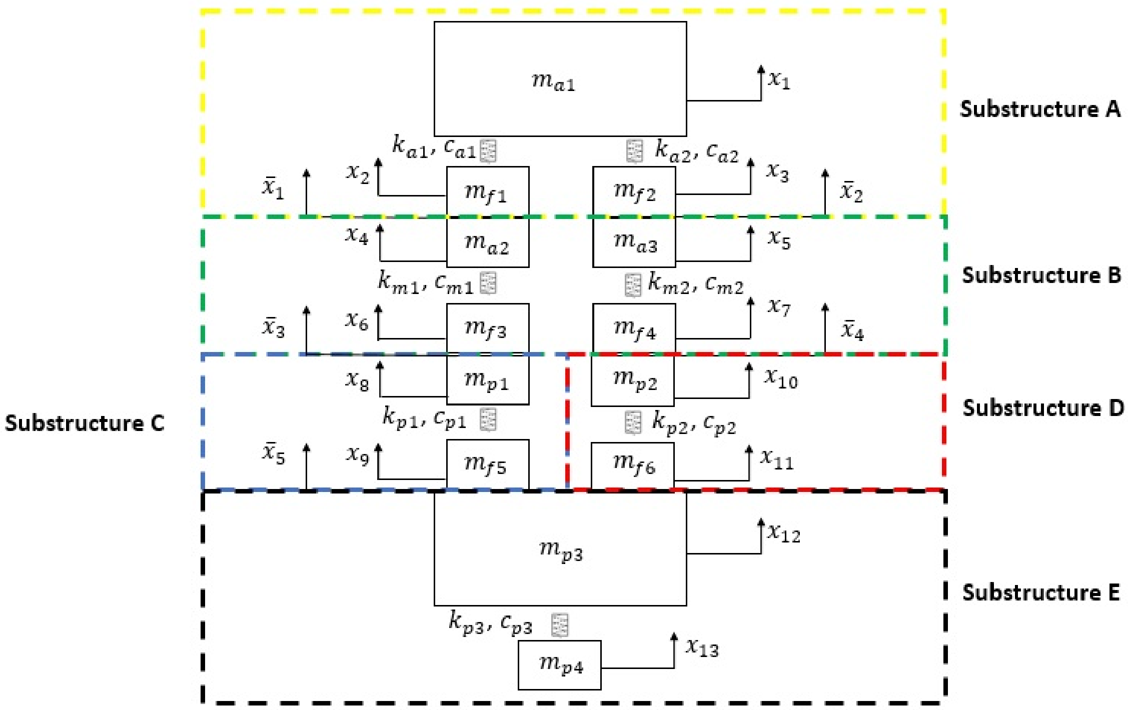

Figure 3.4: Mechanical System nº 2: after fictitious masses insertion

Due this mechanical system complexity all the steps to couple it will be analysed. This example is going to be solved just by the method proposed by Su and Juang [Su and Juang, 1994], because of the connection between the substructures C, D and E. Remember that, the approach suggested by Sjövall [Sjövall, 2004] is not able to deal with matching DOFs related to more than 2 different substructures (see section 2.7.2). Thus, this example emphases a disadvantage of this method.

The first step in order to perform coupling will be the $[T]$ matrix construction, which for this example could be not clear. Remembering the compatibility and equilibrium conditions, expressions (2.43) and (2.44), and by remembering the mathematical expressions (2.45) and (2.46) the matrix $[T]$ can be computed in the following steps.

Firstly, it has to be identified the matching DOFs, in this case it will be x_2 and x_4, x_3 and x_5, x_6 and x_8, x_7 and x_{10} and x_9, x_{11} and x_{12}. A first sketch of the $[T]$ matrix can be computed. Before this construction, the reader should understand that the $[T]$ matrix has the function of enforcing the compatibility and equilibrium condition. Therefore, it is only related to the matching DOFs. After the introduction of the fictitious masses the mechanical system has 13 DOFs, from which 11 are interface ones. Thus, a first sketch of this transformation matrix will be a square matrix with 11 rows and 11 columns (see table 3.1).

Table 3.1: Mechanical System nº 2 - $[T]$ matrix sketch

x_2	x_3	x_4	x_5	x_6	x_7	x_8	x_9	x_{10}	x_{11}	x_{12}	
1	0	1	0	0	0	0	0	0	0	0	$\bar{x}_1$
0	1	0	1	0	0	0	0	0	0	0	$\bar{x}_2$
1	0	1	0	0	0	0	0	0	0	0	$\bar{x}_1$
0	1	0	1	0	0	0	0	0	0	0	$\bar{x}_2$
0	0	0	0	1	0	1	0	0	0	0	$\bar{x}_3$
0	0	0	0	0	1	0	0	1	0	0	$\bar{x}_4$
0	0	0	0	1	0	1	0	0	0	0	$\bar{x}_3$
0	0	0	0	0	0	0	1	0	1	1	$\bar{x}_5$
0	0	0	0	0	1	0	0	1	0	0	$\bar{x}_4$
0	0	0	0	0	0	0	1	0	1	1	$\bar{x}_5$
0	0	0	0	0	0	0	1	0	1	1	$\bar{x}_5$

Analysing the obtained $[T]$ matrix sketch, it can be realised that rows related to matching DOFs are equals as it obviously has to be. However, this matrix is not the final $[T]$ matrix. Remember that the transformation matrix $[T]$ should has a number of columns equal to the number of matching DOFs and a number of rows equal to the number of coupled DOFs, which are going to be present in the coupled structure state-space model (see section 2.7.1). Thus, it is time to select just one row related to each matching DOFs.

The chosen rows were the ones related to the following states x_2, x_3, x_6, x_7 and x_{12}. However, another choice could be made and the same result would be achieved. The final transformation $[T]$ matrix is presented in table 3.2.

It is of interest to observe the last row of the $[T]$ matrix, where it can be observed that this row has three coefficients which value is 1, while the other ones just has two. This is the reason why Sjövall approach [Sjövall, 2004] is not able to deal with this problem. The last row of $[T]$ matrix enforces compatibility and equilibrium equations between three DOFs related to three different structures. In fact, Sjövall method [Sjövall, 2004] cannot enforce coupling between DOFs that are shared by more than two substructures.

Table 3.2: Mechanical System nº 2 - $[T]$ matrix

x_2	x_3	x_4	x_5	x_6	x_7	x_8	x_9	x_{10}	x_{11}	x_{12}	
1	0	1	0	0	0	0	0	0	0	0	$\bar{x}_1$
0	1	0	1	0	0	0	0	0	0	0	$\bar{x}_2$
0	0	0	0	1	0	1	0	0	0	0	$\bar{x}_3$
0	0	0	0	0	1	0	0	1	0	0	$\bar{x}_4$
0	0	0	0	0	0	0	1	0	1	1	$\bar{x}_5$

Returning to the numerical example resolution by the technique proposed by Su and Juang [Su and Juang, 1994]. The following step is the computation of the uncoupled diagonal state-space model (see expression (2.48)). The next step is the achievement of the coupled state-space model as presented in expression (2.57).

Lastly, it is missing the state and input vectors rearrangement, and also the elimination of the redundant states. The obtained state vector and the intended one are following presented

$$\{\bar{x}_{obt}\} = \begin{bmatrix} x^A \\ \dot{x}^A \\ x^B \\ \dot{x}^B \\ x^C \\ \dot{x}^C \\ x^D \\ \dot{x}^D \\ x^E \\ \dot{x}^E \end{bmatrix}, \quad \{\bar{x}_{int}\} = \begin{bmatrix} x^A \\ x^B \\ x^C \\ x^D \\ x^E \\ \dot{x}^A \\ \dot{x}^B \\ \dot{x}^C \\ \dot{x}^D \\ \dot{x}^E \end{bmatrix} \tag{3.35}$$

where,

$$\{x^A\} = \begin{bmatrix} x_1 \\ x_2 \\ x_3 \end{bmatrix}, \quad \{x^B\} = \begin{bmatrix} x_4 \\ x_5 \\ x_6 \\ x_7 \end{bmatrix}, \quad \{x^C\} = \begin{bmatrix} x_8 \\ x_9 \end{bmatrix}, \quad \{x^D\} = \begin{bmatrix} x_{10} \\ x_{11} \end{bmatrix}, \quad \{x^E\} = \begin{bmatrix} x_{12} \\ x_{13} \end{bmatrix} \tag{3.36}$$

Note that, superscripts A, B, C, D and E are related to the different substructures that compose the structure under analysis (see figure 3.4). The obtained and the intended input vector are following presented

$$\{\bar{u}_{obt}\} = \begin{bmatrix} u_1 \\ u_{13} \\ \bar{u}_1 \\ \bar{u}_2 \\ \bar{u}_3 \\ \bar{u}_4 \\ \bar{u}_5 \end{bmatrix}, \quad \{\bar{u}_{int}\} = \begin{bmatrix} u_1 \\ \bar{u}_1 \\ \bar{u}_2 \\ \bar{u}_3 \\ \bar{u}_4 \\ \bar{u}_5 \\ u_{13} \end{bmatrix} \tag{3.37}$$

Note that, subscript *obt* is related to the obtained vector arrangement, while subscript *int* is related to the intended vector arrangement.

Remember that the $[\bar{A}]$ rows and columns, as well $[\bar{B}]$ rows should be rearranged in accordance with the state vector rearrangement. However, $[\bar{B}]$ columns should be rearranged in accordance with input vector rearrangement (see equation (2.2)).

Lastly, it is needed to perform the sum of the $[\bar{A}]$ matrix columns related to the matching DOFs and perform the elimination of the redundant states, in order to achieve a minimal-order coupled state-space model. The matching DOFs have already been identified, when the transformation matrix was computed. Therefore, the related columns of each group of matching DOFs should be now summed. Remembering the pointed matching DOFs it can be stated that the following $[\bar{A}]$ matrix columns should be added:

- x_2 and x_4 (2^{nd} and 4^{th} columns from $[\bar{A}]$ matrix);
- $\dot{x}_2$ and $\dot{x}_4$ (15^{th} and 17^{th} columns from $[\bar{A}]$ matrix);
- x_3 and x_5 (3^{rd} and 5^{th} columns from $[\bar{A}]$ matrix);
- $\dot{x}_3$ and $\dot{x}_5$ (16^{th} and 18^{th} columns from $[\bar{A}]$ matrix);
- x_6 and x_8 (6^{th} and 8^{th} columns from $[\bar{A}]$ matrix);
- $\dot{x}_6$ and $\dot{x}_8$ (19^{th} and 21^{th} columns from $[\bar{A}]$ matrix);
- x_7 and x_{10} (7^{th} and 10^{th} columns from $[\bar{A}]$ matrix);
- $\dot{x}_7$ and $\dot{x}_{10}$ (20^{th} and 23^{th} columns from $[\bar{A}]$ matrix);
- x_9, x_{11} and x_{12} (9^{th}, 11^{th} and 12^{th} columns from $[\bar{A}]$ matrix);
- $\dot{x}_9$, $\dot{x}_{11}$ and $\dot{x}_{12}$ (22^{th}, 24^{th} and 25^{th} columns from $[\bar{A}]$ matrix);

After this procedure, just one row and column of the $[A]$ matrix related to the matching DOF should be kept and the remaining ones has to be eliminated. On other hand, to achieve the coupled $[\bar{B}]$ matrix, just the same meaning rows has to be eliminated (see section 2.7.1).

The final state vector will be the following one

$$\{\bar{x}\} = \begin{bmatrix} x_1 \\ \bar{x}_1 \\ \bar{x}_2 \\ \bar{x}_3 \\ \bar{x}_4 \\ \bar{x}_5 \\ x_{13} \\ \dot{x}_1 \\ \dot{\bar{x}}_1 \\ \dot{\bar{x}}_2 \\ \dot{\bar{x}}_3 \\ \dot{\bar{x}}_4 \\ \dot{\bar{x}}_5 \\ \dot{x}_{13} \end{bmatrix} \tag{3.38}$$

Finishing this last step, $[\bar{A}]$ and $[\bar{B}]$ matrices are deduced. The $[\bar{C}]$ and $[\bar{D}]$ matrices are obtained from the bottom block row of $[\bar{A}]$ and $[\bar{B}]$ matrices, when the chosen output is acceleration (see section 2.2). Afterwards, the state-space model of the coupled structure is obtained.

The FRFs obtained from the coupled state-space modes deduced by the method proposed by Su and Juang [Su and Juang, 1994] were computed and compared with the analytical FRFs. It was observed a perfect fit between the two solutions for all of the FRFs. In figure 3.5 are represented 2 different curves, representative of the assembled structure FRF considering as output the DOF related to the mass m_{p4} and as input the DOF related to the sum of the masses m_{f2} and m_{a3}. The black curve represents the analytical accelerance FRF and the blue curve represents the same accelerance FRF computed from the coupled state-space model obtained with the method proposed by Su and Juang [Su and Juang, 1994].

Note that, the performed coupling in this numerical example was performed with the presented approach at section 2.10.2, however it could be also performed by the use of the approach presented at section 2.10.3. That approach will be applied to perform the coupling of two non-rigidly connected substructures at section 3.2.2.

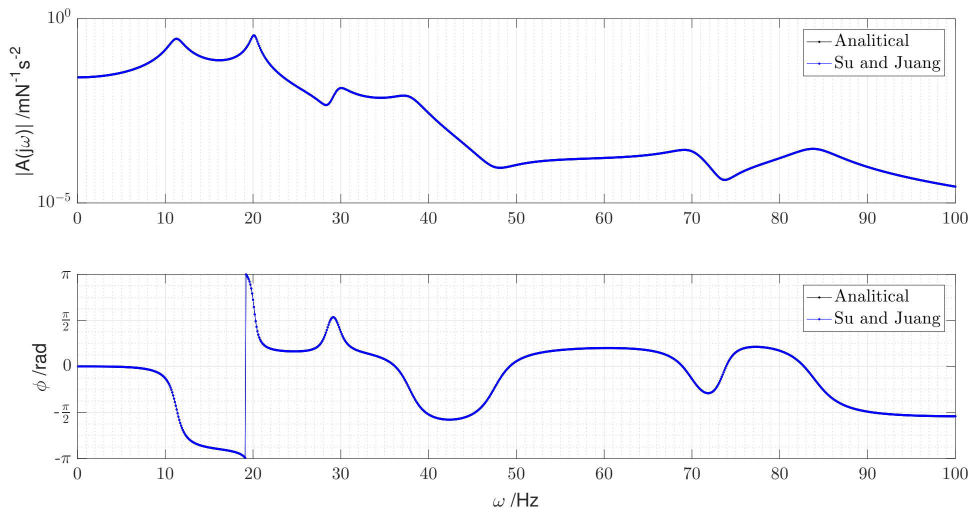

Figure 3.5: Mechanical System nº 2: Accelerance FRF considering as output the DOF related to mass m_{p4} and as input the DOF related to the sum of the masses m_{f2} and m_{a3}

3.2 Numerical Results - Coupling state-space models expressed in modal coordinates

3.2.1 Numerical example nº 1

In this numerical example the coupling between the substructures presented in figure 3.6 will be performed. The substructure mechanical properties are presented in table F.3.

The coupling will be performed with a state-space model expressed in modal coordinates. Using the method proposed by Su and Juang [Su and Juang, 1994], in order to perform coupling, the steps to follow are basically the same as described in the section 3.1.1. The unique difference is that the rearrangement of the state vector and the elimination of states must not be performed, since the used system identification method exactly identifies the number of poles of the mechanical system (see section 2.8). Thus, a minimal number of states will be instantly obtained in the identification procedure. Despite no states elimination or rearrangement is needed, the rearrangement of $[\bar{B}]$ and $[\bar{D}]$ matrices columns in accordance with input vector rearrangement has to be performed. Meanwhile, the rearrangement of $[\bar{C}]$ and $[\bar{D}]$ matrices rows in accordance with output vector rearrangement continue to be performed. As explained in section 2.8.3, the coupled state-space matrices (see expression (2.57)) of the method proposed by Su and Juang [Su and Juang, 1994] are derived from the diagonal uncoupled acceleration state-space model (see appendix A). Therefore, the computation of the coupled acceleration state-space model has to be performed from the uncoupled diagonal acceleration state-space model.

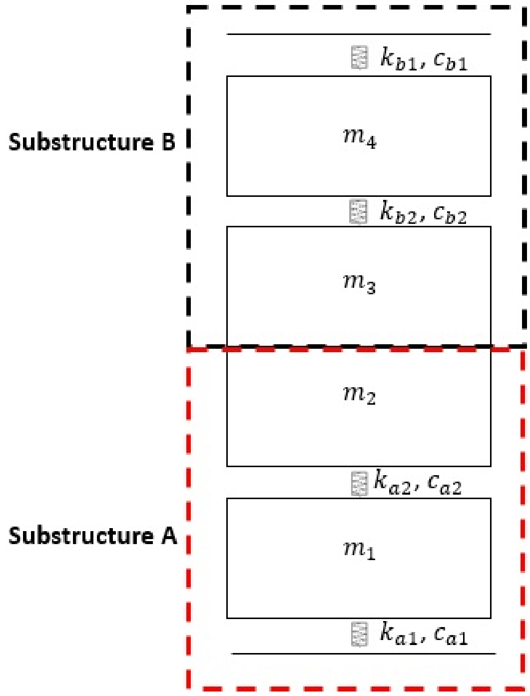

Figure 3.6: Mechanical System nº 3

In fact, the uncoupled diagonal state-space model is simpler obtained by the use of the acceleration substructure state-space models. However, as exposed at appendix D it is also possible to obtain the uncoupled diagonal acceleration state-space model directly from the substructure displacement state-space models. In order to prove the applicability of that theoretical demonstration, the achievement of the diagonal uncoupled acceleration state-space model and, then the achievement of the coupled acceleration state-space model was also performed from the substructure displacement state-space models. Note that, this will not influence the results, since the coupling is performed between a numerical substructures. However, the use of this approach does not take in account any lower or upper residuals, which will, certainly, be important when coupling experimentally measured data.

The FRFs obtained from both of coupled state-space models computed by both of exposed procedures were computed and compared with the analytical FRFs. It was observed a perfect fit between the three solutions for all of the FRFs. In figure 3.7 are represented 3 different curves, representative of the assembled structure FRF considering as output the DOF related to the mass m_4 and as input the DOF related to the mass m_1. The black curve represents the analytical accelerance FRF, the blue and red curves represents the same accelerance FRF computed from the coupled state-space model obtained with the method proposed by Su and Juang [Su and Juang, 1994]. However, the blue curves represents the accelerance FRF computed from a coupled state-space model obtained with the substructure acceleration state-space models, while the red curve represents the accelerance FRF computed from a coupled state-space model obtained with the substructure displacement state-space models

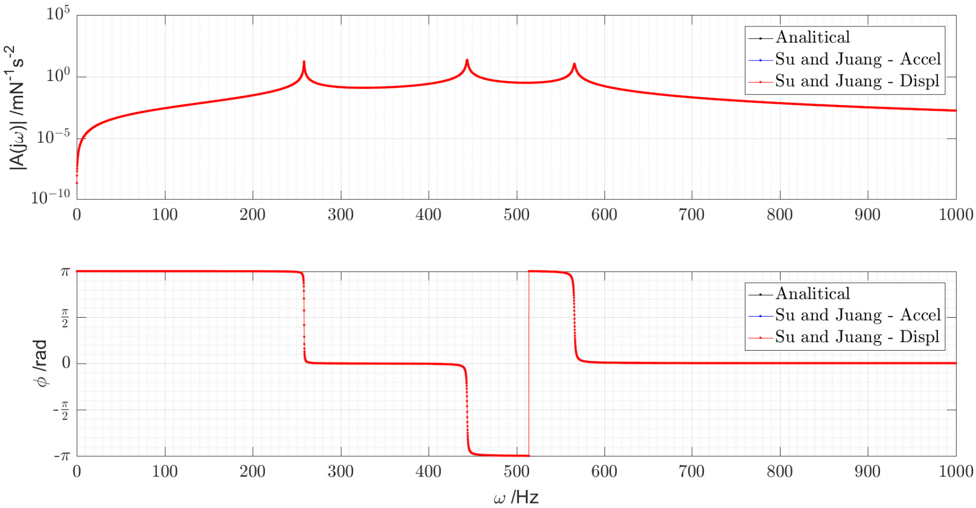

Figure 3.7: Mechanical System nº 3: Accelerance FRF considering as output the DOF related to the mass m_4 and the input as the DOF related to the mass m_1

3.2.2 Numerical example nº 2

In this numerical example the coupling between two non-rigidly connected substructures will be performed. This coupling will be performed with the performance of two different couplings, one realized in a regular form and the other in a negative form (see section 2.10.3). The structure, which will be analysed can be observed in figure 3.8. The structure mechanical properties are presented in table F.4. In figure 3.9 it can be observed the division of the structure in four different substructures, which will be coupled.

As described in section 2.10.3 the inserted masses between the interface of the substructures and the connecting elements are not negligible. Thus, its influence should be removed by coupling another state-space model, defined in a negative form. As this negative state-space model cannot be defined just by mass, the stiffness and damping matrices of both connecting elements substructures should be wisely chosen.

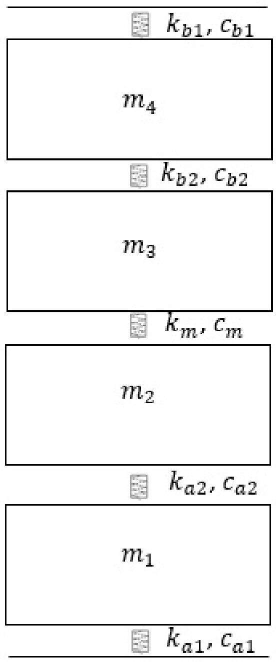

Figure 3.8: Mechanical System nº 4

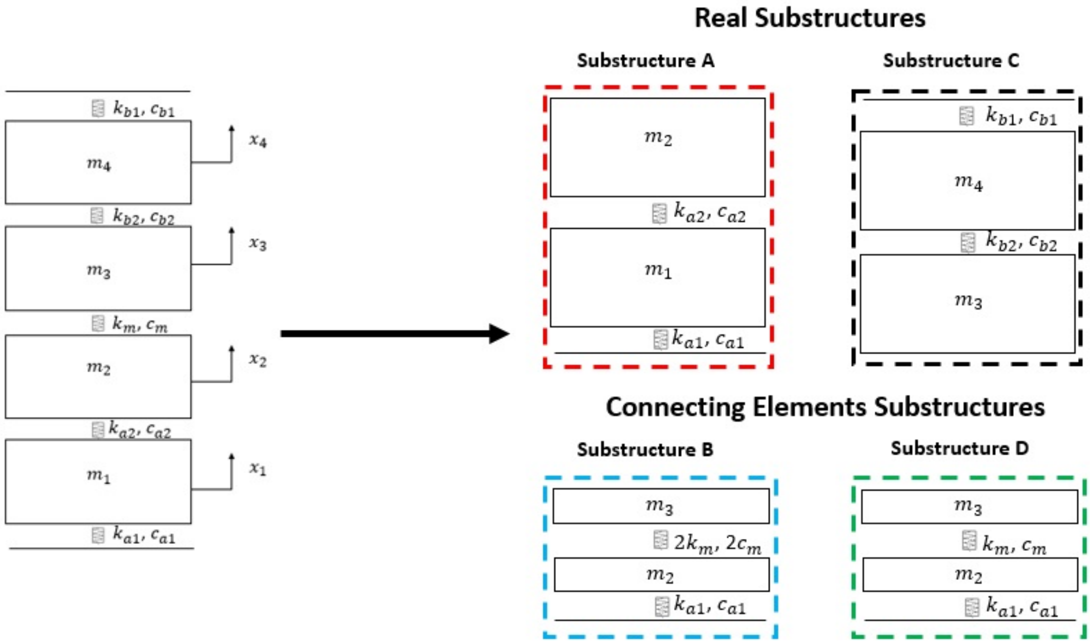

Figure 3.9: Mechanical System nº 4 - Coupling with a positive and a negative state-space model - dividing in different substructures

Firstly, the substructures B and D must have the same mass properties, in order to remove the influence of the inserted masses between the substructure interface. Secondly, as the substructure B will be coupled in a regular form, while the substructure D will be coupled in a negative form, the stiffness and damping properties of the substructure B were selected to be twice the value of the real ones and the stiffness and damping properties of the substructure D were selected to be equal to the real ones. Therefore, it will be guaranteed that the obtained coupled state-space model will correspond to the structure state-space model. The mechanical properties of each connecting elements substructure could be others, since it guarantees the achievement of a coupled state-space model, which represents the structure in analysis (see figure 3.9).

This coupling procedure is done in two different steps. Firstly the substructures A, B and C are coupled in a regular form. Afterwards, the coupling of the substructure D with its state-space model defined in a negative form should be performed, achieving the intended coupled state-space model.

The FRFs obtained from the coupled state-space model were computed and compared with the analytical FRFs. It was observed a perfect fit between both for all the FRFs. In figure 3.10 are represented 2 different curves, representative of the assembled structure FRF considering as output the DOF related to the mass m_4 and as input the DOF related to the mass m_2. The black curve represents the analytical accelerance FRF and the blue curve represents the same accelerance FRF computed from the coupled state-space model obtained with the method proposed by Su and Juang [Su and Juang, 1994].

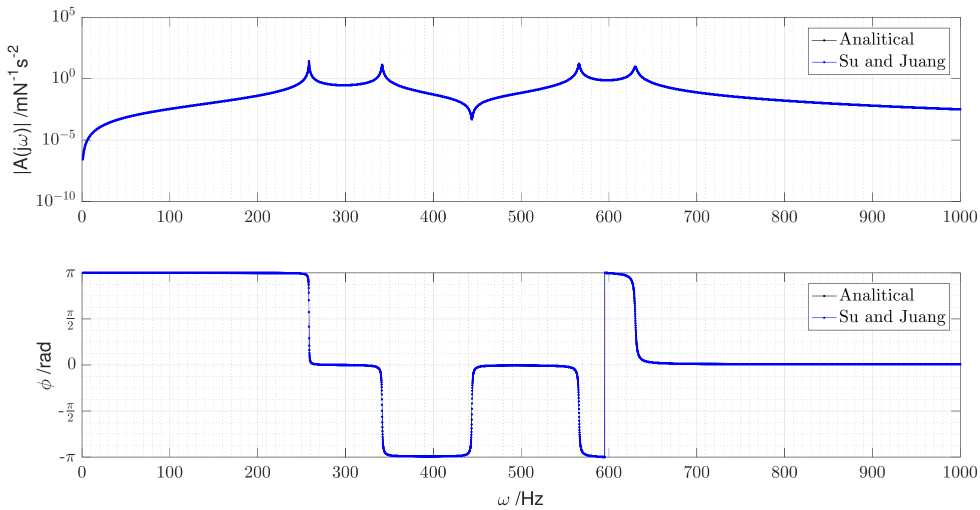

Figure 3.10: Mechanical System nº 4: Accelerance FRF considering as output the DOF related to the mass m_4 and as input the DOF related to the mass m_2

Note that, the coupling realized in this numerical example was not performed by the use of the presented approach at section 2.10.2. In fact, this approach is not recommended, when coupling state-space models expressed in modal coordinates and therefore, is not recommended when coupling experimental data. The reason for this affirmation is the fact of the estimation of a state-space model from experimental data should be performed in a frequency band which includes system poles. However, since the inserted masses would be low, the resonance frequencies of the system, would be localized at high frequencies, hence the state-space model estimation would be more difficult (see section 2.10.1).

Chapter 4

Experimental Results

In this chapter, two real mechanical systems will be analyzed. The first one is an eletric motor rigidly connected to a metal support frame. The second is a system composed by two components, a source and a receiver rigidly connected.

For the first mechanical system, it was provided by Siemens Industry Software NV the measured FRFs of the eletric motor and the metal support frame and as well the measured FRFs of the assembled structure. Therefore, the coupling will be performed between both substructures with the Su and Juang state-space coupling method [Su and Juang, 1994] and with FBS method, then both of obtained solutions will be compared with the measured FRFs of the assembled system.

For the second mechanical system, it is available the measured FRFs of each substructures, but is not available the measured FRFs of the assembled structure. Therefore, the evaluation of the results accuracy obtained by the technique proposed by Su and Juang [Su and Juang, 1994] will be performed by comparing with the solution obtained with FBS method.

Since, the estimated state-space model from measured data presents a non negligible error, the FBS solution will be obtained by the use of the measured FRFs and also by the use of the FRFs computed from the estimated state-space models.

Note that, it will not be performed a description of the material used in the FRFs measurements, neither the performed procedures, since no experimental work has been done. It will be performed just a description of each mechanical system, the position of each accelerometers and the inputs and outputs, which were considered to characterize each substructure.

This chapter will be composed by two main sections related to each analyzed mechanical system. Each of these composed by three different subsections. Firstly, the description of the mechanical system and respective substructures. Secondly, the estimation of the state-space model from the measured data will be explained and the FRFs computed from the estimated state-space models will be compared with the measured ones. Lastly, the coupling procedure will be explained and the obtained coupling results will be presented.

Note that, both of the experimental couplings have the aim to reveal that the coupling with the method proposed by Su and Juang [Su and Juang, 1994] does not impose the necessity of internal and interface inputs and outputs. In fact, with simple adjustments to the coupled state-space model (see mathematical expression (2.57)) it will be possible for the first mechanical system perform coupling just by consider interface inputs and outputs. For the second mechanical system the coupling will be performed by considering just interface inputs and considering interface and internal outputs. The minimum requirement to perform coupling is the presence of interface inputs and outputs.

4.1 Experimental example nº 1

4.1.1 Mechanical System Description

The first mechanical system is composed by two structures, an electric motor and a metal support frame consisting of 3 metal brackets. Both of substructures are connected by 3 connecting points. In order to measure the accelerance FRFs of each substructure it is necessary to perform excitation and measure the acceleration responses at the intended locations. The acceleration measurements were performed by the use of accelemrometers *PCB Piezotronics* with reference $333B30$. All the information about this accelerometers can be found at the following reference [Piezotronics, 2020].

On other hand, the excitation was performed by the use of mechanical shakers *Simcenter* $Q-HSH$. This shaker is a miniature shaker that has been developed to perform highly repeatable and high-frequency structural excitation in minimum space. In fact, this shaker is suitable to perform excitation between 500 Hz and 10000 Hz, therefore, this is not a suitable choice to perform low frequency excitation, but can also provide reliable excitation down to frequencies between 200 Hz and 300 Hz for small application cases where not much energy (force) is required. In this application case the excitation started at 300 Hz. This fact justifies the starting of the analysis of this experimental measured data at 300 Hz. All the information about the used excitation shakers can be found at the following reference [Siemens, 2020]. The upper limit of the frequency band of interest was selected to be 4000 Hz, since for frequencies higher than 4000 Hz the measured data showed to be very noisy.

The electric engine is presented in figure 4.1. In order to measure its accelerance FRFs, the electric engine was excited at the 3 connecting locations in each of the 3 dimensional axis (x, y and z). The acceleration measurements were performed at the same locations as the excitation, therefore this substructure is modeled by 9 interface inputs and outputs. In figure 4.1a it is presented a schematic representation of the tested engine, where it can be seen the position of the inputs and outputs. In that figure the DOFs are denominated by *Engi*:1, *Engi*:2 and *Engi*:3. However, for simplicity from this moment and until the end of this dissertation these DOFs will be denominated by C_1, C_2 and C_3, respectively. In figure 4.1b it can be observed the electric engine in test and can be realized that the accelerance FRFs have been measured in free-free boundary conditions.

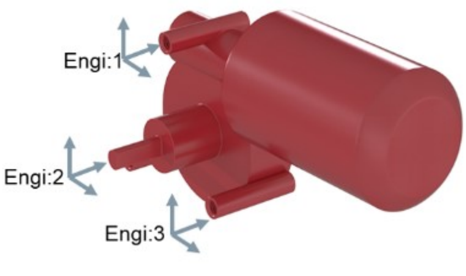

(a) Schematic representation [Siemens, n.d]

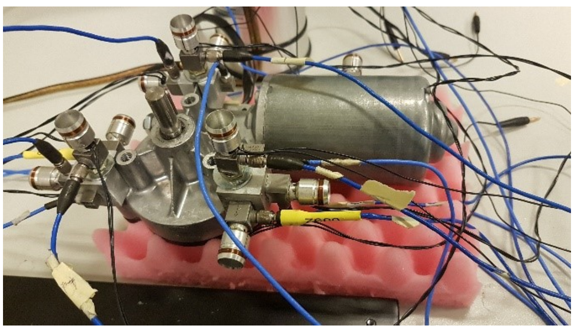

(b) Measuring accelerance FRFs [Siemens, n.d]

Figure 4.1: Eletric engine

In its turn, the support frame is presented at figure 4.2. This structure has been excited and the response have been measured not only at the connection locations but also in another locations. However, it will be just taken in account the 3 connection point locations, in order to practical demonstrate the possibility of perform coupling with the technique proposed by Su and Juang [Su and Juang, 1994] when the substructures are just modelled with interface inputs and outputs. Therefore, this substructure is modeled with 9 interface inputs and outputs.

In figure 4.2a it can be observed the location of the excitation and measurement points. The considered locations to model this substructure are denominated by *subBconn*:1, *subBconn*:2 and *subBconn*:3. However, from this moment and until the end of the present dissertation, these DOFs will be denominated by C_1, C_2 and C_3, respectively. In figure 4.2b it can be observed a real figure of the support frame.

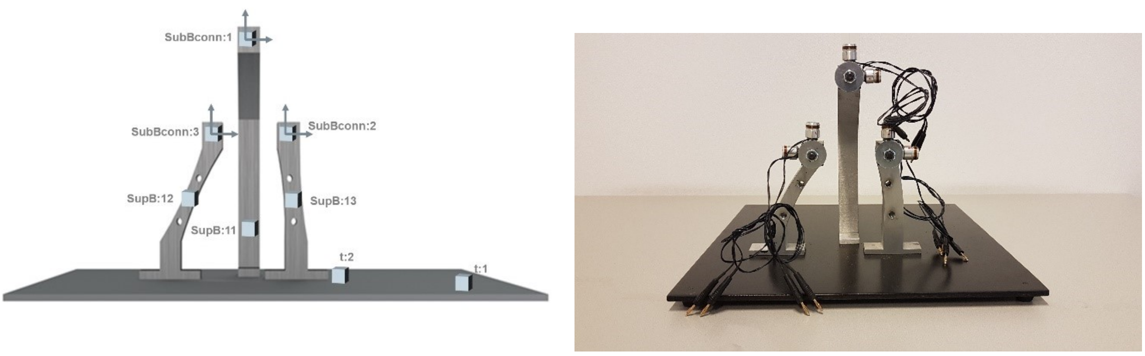

(a) Schematic representation [Siemens, n.d] (b) Real image [Siemens, n.d]

Figure 4.2: Support frame

The assembled structure can be observed at figure 4.3. This structure will be modeled by 9 interface inputs and outputs, since for the pointed reasons the support frame will be just modeled by the connecting points. In figure 4.3a it can be observed a schematic representation of the assembled structure and the location of all the excitation and measurement points. The points considered to model this structure are denominated by *engi*:1, *engi*:2 and *engi*:3. However, from this moment and until the end of the present dissertation, these DOFs will be denominated by C_1, C_2 and C_3, respectively. In figure 4.3b it can be observed a real image of the assembled structure.

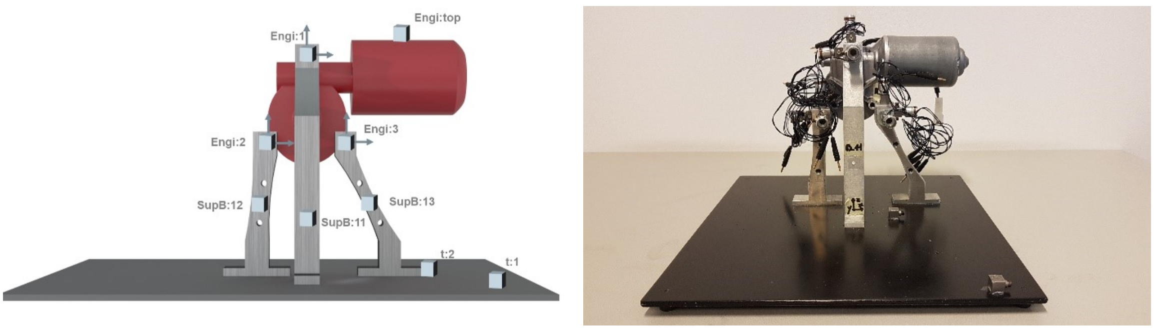

(a) Schematic representation [Siemens, n.d] (b) Real image [Siemens, n.d]

Figure 4.3: Assembled structure

4.1.2 Identification Results

The estimation of state-space models from measured data was performed in two different steps. Firstly, the modal model estimation was performed with software *Simcenter Testlab®* and secondly the state-space model estimation from the estimated modal model was performed with a *MATLAB®* script provided by Siemens Industry Software NV.

The first step was performed by the use of the presented method at section 2.8. This method already was implemented in software *Simcenter Testlab®*, justifying the use of this software in the modal model estimation. The electrical engine (see figure 4.1) measured data was analyzed in four different frequency bands between 300 Hz and 4000 Hz. The analyzed frequency bands are presented as follows:

1. 300 Hz to 850 Hz;
2. 850 Hz to 1840 Hz;
3. 1840 Hz to 2740 Hz;
4. 2740 Hz to 4000 Hz.

The support frame (see figure 4.2) measured data was analyzed in 4 different frequency bands, presented as follows:

1. 300 Hz to 1025 Hz;
2. 1025 Hz to 2050 Hz;
3. 2050 Hz to 3050 Hz;
4. 3050 Hz to 4050 Hz.

For the construction of the stabilization diagram, the chosen modal size was 1000. The chosen pre-set tolerances were the default ones, which are presented as follows:

- Maximum variation of MAC value for the modal participation vectors: 2%;
- Maximum frequency variation: 1%;
- Maximum damping ratio variation: 5%.

For both parts, the poles selection was made with the automatic modal parameter selection tool of software *Simcenter Testlab®*. For this automatic selection it was defined a default modal density and a default limit for the maximum damping ratio of the selected poles (7%).

The choice to perform the modal parameters estimation in several bands is justified for both of the systems have a great number of poles. On other hand, it was verified that performing the identification by the use of one band would require the selection of an huge modal size, which would turn the estimation procedure slower and issues of memory would be faced. The criteria for the chosen frequency bands is simple. It was chosen in order to the beginning and the end of each frequency band be localized at one anti-resonance of the FRF representative of the sum of all the measured FRFs. This criteria is justified in order to guarantee that the frequency band ends in a far location from a FRF peak, which will guarantee that the information about the in-band poles is totally included. Otherwise, some pole information could miss and the identification of that pole would not be properly performed.

The pre-set tolerances should be chosen, in order to obtain the best possible modal model estimation. Usually, if the system has a lot of poles the pre-set tolerances should be greater. However, start by the default pre-set tolerances is always a good choice, if the estimated modal model is not of the intended quality, these tolerances should be readjusted. The maximum damping ratio for the selection of poles is dependent of the mechanical system. If it is known that the damping is low, this parameter should be lower, otherwise if it is known that the system is highly damped, this parameter should be greater. The chosen modal density should be readjusted if in a specific frequency band it is known that the system presents a low or a high number of poles, otherwise the default density should be used. In general, the modal model estimation procedure is an iterative procedure and there is no strict rule for the choice of the involved parameters.

After the poles selection, the participation factors and the damping ratios are known. In order to compute the mode shapes and the lower and upper residuals the modal model expression (2.85) should be solved in a linear least-square sense. In this step it was enforced real mode constraint. This constraint corresponds to estimate real valued mode shapes and participation factors [El-Kafafy et al., 2015]. As stated at section 2.8.3, this means that is assumed that the structure under testing has a proportional damping. The reason for the introduction of this assumption is to low the numerical complexity of the calculations. On other hand, the estimation of the state-space model from the estimated modal model is simpler. In fact for both substructures it was verified that this assumption did not decreased the estimation quality of the modal model.

In order to refine the obtained modal model, 100 ML-MM iterations were applied (see section 2.8). In this step, the selected relative error between two consecutive calculated cost-functions, in order to end the optimization procedure was 3×10^{-5} %. After the optimization procedure for each of the analyzed frequency bands, the estimated modal models were merged and the modal model for the frequency band between 300 Hz and 4000 Hz for the electrical motor and between 300 Hz and 4050 Hz for the support frame was obtained. Afterwards, an acceleration state-space model was computed from the estimated modal model as exposed in section 2.8.3.

In figure 4.4 it can be observed the electrical engine FRF considering as output the DOF C_3^z and as input the DOF C_1^x (see figure 4.1). The figure 4.5 presents the support frame FRF considering as output the DOF C_1^y and as input the DOF C_1^z (see figure 4.2). Both figure presents 3 different curves, the black curve is the measured FRF, the red represents the estimated modal model in software *Simcenter Testlab®* and the blue represent the FRF computed from the estimated acceleration state-space model. The presented FRFs are represented between a frequency band 300 Hz and 4000 Hz.

Analyzing both figures 4.4 and 4.5 it can be realized that the blue curve perfect match with the red one, which proves that the acceleration state-space model is correctly computed from the estimated modal model. Therefore, the theoretical deduction performed at appendix E, in order to take in account the lower residuals and the conversion of the upper residuals into residuals modes (see section (2.8.3)) are here verified in practice. On other hand, it can be realized that the FRF computed from the estimated state-space model and the measured one almost perfect fit, which proofs that the modal model estimation was performed with high quality.

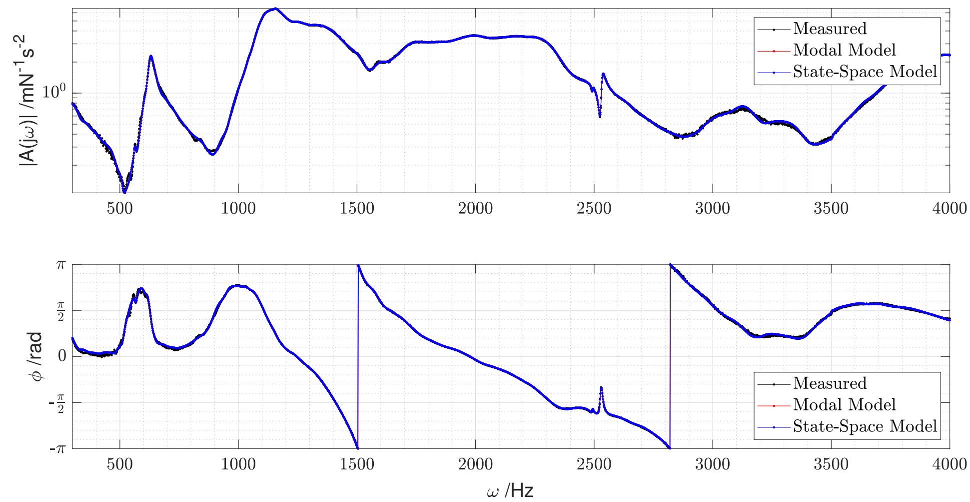

Figure 4.4: Identification results: Electric engine accelerance FRF considering as output the DOF C_3^z and as input the DOF C_1^x

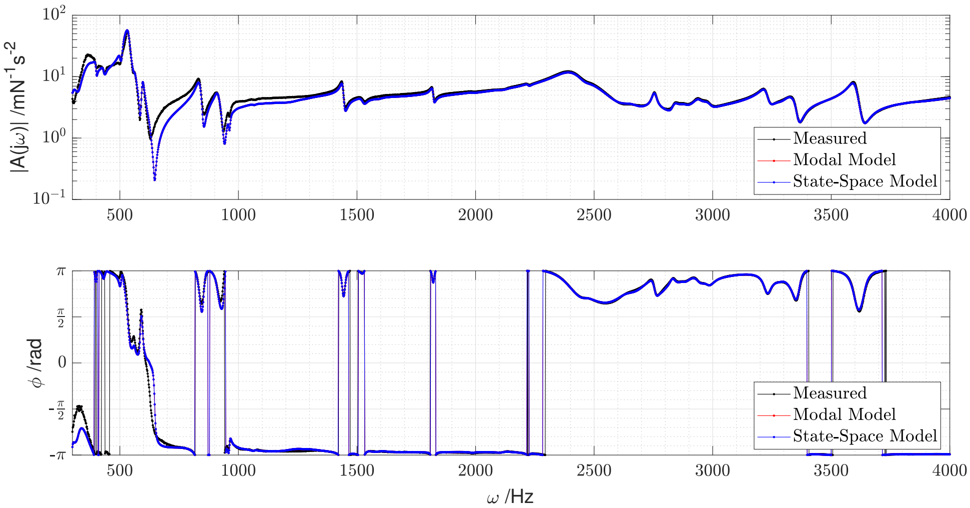

Figure 4.5: Identification results: Support frame accelerance FRF considering as output the DOF C_1^y and as input the DOF C_1^z

4.1.3 Coupling Results

The coupling between both substructures was enforced at the 3 connecting points (see figures 4.1 and 4.2). In order to enforce coupling, the compatibility and equilibrium conditions (see section 2.7.1) have to be established. This coupling will be performed by the use of the method proposed by Su and Juang [Su and Juang, 1994], therefore, a $[T]$ matrix based on the established equilibrium and compatibility conditions should also be computed.

Starting by expressing the equilibrium and compatibility conditions by mathematical expressions

$$
\begin{aligned}
&\bar{u}_{C_1^x} = u^E_{C_1^x} + u^{SF}_{C_1^x} && \bar{u}_{C_1^y} = u^E_{C_1^y} + u^{SF}_{C_1^y} && \bar{u}_{C_1^z} = u^E_{C_1^z} + u^{SF}_{C_1^z} && (4.1a)\\
&\bar{u}_{C_2^x} = u^E_{C_2^x} + u^{SF}_{C_2^x} && \bar{u}_{C_2^y} = u^E_{C_2^y} + u^{SF}_{C_2^y} && \bar{u}_{C_2^z} = u^E_{C_2^z} + u^{SF}_{C_2^z} && (4.1b)\\
&\bar{u}_{C_3^x} = u^E_{C_3^x} + u^{SF}_{C_3^x} && \bar{u}_{C_3^y} = u^E_{C_3^y} + u^{SF}_{C_3^y} && \bar{u}_{C_3^z} = u^E_{C_3^z} + u^{SF}_{C_3^z} && (4.1c)
\end{aligned}
$$

In its turn, the compatibility equations are following presented

$$
\begin{aligned}
&\bar{y}_{C_1^x} = y^E_{C_1^x} = y^{SF}_{C_1^x} && \bar{y}_{C_1^y} = y^E_{C_1^y} = y^{SF}_{C_1^y} && \bar{y}_{C_1^z} = y^E_{C_1^z} = y^{SF}_{C_1^z} && (4.2a)\\
&\bar{y}_{C_2^x} = y^E_{C_2^x} = y^{SF}_{C_2^x} && \bar{y}_{C_2^y} = y^E_{C_2^y} = y^{SF}_{C_2^y} && \bar{y}_{C_2^z} = y^E_{C_2^z} = y^{SF}_{C_2^z} && (4.2b)\\
&\bar{y}_{C_3^x} = y^E_{C_3^x} = y^{SF}_{C_3^x} && \bar{y}_{C_3^y} = y^E_{C_3^y} = y^{SF}_{C_3^y} && \bar{y}_{C_3^z} = y^E_{C_3^z} = y^{SF}_{C_3^z} && (4.2c)
\end{aligned}
$$

In expressions (4.1) and (4.2) and until the end of this section, letter u is related to inputs, y is related to outputs, subscripts refers to the DOFs, top bar variables are referred to the assembled structure and the superscripts E and SF are respectively referred to the electric engine and to the support frame.

Expressing the equilibrium and compatibility conditions (equations (4.3) and (4.4), respectively) by the use of the $[T]$ matrix

$$
\begin{bmatrix} \bar{u}_{C_1} \\ \bar{u}_{C_2} \\ \bar{u}_{C_3} \end{bmatrix} = \begin{bmatrix} T \end{bmatrix} \begin{bmatrix} u^E_{C_1} \\ u^E_{C_2} \\ u^E_{C_3} \\ u^{SF}_{C_1} \\ u^{SF}_{C_2} \\ u^{SF}_{C_3} \end{bmatrix} \quad (4.3) \qquad \begin{bmatrix} y^E_{C_1} \\ y^E_{C_2} \\ y^E_{C_3} \\ y^{SF}_{C_1} \\ y^{SF}_{C_2} \\ y^{SF}_{C_3} \end{bmatrix} = \begin{bmatrix} T \end{bmatrix}^T \begin{bmatrix} \bar{y}_{C_1} \\ \bar{y}_{C_2} \\ \bar{y}_{C_3} \end{bmatrix} \quad (4.4)
$$

where, $[T]$ matrix is given as follows

$$
[T] = [I \quad I] \tag{4.5}
$$

with matrix $[I]$ being an identity matrix with 9 rows and 9 columns.

Note that, each of the inputs and outputs presented at equations (4.3) and (4.4) represent in fact three different inputs and outputs, respectively. Being each, related to each of the three dimensional axis x, y and z.

In order to perform coupling, the presented procedure at section 2.9.1 must be followed. However, analyzing the presented coupled state-space matrices (see equation (2.57)) it can be noted the presence of internal outputs and inputs. In this experimental coupling, just interface inputs and outputs are used to characterize the assembled structure (see section 4.1.1). Therefore, the variables related to the internal inputs and outputs should be eliminated. After this elimination the following coupled state-space matrices are obtained

$$
\begin{aligned}
[\bar{A}] &= A_D + B_D^J Q C_D^J \\
[\bar{B}] &= \left[B_D^J (D_D^{JJ})^{-1} T^T S^{-1}\right] \\
[\bar{C}] &= \left[S^{-1} T (D_D^{JJ})^{-1} C_D^J\right] \\
[\bar{D}] &= \left[S^{-1}\right]
\end{aligned}
\tag{4.6}
$$

where the auxiliary variables $[S]$ and $[Q]$ are given by

$$
[S] = T(D_D^{JJ})^{-1} T^T \tag{4.7}
$$

$$
[Q] = (D_D^{JJ})^{-1} T^T S^{-1} T (D_D^{JJ})^{-1} - (D_D^{JJ})^{-1} \tag{4.8}
$$

The obtained coupled state-space model does not need the matrices $[\bar{B}]$, $[\bar{C}]$ and $[\bar{D}]$ rearrangements presented at section 2.9.1. This is justified for no internal inputs and outputs be used to characterize the assembled structure. The input and output vectors are, instantly, obtained as follows

$$
\{\bar{u}\} = \begin{bmatrix} \bar{u}_{C_1} \\ \bar{u}_{C_2} \\ \bar{u}_{C_3} \end{bmatrix}, \quad \{\bar{y}\} = \begin{bmatrix} \bar{y}_{C_1} \\ \bar{y}_{C_2} \\ \bar{y}_{C_3} \end{bmatrix} \tag{4.9}
$$

Again, each of the inputs and outputs presented in input and output vectors (see equation 4.9) represent in fact three different inputs and outputs, respectively. Being each, related to each of the three dimensional axis x, y and z.

In order to compare the accuracy of the obtained coupled results by the use of the FBS method (see section 2.6) and Su and Juang technique [Su and Juang, 1994], this coupling was also performed by FBS method. In fact, two FBS solutions were computed by the use of software *Simcenter Testlab*®. One FBS solution was computed by the use of the measured FRFs and the other by the use of the identified FRFs (see section 4.1.2).

In figure 4.6 are represented 4 different curves, representative of the assembled structure FRF considering as input the DOF C_1^z and as output the DOF C_3^x. The black one is related to the measured FRF, the blue represents the FRF computed from the coupled state-space model obtained with Su and Juang method [Su and Juang, 1994], the red represents the FRF obtained by the use of the FBS method with the identified substructure FRFs and the green represents the FRF obtained by the application of FBS method to the measured substructure FRFs. It was observed a perfect match between blue and red curves for all of the FRFs. The 4 obtained coupled FRFs solutions are represented for a frequency band between 300 Hz and 4000 Hz.

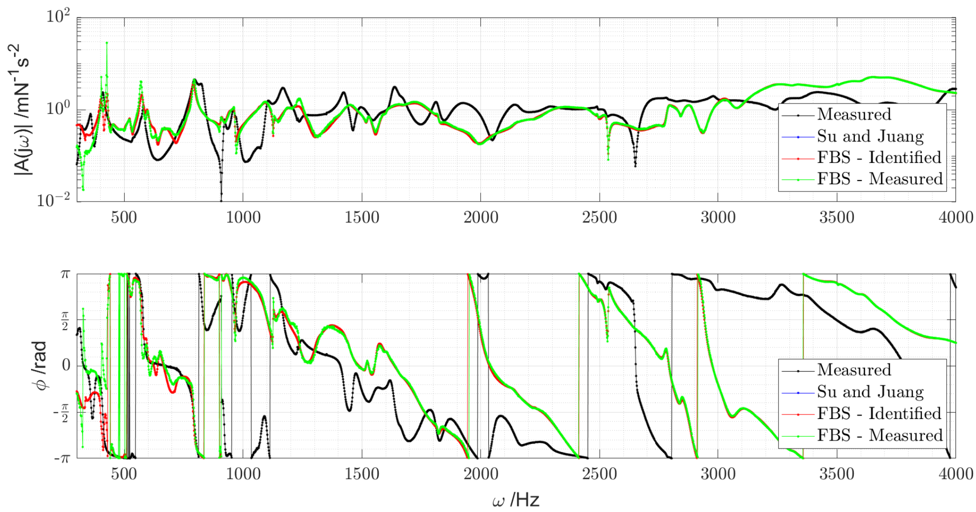

Figure 4.6: Coupling results: Assembled structure accelerance FRF considering as output the DOF C_1^z and as input the DOF C_3^x

4.2 Experimental example nº 2

4.2.1 Mechanical System Description

The second mechanical system is composed by two structures, which here will be denominated as source and receiver. The measured data from source substructure (presented in figure 4.7) is characterized by 4 different excitation and response measurements locations, which are represented by red cross markers. In each of these locations, the excitation and response measurement was performed for each of the three dimensional axis, x, y and z. Therefore, this substructure is characterized by 12 outputs and 12 inputs.

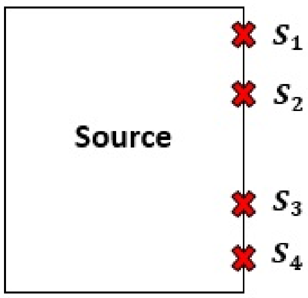

Figure 4.7: Source

In its turn, the receiver is presented at figure 4.8. The 4 red cross markers represent excitation and response measurements locations for each of the three dimensional axis (x, y and z), which perform 12 outputs and 12 inputs. On other hand, the 4 represented green cross markers represent response measurements locations for each of the three dimensional axis, which corresponds to 12 outputs. Thus, this substructure is characterized by 24 outputs and 12 inputs.

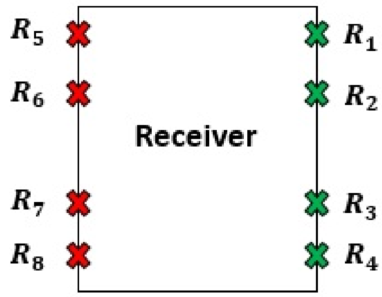

Figure 4.8: Receiver

In its turn, the coupled structure can be observed in figure 4.9. The assembled substructure is characterized by 24 outputs and 12 inputs. Again, the 4 red cross markers represent excitation and response measurements locations for each of the three dimensional axis (x, y and z), while the 4 presented green cross markers represent response measurements locations for each of the three dimensional axis.

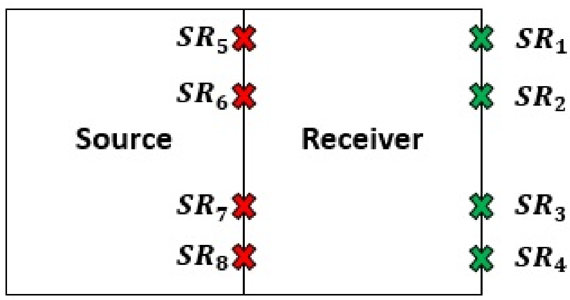

Figure 4.9: Assembled structure

4.2.2 Identification Results

The estimation of the state-space models from the measured data was performed by following the same steps as described at section 4.1.2. The source substructure (see figure 4.7) measured data was analyzed in four different frequency bands between 20 Hz and 4000 Hz. The analyzed frequency bands are presented as follows:

1. 20 Hz to 1015 Hz;
2. 1015 Hz to 2000 Hz;
3. 2000 Hz to 3000 Hz;
4. 3000 Hz to 4000 Hz.

In its turn, the receiver part (see figure 4.8) measured data was analyzed in 8 different frequency bands. The choice of twice the bands compared to the source part is justified because of the receiver part has more poles. This implies the selection of an higher model size for the computation of the stabilization diagram or the use of the same model size but in smaller frequencies bands, in order to achieve an high quality modal model estimation.

To overcome possible problems related to lack of memory or a slow modal model estimation, it was preferred to divide the frequency band of interest in smaller frequency bands. The analyzed frequency bands are presented as follows:

1. 20 Hz to 495 Hz;
2. 495 Hz to 985 Hz;
3. 985 Hz to 1500 Hz;
4. 1500 Hz to 2000 Hz;
5. 2000 Hz to 2500 Hz;
6. 2500 Hz to 2975 Hz;
7. 2975 Hz to 3520 Hz;
8. 3520 Hz to 4000 Hz.

The choice of this bands follows the same presented advises at section 4.1.2. For the PolyMAX step, the chosen model size for the stabilization diagram construction was 1000 and the pre-set tolerances for the identification of the physical poles were the following:

- Maximum variation of MAC value for the modal participation vectors: 10%;
- Maximum frequency variation: 5%;
- Maximum damping ratio variation: 10%.

For both parts, the poles selection was made with the defined default modal density of the software *Simcenter Testlab*®, it was also limited a maximum damping ratio of 70% for the selected poles. In section 4.1.2 it was advised to use the *Simcenter Testlab*® default pre-set tolerances, however it was found that with such strict tolerances many poles of both parts would be erroneously rejected. Therefore, the used pre-set tolerances were higher. On other hand, it is known that both substructures under test present high damping which justifies the choice of maximum damping ratio of 70% for the poles selection.

After the poles selection, the participation factors and the damping ratios are known. Then, to compute the mode shapes and the lower and upper residuals the modal model expression (2.85) should be solved in a linear least-square sense. In this step it was enforced real mode constraint as it already have been done for the mode shapes computation at section 4.1.2. It was verified, for both parts, that this assumption did not decreased the estimation quality of the modal model.

In order to refine the obtained modal model, 100 ML-MM iterations were applied (see section 2.8). For each substructure, the estimated modal models were merged and the modal model for the frequency band between 20 Hz and 4000 Hz was achieved. Afterwards, an acceleration state-space model was computed from the estimated modal model as exposed in section 2.8.3.

In figure 4.10 it can observed the source substructure FRF considering as output the DOF S_3^x and input the DOF S_1^x. The figure (4.11) presents the receiver substructure FRF considering as output the DOF R_8^z and as input the DOF R_8^y. Both figures presents the referred FRFs for a frequency band between 20 Hz and 4000 Hz. In each of these figures are represented 3 different curves, the black curve is the measured FRF, the red represents the estimated modal model in *Simcenter Testlab*® and the blue represents the FRF computed from the estimated acceleration state-space model.

Analyzing both figures 4.10 and 4.11 it can be realized that the blue curve perfect match with the red one, which proves that the acceleration state-space model is correctly computed from the estimated modal model. Comparing the black curve with the blue one it can be observed that the estimated modal model is of high quality for the majority of the frequency band.

It is important to refer that the majority of test conditions for the measured accelerance FRFs for the both substructures and respective assembled structure are unknown. This fact justifies the analyze of this experimental coupling starting at the lower frequency that measured data is available, 20 Hz. The upper frequency of the band of interest was selected to be 4000 Hz, since for frequencies higher than 4000 Hz the measured data showed to be very noisy.

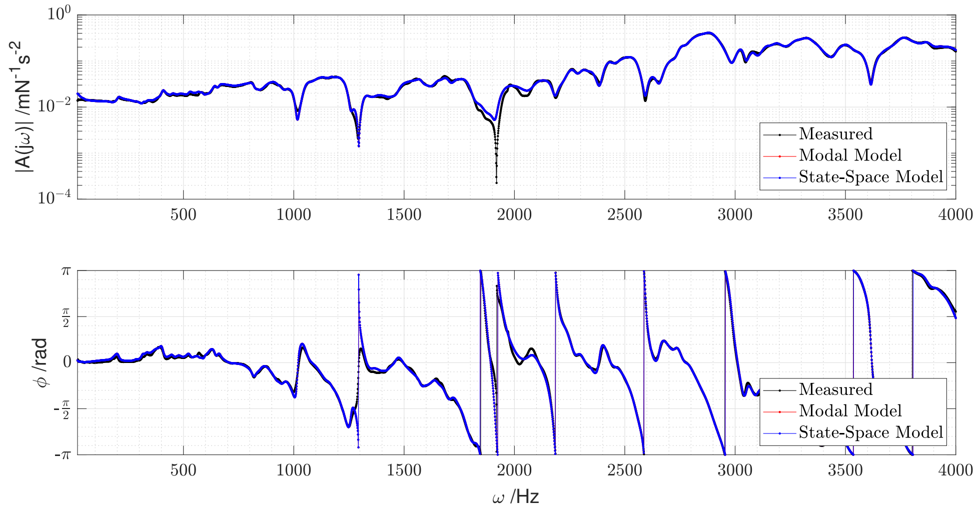

Figure 4.10: Identification results: Source part accelerance FRF considering as output the DOF S_3^x and as input the DOF S_1^x

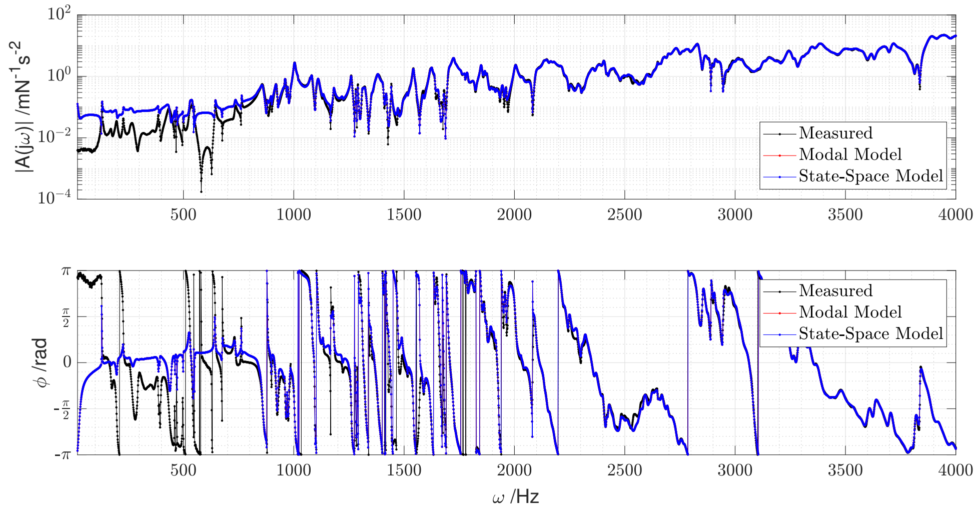

Figure 4.11: Identification results: Receiver part accelerance FRF considering as output the DOF R_8^z and as input the DOF R_8^y

4.2.3 Coupling Results

The connection between both substructures is performed at red cross markers location (see figures 4.7 and 4.8). Thus, in order to enforce coupling, the equilibrium and compatibility conditions (see section 2.7.1) have to be established between the DOFs related to these locations. These conditions can be established by the following mathematical expressions

$$u_{SR_5^x} = u_{S_1^x} + u_{R_5^x} \qquad u_{SR_5^y} = u_{S_1^y} + u_{R_5^y} \qquad u_{SR_5^z} = u_{S_1^z} + u_{R_5^z} \tag{4.10a}$$
$$u_{SR_6^x} = u_{S_2^x} + u_{R_6^x} \qquad u_{SR_6^y} = u_{S_2^y} + u_{R_6^y} \qquad u_{SR_6^z} = u_{S_2^z} + u_{R_6^z} \tag{4.10b}$$
$$u_{SR_7^x} = u_{S_3^x} + u_{R_7^x} \qquad u_{SR_7^y} = u_{S_3^y} + u_{R_7^y} \qquad u_{SR_7^z} = u_{S_3^z} + u_{R_7^z} \tag{4.10c}$$
$$u_{SR_8^x} = u_{S_4^x} + u_{R_8^x} \qquad u_{SR_8^y} = u_{S_4^y} + u_{R_8^y} \qquad u_{SR_8^z} = u_{S_4^z} + u_{R_8^z} \tag{4.10d}$$

In its turn, the compatibility equations are following presented

$$y_{SR_5^x} = y_{S_1^x} = y_{R_5^x} \qquad y_{SR_5^y} = y_{S_1^y} = y_{R_5^y} \qquad y_{SR_5^z} = y_{S_1^z} = y_{R_5^z} \tag{4.11a}$$
$$y_{SR_6^x} = y_{S_2^x} = y_{R_6^x} \qquad y_{SR_6^y} = y_{S_2^y} = y_{R_6^y} \qquad y_{SR_6^z} = y_{S_2^z} = y_{R_6^z} \tag{4.11b}$$
$$y_{SR_7^x} = y_{S_3^x} = y_{R_7^x} \qquad y_{SR_7^y} = y_{S_3^y} = y_{R_7^y} \qquad y_{SR_7^z} = y_{S_3^z} = y_{R_7^z} \tag{4.11c}$$
$$y_{SR_8^x} = y_{S_4^x} = y_{R_8^x} \qquad y_{SR_8^y} = y_{S_4^y} = y_{R_8^y} \qquad y_{SR_8^z} = y_{S_4^z} = y_{R_8^z} \tag{4.11d}$$

Note that, letter u is related to inputs and letter y is related to outputs.

Since, this mechanical coupling will be performed by the use of the method proposed by Su and Juang [Su and Juang, 1994], a $[T]$ matrix based on the established equilibrium and compatibility conditions should be computed. Starting for express the equilibrium and compatibility conditions (equations (4.10) and (4.11), respectively) by the introduction of the $[T]$ matrix

$$\begin{bmatrix} u_{SR_5} \\ u_{SR_6} \\ u_{SR_7} \\ u_{SR_8} \end{bmatrix} = [T] \begin{bmatrix} u_{S_1} \\ u_{S_2} \\ u_{S_3} \\ u_{S_4} \\ u_{R_1} \\ u_{R_2} \\ u_{R_3} \\ u_{R_4} \end{bmatrix} \tag{4.12}$$

$$\begin{bmatrix} y_{S_1} \\ y_{S_2} \\ y_{S_3} \\ y_{S_4} \\ y_{R_1} \\ y_{R_2} \\ y_{R_3} \\ y_{R_4} \end{bmatrix} = [T]^T \begin{bmatrix} y_{SR_5} \\ y_{SR_6} \\ y_{SR_7} \\ y_{SR_8} \end{bmatrix} \tag{4.13}$$

where, $[T]$ matrix is given as follows

$$[T] = [I \quad I] \tag{4.14}$$

with matrix $[I]$ being an identity matrix with 12 rows and 12 columns.

Note that, each of the inputs and outputs presented at equations (4.12) and (4.13) represent in fact three different inputs and outputs, respectively. Being each, related to each of the three dimensional axis x, y and z.

At this moment, to perform coupling, the presented procedure at section 2.9.1 must be followed. However, analyzing the presented coupled state-space matrices (see equation (2.57)) it can be noted the presence of internal inputs. In this experimental coupling, in order to characterize the assembled structure are used interface inputs and internal and interface outputs (see section 4.2.1). Therefore, the variables related to the internal inputs should be eliminated. After this elimination the following coupled state-space matrices are obtained

$$
\begin{aligned}
[\bar{A}] &= A_D + B_D^J Q C_D^J \\
[\bar{B}] &= \begin{bmatrix} B_D^J (D_D^{JJ})^{-1} T^T S^{-1} \end{bmatrix} \\
[\bar{C}] &= \begin{bmatrix} C_D^I + D_D^{IJ} Q C_D^J \\ S^{-1} T (D_D^{JJ})^{-1} C_D^J \end{bmatrix} \\
[\bar{D}] &= \begin{bmatrix} D_D^{IJ} (D_D^{JJ})^{-1} T^T S^{-1} \\ S^{-1} \end{bmatrix}
\end{aligned}
\tag{4.15}
$$

where the auxiliary variables $[S]$ and $[Q]$ are given by

$$[S] = T(D_D^{JJ})^{-1} T^T \tag{4.16}$$

$$[Q] = (D_D^{JJ})^{-1} T^T S^{-1} T (D_D^{JJ})^{-1} - (D_D^{JJ})^{-1} \tag{4.17}$$

The obtained coupled state-space model does not need any rearrangement of matrices $[B]$, $[C]$ or $[D]$ as explained in section 2.9.1. This is justified because just the receiver substructure is characterized by internal outputs. The input and output vectors are, instantly, obtained as follows

$$
\{\bar{u}\} = \begin{bmatrix} u_{SR_5} \\ u_{SR_6} \\ u_{SR_7} \\ u_{SR_8} \end{bmatrix}, \quad \{\bar{y}\} = \begin{bmatrix} y_{SR_1} \\ y_{SR_2} \\ y_{SR_3} \\ y_{SR_4} \\ y_{SR_5} \\ y_{SR_6} \\ y_{SR_7} \\ y_{SR_8} \end{bmatrix}
\tag{4.18}
$$

Again, each of the inputs and outputs presented in input and output vectors (see equation 4.18) represent in fact three different inputs and outputs, respectively. Being each, related to each of the three dimensional axis x, y and z.

In order to compare the accuracy of the obtained coupled results by the use of the FBS method (see section 2.6) and by the use of the proposed by Su and Juang [Su and Juang, 1994], this coupling was also performed by FBS method. In fact, two FBS solutions were computed by the use of software *Simcenter Testlab*®. One FBS solution was computed by the use of the measured FRFs, while the other by the use of the identified FRFs (see section 4.1.2).

In figure 4.12 are represented 3 different curves, representative of the assembled structure FRF considering as output the DOF SR_1^x and as input the DOF SR_8^x. The blue curve represents the FRF computed from the coupled state-space model obtained with the method proposed by Su and Juang [Su and Juang, 1994], the red represents the FRF obtained by the use of the FBS method with the identified substructure FRFs and the green represents the FRF obtained by the application of FBS technique to the measured substructure FRFs. It was observed a perfect match between blue and red curves for all of the FRFs.

Unfortunately, no measured FRFs of the assembled structure were available. The 3 obtained coupled FRFs solutions are represented for a frequency band between 20 Hz and 4000 Hz.

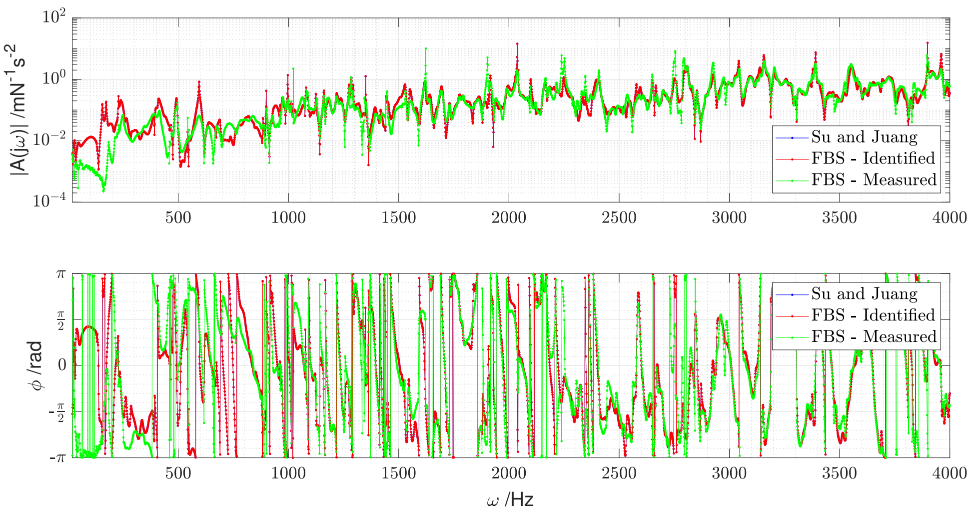

Figure 4.12: Coupling results: Assembled structure accelerance FRF considering as output the DOF SR_1^x and as input the DOF SR_8^x

4.3 Discussion

Analyzing the obtained results for the experimental couplings performed at sections 4.1 and 4.2, it can be realized that the FRFs computed from the coupled state-space model obtained by the use of the method proposed by Su and Juang [Su and Juang, 1994] perfects match the solution obtained by the application of the FBS method to the identified substructures FRFs. This means that starting from the same set of identified substructures FRFs, the method proposed by Su and Juang [Su and Juang, 1994] is able to provide coupling results with the same accuracy of the obtained ones by the use of FBS method. Therefore, the differences verified between the coupled FRFs obtained by the application of the FBS method to the measured FRFs and the obtained by the use of Su and Juang method [Su and Juang, 1994] are, uniquely, explained by errors in the modal model estimation of each substructure involved in coupling.

Even thought, the modal model estimation was not perfectly performed, the estimation is of high quality for the majority of the frequency band, even for the identification of more complex systems as the identified at section 4.2. This justifies the perfect match at many frequencies between the coupled FRFs obtained by the method proposed by Su and Juang [Su and Juang, 1994] and the ones obtained by the FBS method applied to the measured data, for both performed experimental couplings.

Observing the obtained coupling results for the first performed experimental coupling presented at figure 4.6 it can be observed that for frequencies below 500 Hz the coupling results obtained by the use of FBS method applied to the identified FRFs are closer to the measured FRFs than the coupled FRFs obtained by the application of the FBS method to the measured FRFs.

In fact, as already stated the FBS method suffers from numerical problems, in special related to ill-conditioned matrix inversions. A criteria to evaluate if the obtained coupled FRFs matrices are not numerically ill-conditioned is the analysis of its condition number. The condition number is given by the ratio between the highest and smallest singular values of the FRFs. These singular values are obtained by the application of the singular value decomposition (SVD) to the obtained coupled FRFs at each frequency as presented at section 2.5. A practical rule is to assume that the obtained coupled FRFs by the use of FBS method does not suffer of numerical ill-conditioned problems if the condition value is bellow 100 [Siemens, 2018].

Therefore, in order to evaluate the reason for the better results obtained by the computation of the coupled FRFs by the use of the measured and identified FRFs the condition values have been represented for a frequency range between 300 Hz and 4000 Hz in figure 4.13. In this figure it can be observed the condition number for the coupled FRFs obtained by the application of FBS method to the measured FRFs (black curve) and to the identified ones (blue curve). The condition values for both sets of coupled FRFs were obtained by the use of software *Simcenter Testlab*®.

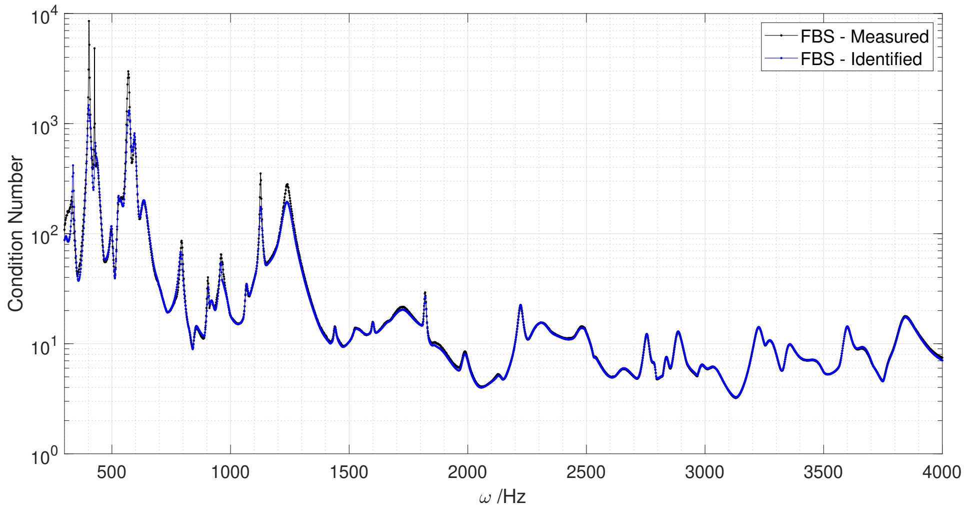

Figure 4.13: Condition Number: Experimental example nº1

In fact, it can be realized that the condition number for the solution obtained by the use of the identified FRFs is lower than by the use of the measured FRFs, specially, for frequencies bellow 600 Hz. Thus, the coupling FRFs computed by the application of FBS method to the identified FRFs are closer to the measured ones, because of the verified improvement in the condition number. Indeed, the identification procedure, even though not being perfect (see section 4.1.2) improved the solution obtained for the coupling FRFs. In fact, the identification procedure described at section 2.8 have the effect of filtering the noise from the measured data, not being a totally surprise. This phenomena as already been observed for others applications, which motivated the development of PolyMAX Plus. This PolyMAX based method is specialized in filtering noise of the measured FRFs [Siemens, 2019].

Moreover, the condition number is lower than 100 for the majority of frequencies values higher than 600 Hz, which suggest that in fact, the obtained coupled FRFs are of high quality. Suggesting that the main reason for the observed differences between the coupled FRFs and the measured ones are due to measurements errors.

Unfortunately, no measured solution is available for the rigidly connected system analyzed in section 4.2, not permitting the understand of which the FBS solution is closer to the measured ones. However, the analyze of the condition number continues to be of interest, in order to understand if the identification procedure has the effect of the decrease this parameter as verified for the first experimental coupling. In figure 4.14 it can be observed the condition number for the coupled FRFs obtained by the application of

FBS method to the measured FRFs (black curve) and to the identified ones (blue curve) represented between 20 Hz and 4000 Hz. Again, the condition values for both sets of coupled FRFs were obtained by the use of software *Simcenter Testlab®*.

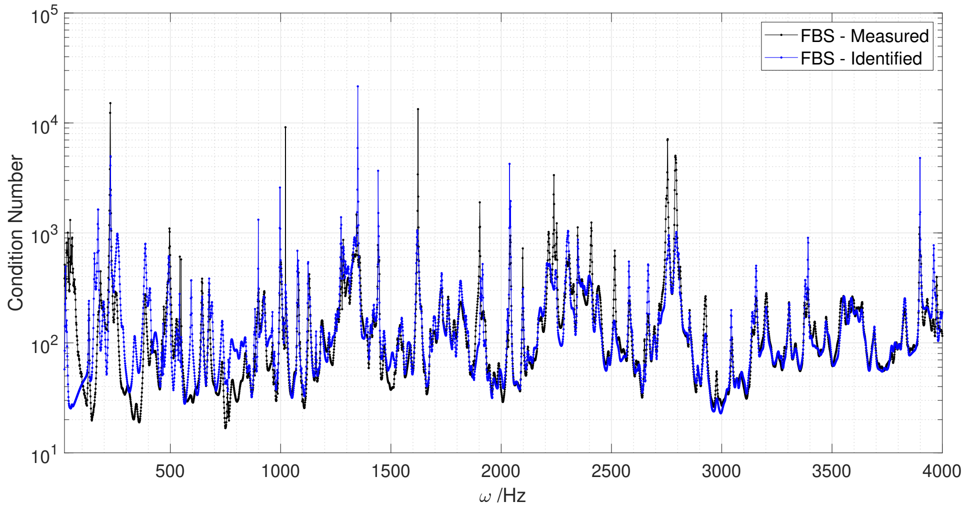

Figure 4.14: Condition Number: Experimental example nº2

Observing the figure 4.14 it can be realized that the same decrease of condition number for the FBS solution computed by the identified FRFs was observed for some frequencies of the band of interest. However, for other frequencies it was observed the opposite, being observed a increase of the condition number. Furthermore, overall the condition number is very high in order to assume that the obtained coupled FRFs are of high quality.

Another important conclusion that can be made is that the method proposed by Su and Juang [Su and Juang, 1994] suffers of same ill-conditioned problems as FBS. In fact, when applied to the same set of FRFs both techniques provide same coupled results for both performed experimental couplings. However, since for the second experimental coupling it was observed that the condition number was high for the majority of frequency band, thus, it is expected that FBS method suffers of ill-conditioned problems. Hence, the obtained coupled FRFs obtained by the use of the method proposed by Su and Juang [Su and Juang, 1994] should not perfect fit the ones obtained by FBS method, if the Su and Juang technique [Su and Juang, 1994] did not suffers of ill-condition problems as well. The same is valid for the first experimental coupling up to 600 Hz, where it was verified high condition numbers. Therefore, these facts strongly support the idea that the method proposed by Su and Juang [Su and Juang, 1994] suffers from the same numerical problems as FBS method. However, further research on systems that suffers of numerical ill-conditioned problems is required to better assess the performance of this state-space coupling method.

Comparing the results obtained by the method proposed by Su and Juang [Su and Juang, 1994] with the measured ones, which are just available for the coupling performed at section 4.1, it can be seen that both solutions are not equal. Despite the evident differences between both solutions, it is observed that for some frequencies both of the obtained FRFs are close. This fact, the fact of the coupled FRFs obtained by the method proposed by Su and Juang [Su and Juang, 1994] perfect match the ones computed by FBS method, when it is applied to the identified FRFs and the fact of the perfect results obtained for numerical couplings (see chapter 3), suggest that the encountered differences are mainly due to measurement errors.

The pointed measurement errors can be caused by several factors. One of these factors is related to the way that the excitation is performed. This excitation can be either impact excitation by the use of hammer or by the use of shakers. As stated, it was used shakers to perform the excitation. By the use of shakers the excitation force is obtained by the motion of the vibrating piston, through the shaker stinger. The transmitted force from the stinger to the structure under testing is supposed to be just in stinger direction, which never occur. Moreover, the stinger also has natural modes which can introduce false modes into the FRFs. The force gage associated with a shaker may pollute the measured FRFs by adding shear and rotation masses [Allen et al., 2020]. On other hand, the measured substructure accelerance FRFs were obtained by simulating free-free boundary conditions. However, these boundary conditions does not, correctly, simulates boundary conditions of the substructure when it is coupled. In order to better simulates the coupling conditions when measuring substructure accelerance FRFs, the use of the transmission simulator method in future substructure accelerance FRFs measurements is suggested.

The transmission simulator method assumes that if the accelerance FRFs of a substructure are wanted to be known, these FRFs measurement should be performed with the substructure coupled to another substructure, which accelerance FRFs are known (transmission simulator). Afterwards, the influence of the transmission simulator should be removed by substructure decoupling. When using state-space coupling methods, this decoupling can be performed in a similar way to the negative coupling presented at section 2.10.3. In order to implement this method, an analytical and a real model of the transmission simulator have to be manufactured. In the measurement FRFs procedure, the transmission simulator should be mounted to the substructure under test with exactly the same joint geometry as that to which the substructure will be connected. Moreover, the transmission simulator should be manufactured with the same material as the substructure that will be coupled with the substructure under test. Then, the constructed analytical model of the transmission simulator is used in the decoupling procedure, in order to obtain the substructure FRFs [Allen et al., 2020].

The use of this approach will permit the measurement of the substructure accelerance FRFs better simulating the coupling boundary conditions. In theory this procedure may seems useless, however it has been verified a significant improvement in the obtained coupling FRFs of the assembled system, when the accelerance FRFs of the substructures are obtained by the use of this method. This fact is related to two main reasons. Firstly, the dynamics of the substructure under testing if coupled to the transmission simulator will be similar to its dynamics when is incorporated into the real assembled structure. Moreover, the obtained substructure FRF after the decoupling procedure will not only present the dynamics of the isolated substructure, but also the dynamic of the interface as it presents in the assembled structure.

In fact, this method has been mostly applied to the FBS method being obtained higher accuracy in the obtained coupled results. Recently, this method have been translated for state-space substructuring by Scheel et al. in [Scheel et al., 2019], and used to couple an wind turbine being found that the transmission simulator method was successful implemented. This fact motivates even more the repetition of the substructure FRFs measurements by the use of transmission simulator method, suggesting that the obtained results will be improved. For a deeper exploration on transmission simulator method the following references are suggested [Mayes and Arviso, 2010],[Scheel, 2015],[Scheel et al., 2019],[Allen et al., 2020].

Chapter 5

Conclusion

5.1 Conclusions

The present work was developed with the aim of explore state-space coupling techniques for experimental dynamic substructuring. By the realization of this dissertation, was found that by the use of the state-space coupling technique proposed by Su and Juang [Su and Juang, 1994] it is possible to obtain reliable coupling results, for couplings performed between analytical models and also performed between real substructures.

The coupling of analytical models was verified for rigid connections and also for non-rigid ones (see chapter 3). It was verified that this technique provide high quality results, no mattering the complexity of the structure and the number of substructures that compose it. On other hand, the coupled DOFs can be shared for several substructures, high quality coupling results continue to be obtained. Focusing on non-rigid coupling, two different approaches were presented and validated on numerical models. Firstly, one based on the insertion of small fictitious masses between the connections of each substructure with the connecting elements 2.10.2. Secondly, one approach based in the construction of two fictitious models, which one of those should be coupled in a regular way and the other in a negative way (see section 2.10.3). Both of these approaches were verified when coupling numerical models. The first was verified for the coupling of the theoretical state-space models (see section 2.2) and the second for coupling state-space models expressed in modal coordinates (see section 2.8.3).

The coupling of real substructures was only performed for rigid connections (see chapter 4). It was found that the coupling results obtained by the method proposed by Su and Juang [Su and Juang, 1994] and the results obtained by the application of the FBS method to the identified FRFs perfect matched for both of performed experimental couplings. This reveals that the method proposed by Su and Juang [Su and Juang, 1994] provides results of the same accuracy as the FBS method. Therefore, the use of the method proposed by Su and Juang [Su and Juang, 1994] to couple real substructures rigidly connected is validated.

Although the validation of Su and Juang method [Su and Juang, 1994] for coupling rigidly connected substructures, it was experimentally found that this method possible suffers from the same ill-conditioned problems as the FBS method. Indeed, for the second performed experimental rigid coupling it was found that the obtained coupled FRFs by the use of both methods, perfect fits. However, analyzing the condition number of the obtained coupled FRFs, it was found that this parameter is very high. This suggest that the obtained coupled FRFs are not of high quality and ill-conditioned problems have been faced in the computation of the FBS solution. Since, the coupled FRFs obtained by the method proposed by Su and Juang [Su and Juang, 1994] perfect fits the ones obtained by FBS method, it can be realized that the method proposed by Su and Juang [Su and Juang, 1994] is suffering by the same numerical problems. However, this conclusion still is premature. Indeed, this is a first study of the state-space techniques, without any background or experience in the field. Therefore, more experimental work and experimental couplings are needed to be performed in future, in order to really evaluate which could be the advantages of the state-space coupling methods over the FBS.

Moreover, it was found that for the first performed experimental coupling, the identification procedure worked as a noise filtering, decreasing the condition number of the coupled FRFs. This fact permitted to obtain for frequencies lower than 500 Hz better coupling results by the application of the FBS method to the identified FRFs than the application of the same method for the measured ones. This phenomena must be further analyzed, in order to understand in which situations it would be preferable to apply the FBS technique directly to the measured FRFs and the situations when the application of the FBS method to the identified FRFs would be profitable.

Even though the possibility of the method proposed by Su and Juang [Su and Juang, 1994] suffers of the same numerical problems as FBS method, a possible advantage can be pointed. In fact, the coupling of two or more substructures and the coupling of DOFs that are shared by more than two substructures is not a problem for the method proposed by Su and Juang [Su and Juang, 1994]. In fact this method showed to be very flexible and continue to be simple even if a really complex structure composed by several substructures is intended to be coupled. In section 2.6 a similar formulation to the state-space coupling proposed by Su and Juang [Su and Juang, 1994] is presented for FBS method, which also permits the enforcement of coupling by the use of the same $[T]$ matrix and the coupling of several substructures at same time. However, this possibility have not been yet analyzed. Up to this moment the FBS coupling has been just analyzed for coupling two substructures at same time not being known if for the FBS method will be observed the same simplicity and flexibility to perform more complex couplings.

The realization of the present dissertation adds a deep analysis on the two mostly developed state-space coupling methods, containing several mathematical deductions that are not present on the literature analyzed by the author. Furthermore, it comprises coupling procedures and results for analytical cases by the use of two state-space coupling methods, one developed by Su and Juang [Su and Juang, 1994] and another by Sjövall [Sjövall, 2004]. As well as coupling procedures and results for experimental couplings by the use of the same two state-space coupling methods and by the use of FBS method.

5.2 Future work

The present dissertation comprises a initial study in the state-space coupling methods. At this moment, it is not possible to find any advantage of the use of state-space coupling methods instead of the use of FBS method, since the accuracy of the obtained results by both for the performed experimental couplings showed to be equal. Indeed, just analyzing the presented content in this dissertation, the great motivation for the exploration of state-space coupling techniques vanish, since the analysis of the obtained experimental coupling results suggest that the technique proposed by Su and Juang [Su and Juang, 1994] suffers of the same ill-conditioned problems as FBS method. However, this is just a first initial study on the field and more experimental work and experimental couplings should be performed to understand the limitations and the problems of the method proposed by Su and Juang [Su and Juang, 1994].

On other hand, the greater observed problems when coupling with the FBS method were verified when coupling substructures that present translational and rotational degrees of freedom and also substructures that work under non-linear mechanical behaviour. Therefore, future works must for sure include couplings of the substructures that presented these characteristics by the use of the method proposed by Su and Juang [Su and Juang, 1994].

Summarizing some possible future work

- Use of the transmission simulator method to measure the substructure FRFs;
- Further analysis to the possible ill-condition numerical problems of the method proposed by Su and Juang [Su and Juang, 1994];
- Analyze the possibility of use FBS method to perform couplings between several substructures and DOFs that are shared by more than two substructures;
- Analyze the circumstances for which the application of the FBS method to the identified FRFs instead to the measured FRFs would drive to better coupling results;
- Validation of the method proposed by Su and Juang [Su and Juang, 1994] for numerical and experimental couplings that include coupling of both translational and rotational DOFs;
- Validation of the method proposed by Su and Juang [Su and Juang, 1994] for experimental couplings of real substructures non-rigidly connected;
- Validation of the method proposed by Su and Juang [Su and Juang, 1994] for numerical and experimental couplings of substructures that presents a non-linear mechanical behaviour;

References

Tzu-Jeng Su and Jer-Nan Juang. Substructure system identification and synthesis. *Journal of Guidance, Control and Dynamics*, 17(5):1087–1095, 1994.

Per Sjövall. *Component System and Identification in Structural Dynamics.* Chalmers University Technology, Götenborg, 2004.

D. de Klerk, D.J. Rixen, and S.N. Voormeeren. General framework for dynamic substructuring: History, review, and classification of techniques. *Journal of the American Helicopter Society*, 46(5):1169–1181, 2008. doi: 10.2514/1.33274.

Krishna Chaitanya Konjerla. *FRF Based Experimental – Analytical Dynamic Substructuring Using Transmission Simulator.* KTH Engineering Sciences, Stockholm, Sweden, 2016.

Bjorn Jetmundsen, Richard L. Bielawa, and William G. Flannelly. Generalized frequency domain substructure synthesis. *Journal of the American Helicopter Society*, pages 55–64, 1988.

Mladen Gibanica. *Experimental-Analytical Dynamic Substructuring.* Chalmers University Technology, Götenborg, Sweden, 2013.

Roy R. Craig and Andrew J. Kurdila. *Fundamentals of Structural Dynamics.* JOHN WILEY & SONS, INC., 2006.

Bart Peeters, Herman Van der Auweraer, Patrick Guillaume, and Jan Leuridan. The polymax frequency-domain method: a new standard for modal parameter estimation? *IOS Press*, pages 395–409, 2004.

Mahmoud El-Kafafy, Bart Peeters, Patrick Guillaume, and Tim De Troyer. Constrained maximum likelihood modal parameter identification applied to structural dynamics. *Elsevier*, pages 567–589, 2015.

Matthew Allen, Daniel Rixen, Maarten van der Seijs, Paolo Tiso, Thomas Abrahamsson, and Randal Mayes. *Emerging Numerical and Experimental Techniques.* Springer, 2020.

Mladen Gibanica, Anders T. Johansson, Anders Liljerehn, Per Sjövall, and Thomas Abrahamsson. Experimental-analytical dynamic substructuring of ampair testbed: A state-space approach. *The Society for Experimental Mechanics, Inc. 2014*, pages 1–14, 2014. doi: 10.1007/978-3-319-04501-6_1.

Peter Van Overschee and Bart de Moor. N4sid*: Subspace algorithms for the identification of combined deterministic-stochastic systems. *Pergamon Press Ltd*, 30(1):75–93, 1994.

Hiiseyin AkCay Tomas McKelvey and Lennart Ljung. Subspace-based multivariable system identification from frequency response data. *IEEE TRANSACTIONS ON AUTOMATIC CONTROL*, 41(7):960–979, 1996.

Mladen Gibanica, Thomas Abrahamsson, and Thomas McKelvey. Physically motivated rank constraint on direct throughput of state-space models. *ELSEVIER*, pages 329–334, 2018.

Suat Gumussoy, Ahmet Arda Ozdemir, Thomas McKelvey, Lennart Ljung, Mladen Gibanica, and Rajiv Singh. Improving linear state-space models with additional iterations. *ELSEVIER*, pages 341–346, 2018.

D.J. Ewins. *Modal Testing: Theory, Practice and Application.* Research Studies Press Ltd., Second Edition, Hertfordshire, England, 2000.

Jimin He and Zhi-Fang Fu. *Modal Analysis.* Butterworth-Heinemann, Oxford, England, 2001.

Siemens. *Simcenter Testlab: Transfer Path Analysis Singular Value Decomposition.* Leuven, Belgium, 2018.

Maarten van der Seijs. *Experimental Dynamic Substructuring.* Delft University of Technology, Delft, Netherlands, 2016.

Thomas Abrahamsson. *State-Space Model Coupling.* Chalmers University, 2018.

J. Dias Rodrigues. *Apontamentos de Vibrações de Sistemas Mecânicos.* Faculdade de Engenharia da U.PORTO, PORTO, 2018 edition, 2018.

LMS International. *The LMS Theory and Background Book.* Leuven, Belgium, 2000.

Patrick Guillaume. *Modal Analysis.* Department of Mechanical Engineering,Vrije Universiteit Brussel, Belgium, n.d.

LMS International. *The LMS Test.Lab Modal Analysis manual.* Leuven, Belgium, 2012.

F. Lembregts, J.Leuridan, and H. Van Brussel. Frequency domain direct parameter identification for modal analysis: State space formulation. *ResearchGate*, pages 1–17, 1988. doi: 10.1016/0888-3270(90)90041-I.

Ahmed El Mahmoudi, Daniel J. Rixen, and Christian H. Meyer. Comparison of different approaches to include connection elements into frequency-based substructuring. *SEM*, 2020. URL `https://doi.org/10.1007/s40799-020-00360-1`.

Maren Scheel, Mladen Gibanica, and Anders Nord. State-space dynamic substructuring with the transmission simulator method. *SEM*, pages 325–340, 2019. URL `https://doi.org/10.1007/s40799-019-00317-z`.

J. Dias Rodrigues. *Diapositivos de Dinâmica de Máquinas: Modelos para Análise Dinâmica de Sistemas Mecânicos e Estruturas.* DEMec, FEUP, 2019.

PCB Piezotronics, 2020. URL `https://www.pcb.com/products?m=333B30`.

Siemens. Simcenter-qsources, 2020. URL `https://www.qsources.be/simcenter/l`.

Siemens. *C-TPA – Wiper electromotor case.* Leuven, Belgium, n.d.

Siemens. *Simcenter Testlab: Modal Analysis.* Leuven, Belgium, 2019.

Randy L. Mayes and Michael Arviso. Design studies for the transmission simulator method of experimental dynamic substructuring. *Proceedings of ISMA 2010*, pages 1929–1938, 2010.

Maren Scheel. *State-Space Experimental-Analytical Dynamic Substructuring Using the Transmission Simulator.* Chalmers University Technology, Götenborg, Sweden, 2015.

Anders Liljerehn. *Component Synthesis of Machine Tool and Cutter for Process Optimisation.* Chalmers University Technology, Götenborg, Sweden, 2012.

Appendix A

Mathematical proof: Coupling matrices - Su and Juang method

In this appendix the coupled acceleration state-space matrices presented in equation (2.57) are going to be deduced from the uncoupled diagonal acceleration state-space model presented in equation (2.48). Starting for work with the bottom block row of the uncoupled diagonal state-space model (2.48) [Su and Juang, 1994].

$$y^J = C_D^J x + D_D^{JI} u^I + D_D^{JJ} u^J \tag{A.1}$$

Recording the compatibility condition (equation (2.43)).

$$T^T \bar{y}^J = C_D^J x + D_D^{JI} u^I + D_D^{JJ} u^J \tag{A.2}$$

For the equality relation between internal uncoupled and coupled DOFs (equations (2.54) and (2.55)), and solving equation (A.2) in order to variable u^J

$$D_D^{JJ} u^J = T^T \bar{y}^J - C_D^J x - D_D^{JI} \bar{u}^I$$

$$<=> u^J = (D_D^{JJ})^{-1} (T^T \bar{y}^J - C_D^J x - D_D^{JI} \bar{u}^I) \tag{A.3}$$

Performing the multiplication of the equation (A.3) by the transformation matrix $[T]$ and solving in order to variable $\bar{y}^J$

$$T u^J = T (D_D^{JJ})^{-1} (T^T \bar{y}^J - C_D^J x - D_D^{JI} \bar{u}^I)$$

$$<=> T u^J = T (D_D^{JJ})^{-1} T^T \bar{y}^J - T (D_D^{JJ})^{-1} C_D^J x - T (D_D^{JJ})^{-1} D_D^{JI} \bar{u}^I$$

$$<=> T (D_D^{JJ})^{-1} T^T \bar{y}^J = T u^J + T (D_D^{JJ})^{-1} C_D^J x + T (D_D^{JJ})^{-1} D_D^{JI} \bar{u}^I$$

$$<=> \bar{y}^J = (T (D_D^{JJ})^{-1} T^T)^{-1} (T u^J + T (D_D^{JJ})^{-1} C_D^J x + T (D_D^{JJ})^{-1} D_D^{JI} \bar{u}^I) \tag{A.4}$$

Remembering the definition of the auxiliary variable $[S]$ presented in equation (2.58) and the equilibrium condition presented in equation (2.44)

$$\bar{y}^J = (S)^{-1} (\bar{u}^J + T (D_D^{JJ})^{-1} C_D^J x + T (D_D^{JJ})^{-1} D_D^{JI} \bar{u}^I) \tag{A.5}$$

Working, now, with the first block row of the uncoupled diagonal state-space model (equation (2.48)) and remembering the mathematical expressions (2.54) and (2.55)

$$\bar{y}^I = C_D^I x + D_D^{II}\bar{u}^I + D_D^{IJ} u^J$$

Recalling the relation established in equation (A.3)

$$\bar{y}^I = C_D^I x + D_D^{II}\bar{u}^I + D_D^{IJ}(D_D^{JJ})^{-1}(T^T\bar{y}^J - C_D^J x - D_D^{JI}\bar{u}^I)$$

By the relation established in equation (A.4)

$$\bar{y}^I = C_D^I x + D_D^{II}\bar{u}^I + D_D^{IJ}(D_D^{JJ})^{-1}((T^T(S)^{-1}(\bar{u}^J + T(D_D^{JJ})^{-1}C_D^J x + T(D_D^{JJ})^{-1}D_D^{JI}\bar{u}^I) - C_D^J x - D_D^{JI}\bar{u}^I) \tag{A.6}$$

Developing just the equation term $\phi = (D_D^{JJ})^{-1}(T^T(S)^{-1}(\bar{u}^J + T(D_D^{JJ})^{-1}C_D^J x) - C_D^J x)$

$$\phi = (D_D^{JJ})^{-1}T^T(S)^{-1}\bar{u}^J + (D_D^{JJ})^{-1}T^T(S)^{-1}T(D_D^{JJ})^{-1}C_D^J x - (D_D^{JJ})^{-1}C_D^J x \tag{A.7}$$

Introducing the auxiliary variable $[Q]$ given by equation (2.59)

$$\phi = (D_D^{JJ})^{-1}(T^T(S)^{-1}(\bar{u}^J + T(D_D^{JJ})^{-1}C_D^J x) - C_D^J x) = (D_D^{JJ})^{-1}T^T(S)^{-1}\bar{u}^J + QC_D^J \tag{A.8}$$

Developing just the equation therm $\delta = (D_D^{JJ})^{-1}(T^T(S)^{-1}(T(D_D^{JJ})^{-1}D_D^{JI}) - D_D^{JI})\bar{u}^I$

$$\delta = ((D_D^{JJ})^{-1}T^T(S)^{-1}T(D_D^{JJ})^{-1} - (D_D^{JJ})^{-1})D_D^{JI}\bar{u}^I \tag{A.9}$$

Introducing the auxiliary variable $[Q]$

$$\delta = ((D_D^{JJ})^{-1}T^T(S)^{-1}T(D_D^{JJ})^{-1} - (D_D^{JJ})^{-1})D_D^{JI}\bar{u}^I = QD_D^{JI}\bar{u}^I \tag{A.10}$$

Introducing the simplified expressions (A.8) and (A.10) in equation (A.6)

$$\bar{y}^I = C_D^I x + D_D^{II}\bar{u}^I + D_D^{IJ}QC_D^J x + D_D^{IJ}(D_D^{JJ})^{-1}T^T(S)^{-1}\bar{u}^J + D_D^{IJ}QD_D^{JI}\bar{u}^I$$

Aggregating x, $\bar{u}^I$ and $\bar{u}^J$ dependent therms

$$\bar{y}^I = (C_D^I + D_D^{IJ}QC_D^J)x + (D_D^{II} + D_D^{IJ}QD_D^{JI})\bar{u}^I + D_D^{IJ}(D_D^{JJ})^{-1}T^T S^{-1}\bar{u}^J \tag{A.11}$$

Aggregating x, $\bar{u}^I$ and $\bar{u}^J$ dependent therms of the equation (A.5)

$$\bar{y}^J = (S)^{-1}T(D_D^{JJ})^{-1}C_D^J x + (S)^{-1}T(D_D^{JJ})^{-1}D_D^{JI}\bar{u}^I + (S)^{-1}\bar{u}^J \tag{A.12}$$

By the equations (A.11) and (A.12) the $[\bar{C}]$ and $[\bar{D}]$ can be defined as

$$[\bar{C}] = \begin{bmatrix} C_D^I + D_D^{IJ}QC_D^J \\ (S)^{-1}T(D_D^{JJ})^{-1}C_D^J \end{bmatrix}, \quad [\bar{D}] = \begin{bmatrix} D_D^{II} + D_D^{IJ}QD_D^{JI} & D_D^{IJ}(D_D^{JJ})^{-1}T^T S^{-1} \\ (S)^{-1}T(D_D^{JJ})^{-1}D_D^{JI} & (S)^{-1} \end{bmatrix} \tag{A.13}$$

At this moment it is just missing the achievement of $[\bar{A}]$ and $[\bar{B}]$ matrices. Working with equation (2.48)

$$\dot{x} = A_D x + B_D^I u^I + B_D^J u^J$$

Remembering the equation (A.3) and also the equality relation between internal uncoupled and internal coupled DOFs (equation (2.54) and (2.55))

$$\dot{x} = A_D x + B_D^I \bar{u}^I + B_D^J (D_D^{JJ})^{-1}(T^T \bar{y}^J - C_D^J x - D_D^{JI} \bar{u}^I) \tag{A.14}$$

Substituting the $\bar{y}^J$ value given at equation (A.12) in equation (A.14)

$$\dot{x} = A_D x + B_D^I \bar{u}^I + B_D^J (D_D^{JJ})^{-1}(T^T (S)^{-1}(\bar{u}^J + T(D_D^{JJ})^{-1} C_D^J x + T(D_D^{JJ})^{-1} D_D^{JI} \bar{u}^I) - C_D^J x - D_D^{JI} \bar{u}^I)$$

For the relations established in equations (A.8) and (A.10)

$$\dot{x} = A_D x + B_D^I \bar{u}^I + B_D^J ((D_D^{JJ})^{-1} T^T (S)^{-1} \bar{u}^J + Q C_D^J x + Q D_D^{JI} \bar{u}^I) \tag{A.15}$$

Aggregating x, $\bar{u}^I$ and $\bar{u}^J$ dependent therms of the equation (A.15)

$$\dot{x} = (A_D + B_D^J Q C_D^J) x + (B_D^I + B_D^J Q D_D^{JI}) \bar{u}^I + B_D^J (D_D^{JJ})^{-1} T^T (S)^{-1} \bar{u}^J \tag{A.16}$$

By the equation (A.16) the $[\bar{A}]$ and $[\bar{B}]$ can be defined as follows

$$[\bar{A}] = \begin{bmatrix} A_D + B_D^J Q C_D^J \end{bmatrix} \quad [\bar{B}] = \begin{bmatrix} B_D^I + B_D^J Q D_D^{JI} & B_D^J (D_D^{JJ})^{-1} T^T (S)^{-1} \end{bmatrix} \tag{A.17}$$

Appendix B

Mathematical proof: Coupling form structure of the uncoupled state-space matrices

In this appendix the mathematical deduction of the coupling form structure of the substructure state-space matrices will be performed. Starting for considering a state-space realization $\{\dot{x}(t)\} = [A]\{x(t)\} + [B]\{u(t)\}$, $\{y(t)\} = [C]\{x(t)\}$ of a second order system $[M]\{\ddot{r}(t)\} + [V]\{\dot{r}(t)\} + [K]\{r(t)\} = \{F(t)\}$. Assuming, that response is equal or a linear combination of $x(t)$ and non singular mass matrix, it can be pointed that the relation between matrices $[B]$ and $[C]$ is such that $CB = 0$ and the relation between matrices $[A]$, $[B]$ and $[C]$ will be such that $CAB \neq 0$. Note that, this state-space model realization was obtained assuming displacement outputs, justifying the fact of the matrix $[D]$ be a null matrix.

In order to prove the previous statements, consider the matrices $[B]$ and $[C]$ of the presented second order system

$$[B] = \begin{bmatrix} 0 \\ M^{-1} \end{bmatrix}, \qquad C = \begin{bmatrix} I & 0 \end{bmatrix} \tag{B.1}$$

Applying an arbitrary transformation $x(t) = Tz(t)$, the state-space model is given by

$$\begin{cases} [T]\{\dot{z}(t)\} = [A][T]\{z(t)\} + [B]\{u(t)\} \\ \{y(t)\} = [C][T]\{z(t)\} + [D]\{u(t)\} \end{cases} \tag{B.2}$$

Thus,

$$\begin{cases} \{\dot{z}(t)\} = [T]^{-1}[A][T]\{z(t)\} + [T]^{-1}[B]\{u(t)\} \\ \{y(t)\} = [C][T]\{z(t)\} + [D]\{u(t)\} \end{cases} \tag{B.3}$$

By the system of equations (B.3), the relation between $[B]$ and $[C]$ matrices will be

$$(CT)(T^{-1}B) = \begin{bmatrix} I & 0 \end{bmatrix} \begin{bmatrix} 0 \\ M^{-1} \end{bmatrix} = 0 \tag{B.4}$$

The equation (B.4) ends the proof related to the relation between $[B]$ and $[C]$ matrices. Note that, also after an arbitrary transformation this relation is verified.

The second stated relation can be verified as follows

$$CAB = \begin{bmatrix} I & 0 \end{bmatrix} \begin{bmatrix} 0 & I \\ -M^{-1}K & -M^{-1}V \end{bmatrix} \begin{bmatrix} 0 \\ M^{-1} \end{bmatrix} \neq 0 \tag{B.5}$$

Which ends the proof for the relation between the matrices $[A]$, $[B]$ and $[C]$.

Now, proving that a given state-space realization $\{\dot{x}(t)\} = [A]\{x(t)\} + [B]\{u(t)\}$, $\{y(t)\} = [C]\{x(t)\}$ ($[A] \in R^{n\times n}, [B] \in R^{n\times n_c}, [C] \in R^{n_c\times n}$) of a second order system $[M]\{\ddot{r}(t)\} + [V]\{\dot{r}(t)\} + [K]\{r(t)\} = \{F(t)\}$, can be transformed in a system with state-space matrices written in a coupling form by the presented $[T_{Sj}]$ matrix in equation (2.62), with $[C; CA]$ being full row rank $2n_c$ and $n_c \leq n$. Note that, the considered output for the state-space model is displacement again.

Recalling the transformation matrix $[T_{Sj}]$ and assuming its inverse Z is such that

$$[T_{Sj}] = \begin{bmatrix} C \\ CA \\ N \end{bmatrix}, \qquad Z = \begin{bmatrix} Z_1 & Z_2 & Z_3 \end{bmatrix} \tag{B.6}$$

Resuming the presented expression (2.63) for the variable $[N]$ presented in the transformation matrix $[T_{Sj}]$

$$N = N_C N_B^T (N_B N_B^T)^{-1} N_B$$

where the null-spaces $[N_B]$ and $[N_C]$ are given according with equations (2.64) and (2.65)

$$N_B B = 0 \qquad \begin{bmatrix} C \\ CA \end{bmatrix} N_C^T = 0$$

Observing the equations (2.64) and (2.65) it can be concluded that the null-space $[N_C]$ will be of full row rank $n - 2n_c$ as well the combined null-space $[N]$, because of matrix $[B]$ is not contained in the null-space $[N_C]$ since the established relation $CAB \neq 0$. On other hand, since $[C; CA]$ and $[N]$ are full row rank and $[N]$ is a null-space of $[C; CA]$, the $[T_{Sj}]$ matrix will be full rank and non singular. By the relation $T_{Sj}Z = I$

$$\begin{bmatrix} CZ_1 & CZ_2 & CZ_3 \\ CAZ_1 & CAZ_2 & CAZ_3 \\ NZ_1 & NZ_2 & NZ_3 \end{bmatrix} = I \tag{B.7}$$

The established relation in equation (B.7) implies that

$$CAZ_1 = 0 \qquad CAZ_2 = I \qquad CAZ_3 = 0 \tag{B.8}$$

Remembering the coupling form of the substructure state-space model (see equation (2.69)), the first block row of the coupling form uncoupled state-space model $[\widetilde{A}]$ matrix will be given as follows

$$[\widetilde{A}] = T_{Sj} A T_{Sj}^{-1} = T_{Sj} A Z \tag{B.9}$$

Therefore,

$$CA \begin{bmatrix} Z_1 & Z_2 & Z_3 \end{bmatrix} = \begin{bmatrix} CAZ_1 & CAZ_2 & CAZ_3 \end{bmatrix} = \begin{bmatrix} 0 & I & 0 \end{bmatrix} \tag{B.10}$$

At this moment the proof for the coupling form structure of $[\widetilde{A}]$ matrix is concluded. The matrix $[\widetilde{B}]$ is given as follows

$$[\widetilde{B}] = T_{Sj} B = \begin{bmatrix} C \\ CA \\ N \end{bmatrix} B = \begin{bmatrix} CB \\ CAB \\ N_C N_B^T (N_B N_B^T)^{-1} N_B B \end{bmatrix} \tag{B.11}$$

Remember that, as proved, $CB = 0$ and $N_B B = 0$. Thus,

$$[\widetilde{B}] = T_{Sj}B = \begin{bmatrix} C \\ CA \\ N \end{bmatrix} B = \begin{bmatrix} CB \\ CAB \\ N_C N_B^T (N_B N_B^T)^{-1} N_B B \end{bmatrix} = \begin{bmatrix} 0 \\ CAB \\ 0 \end{bmatrix} \tag{B.12}$$

Recalling the equation (B.5)

$$CAB = \begin{bmatrix} I & 0 \end{bmatrix} \begin{bmatrix} 0 & I \\ -M^{-1}K & -M^{-1}V \end{bmatrix} \begin{bmatrix} 0 \\ M^{-1} \end{bmatrix} = \begin{bmatrix} 0 & I \end{bmatrix} \begin{bmatrix} 0 \\ M^{-1} \end{bmatrix} = M^{-1} = B_{vv} \tag{B.13}$$

Substituting the value of CAB (equation (B.13)) in expression (B.12)

$$[\widetilde{B}] = \begin{bmatrix} 0 \\ B_{vv} \\ 0 \end{bmatrix} \tag{B.14}$$

which proofs the coupling form structure of matrix $[\widetilde{B}]$ [Allen et al., 2020].

Appendix C

Mathematical proof: Coupling form of the coupled state-space model

In this appendix the deduction of the coupling form of the coupled state-space model will be performed.

Assuming that it is intended to couple two substructures connected by a rigid connection, substructure A and substructure B. Recording the coupling form of a generic uncoupled state-space model

$$\begin{bmatrix} \dot{y}_c^I \\ \ddot{y}_c^I \\ \dot{x}_b^I \end{bmatrix} = \begin{bmatrix} 0 & I & 0 \\ A_{vd}^A & A_{vv}^A & A_{vb}^A \\ A_{bd}^A & A_{bv}^A & A_{bb}^A \end{bmatrix} \begin{bmatrix} y_c^A \\ \dot{y}_c^A \\ x_b^A \end{bmatrix} + \begin{bmatrix} 0 \\ B_{vv}^A \\ 0 \end{bmatrix} (u_c^A) \tag{C.1}$$

$$\begin{bmatrix} \dot{y}_c^B \\ \ddot{y}_c^B \\ \dot{x}_b^B \end{bmatrix} = \begin{bmatrix} 0 & I & 0 \\ A_{vd}^B & A_{vv}^B & A_{vb}^B \\ A_{bd}^B & A_{bv}^B & A_{bb}^B \end{bmatrix} \begin{bmatrix} y_c^B \\ \dot{y}_c^B \\ x_b^B \end{bmatrix} + \begin{bmatrix} 0 \\ B_{vv}^B \\ 0 \end{bmatrix} (u_c^B) \tag{C.2}$$

The compatibility equation can be established as follows

$$\bar{y} = y_c^A = y_c^B \tag{C.3}$$

The equilibrium equation is given as follows

$$u_c^A + u_c^B = \bar{u} \tag{C.4}$$

Extracting the second row of each uncoupled state-space model present in expressions (C.1) and (C.2)

$$\ddot{y}_c^A = A_{vd}^A y_c^A + A_{vv}^A \dot{y}_c^A + A_{vb}^A x_b^A + B_{vv}^A u_c^A \tag{C.5}$$

$$\ddot{y}_c^B = A_{vd}^B y_c^B + A_{vv}^B \dot{y}_c^B + A_{vb}^B x_b^B + B_{vv}^B u_c^B \tag{C.6}$$

Multiplying each equation (C.5) and (C.6) for each corresponding interface inertia and remembering the compatibility equation (C.3)

$$(B_{vv}^A)^{-1}\ddot{\bar{y}} = (B_{vv}^A)^{-1}(A_{vd}^I \bar{y} + A_{vv}^I \dot{\bar{y}} + A_{vb}^A x_b^A) + u_c^A \tag{C.7}$$

$$(B_{vv}^B)^{-1}\ddot{\bar{y}} = (B_{vv}^B)^{-1}(A_{vd}^B \bar{y} + A_{vv}^B \dot{\bar{y}} + A_{vb}^B x_b^B) + u_c^B \tag{C.8}$$

The interface mass inertia of the coupled system will be $(B_{vv}^A + B_{vv}^B)^{-1}$. Thus, the equations (C.7) and (C.8) have to be added[Liljerehn, 2012]

$$
\begin{aligned}
((B_{vv}^A)^{-1} + (B_{vv}^B)^{-1})\ddot{\bar{y}} = (B_{vv}^A)^{-1}(A_{vd}^A\bar{y} + A_{vv}^A\dot{\bar{y}} + A_{vb}^A x_b^A) + u_c^A \\
+ (B_{vv}^B)^{-1}(A_{vd}^B\bar{y} + A_{vv}^B\dot{\bar{y}} + A_{vb}^B x_b^B) + u_c^B
\end{aligned}
\tag{C.9}
$$

Assuming $\bar{B}_{vv} = ((B_{vv}^A)^{-1} + (B_{vv}^B)^{-1})^{-1}$, remembering the both established coupling equations (C.3) and (C.4)

$$
\bar{B}_{vv}^{-1}\ddot{\bar{y}} = (B_{vv}^A)^{-1}(A_{vd}^A\bar{y} + A_{vv}^A\dot{\bar{y}} + A_{vb}^A x_b^A) + \bar{u} + (B_{vv}^B)^{-1}(A_{vd}^B\bar{y} + A_{vv}^B\dot{\bar{y}} + A_{vb}^B x_b^B) \tag{C.10}
$$

Rearranging the equation (C.10)

$$
\begin{aligned}
\ddot{\bar{y}} = \bar{B}_{vv}(((B_{vv}^A)^{-1}A_{vd}^A + (B_{vv}^B)^{-1}A_{vd}^B)\bar{y} + ((B_{vv}^A)^{-1}A_{vv}^A + (B_{vv}^B)^{-1}A_{vv}^B)\dot{\bar{y}} \\
+ (B_{vv}^A)^{-1}A_{vb}^A x_b^A + (B_{vv}^B)^{-1}A_{vb}^B x_b^B + \bar{u})
\end{aligned}
\tag{C.11}
$$

The equation (C.11) can be rewritten as follows

$$
\ddot{\bar{y}} = \bar{A}_{vd}\bar{y}_c + \bar{A}_{vv}\dot{\bar{y}} + \bar{A}_{vb}^A x_b^A + \bar{A}_{vb}^B x_b^B + \bar{B}_{vv}\bar{u} \tag{C.12}
$$

where,

- $\bar{B}_{vv} = ((B_{vv}^A)^{-1} + (B_{vv}^B)^{-1})^{-1}$;
- $\bar{A}_{vd} = \bar{B}_{vv}((B_{vv}^A)^{-1}A_{vd}^A + (B_{vv}^B)^{-1}A_{vd}^B)$;
- $\bar{A}_{vv} = \bar{B}_{vv}((B_{vv}^A)^{-1}A_{vv}^B + (B_{vv}^B)^{-1}A_{vv}^B)$;
- $\bar{A}_{vb}^A = \bar{B}_{vv}(B_{vv}^A)^{-1}A_{vb}^A$;
- $\bar{A}_{vb}^B = \bar{B}_{vv}(B_{vv}^B)^{-1}A_{vb}^B$.

The deduction of the second coupled block row is completed. The others block rows can be computed without difficulties. The first block row represents a dummy equation and the other ones represents rows taken from the uncoupled substructure state-space models. Thus, the coupling form of the coupled state-space model can be build as follows

$$
\begin{bmatrix} \dot{\bar{y}} \\ \ddot{\bar{y}} \\ x_b^A \\ x_b^B \end{bmatrix} = \begin{bmatrix} 0 & I & 0 & 0 \\ \bar{A}_{vd} & \bar{A}_{vv} & \bar{A}_{vb}^A & \bar{A}_{vb}^B \\ \bar{A}_{bd}^A & \bar{A}_{bv}^A & A_{bb}^A & 0 \\ \bar{A}_{bd}^B & \bar{A}_{bv}^B & 0 & A_{bb}^B \end{bmatrix} \begin{bmatrix} \bar{y} \\ \dot{\bar{y}} \\ x_b^A \\ x_b^B \end{bmatrix} + \begin{bmatrix} 0 \\ \bar{B}_{vv} \\ 0 \\ 0 \end{bmatrix} (\bar{u}) \tag{C.13}
$$

Appendix D

Mathematical proof: Diagonal uncoupled acceleration state-space model from displacement state-space models

In this appendix the diagonal uncoupled acceleration state-space model of the method proposed by Su and Juang [Su and Juang, 1994] will be deduced from the uncoupled substructure displacement state-space model. Starting for a generic uncoupled displacement FRF (considering an interface input and output) of one arbitrary substructure α (see equation (2.19)). [Su and Juang, 1994]

$$H_{\alpha}^{JJ} = C_{\alpha}^{J}(s[I] - A_{\alpha})^{-1} B_{\alpha}^{J} \tag{D.1}$$

Note that, the $[D]$ matrix is a null matrix, because there is no direct relation between force and displacement. Justifying the fact of $[D]$ matrix be not null just for acceleration outputs.

In order to achieve the acceleration FRF the equation (D.1) has to be twice differentiated. In Laplace domain the differentiation is given by a s multiplication. Thus, the velocity FRF will be given by

$$sH_{\alpha}^{JJ} = sC_{\alpha}^{J}(s[I] - A_{\alpha})^{-1} B_{\alpha}^{J} \tag{D.2}$$

As the s therm is multiplied by matrices or vectors in expression (D.2), the following expression is true.

$$s = (s[I] - A_{\alpha}) + A_{\alpha} \tag{D.3}$$

By substituting the s value given by expression (D.3) in equation (D.2)

$$sH_{\alpha}^{JJ} = ((s[I] - A_{\alpha}) + A_{\alpha}) C_{\alpha}^{J}(s[I] - A_{\alpha})^{-1} B_{\alpha}^{J}$$

$$<=> sH_{\alpha}^{JJ} = C_{\alpha}^{J} A_{\alpha}(s[I] - A_{\alpha})^{-1} B_{\alpha}^{J} + C_{\alpha}^{J} B_{\alpha}^{J} \tag{D.4}$$

Resuming the generic expression of an FRF obtained from state-space matrices (2.19).

$$\frac{Y(s)}{U(s)} = [C](s[I] - [A])^{-1}[B] + [D] \tag{D.5}$$

Analysing the obtained expression of the velocity FRF (equation (D.4)) and the generic expression (D.5), the therms of the velocity FRF can be identified from, the displacement therms as presented in equation (D.6),

$$[A_{\alpha}]^{vel} = \left[A_{\alpha}\right], \quad [B_{\alpha}^{J}]^{vel} = \left[B_{\alpha}^{J}\right], \quad [C_{\alpha}^{J}]^{vel} = \left[C_{\alpha}^{J} A_{\alpha}\right] \quad [D_{\alpha}^{JJ}]^{vel} = \left[C_{\alpha}^{J} B_{\alpha}^{J}\right] \tag{D.6}$$

where, subscript *vel* is related to velocity FRF therms.

The $[D]$ matrix of a velocity FRF will be a null matrix, therefore

$$C_\alpha^J B_\alpha^J = 0 \tag{D.7}$$

The velocity FRF expression will be given by

$$sH_\alpha^{JJ} = C_\alpha^J A_\alpha (s[I] - A_\alpha)^{-1} B_\alpha^J \tag{D.8}$$

Multiplying the velocity FRF expression by s, the acceleration FRF will be obtained as follows

$$s^2 H_\alpha^{JJ} = sC_\alpha^J A_\alpha (s[I] - A_\alpha)^{-1} B_\alpha^J$$

$$<=> s^2 H_\alpha^{JJ} = ((s[I] - A_\alpha) + A_\alpha) C_\alpha^J A_\alpha (s[I] - A_\alpha)^{-1} B_\alpha^J$$

$$<=> s^2 H_\alpha^{JJ} = C_\alpha^J A_\alpha A_\alpha (s[I] - A_\alpha)^{-1} B_\alpha^J + C_\alpha^J A_\alpha B_\alpha^J \tag{D.9}$$

Analysing the obtained expression of the acceleration FRF (equation (D.9)) and the generic expression (D.5), the therms of the acceleration FRF can be identified from, the displacement therms. Furthermore, generalizing for the others FRFs, it can be identified each of the diagonal uncoupled acceleration state-space model therms as follows

$$\begin{array}{ll} C_{\alpha D}^{I\ accel} = C_\alpha^I A_\alpha A_\alpha & C_{\alpha D}^{J\ accel} = C_\alpha^J A_\alpha A_\alpha \\ D_{\alpha D}^{II\ accel} = C_\alpha^I A_\alpha B_\alpha^I & D_{\alpha D}^{IJ\ accel} = C_\alpha^I A_\alpha B_\alpha^J \\ D_{\alpha D}^{JI\ accel} = C_\alpha^J A_\alpha B_\alpha^I & D_{\alpha D}^{JJ\ accel} = C_\alpha^J A_\alpha B_\alpha^J \end{array} \tag{D.10}$$

where subscript *accel* is related to acceleration FRF therms.

The $[A]$ and $[B]$ matrices are not dependent on the chosen output, thus the diagonal uncoupled matrices $[A]$ and $[B]$ for the acceleration and displacement state-space models are the same.

Note that, in this deduction it was not taken in account the $[D]$ matrix of the obtained estimated displacement state-space model from measured data (see mathematical expression (2.89)). Otherwise it would be obtained a frequency dependent state-space model, because $[D]$ matrix would be frequency dependent.

Observe that, with this deduction, displacement state-space models can be used to directly obtain the acceleration coupled state-space model. To do such achievement the derived diagonal uncoupled acceleration state-space model should be coupled as described in sections 2.7 and 2.9.

Appendix E

Mathematical proof: Acceleration state-space model

In this appendix the presented displacement modal model in equation (2.85) will be derived twice in order to obtain the acceleration modal model and, therefore, obtain the acceleration state-space matrices.

Resuming the presented displacement modal model for a generic FRF (equation (2.87))

$$[H(\omega)] = [\Psi \quad \Psi^*]\left[s[I] - \begin{bmatrix} \Lambda & 0 \\ 0 & \Lambda^* \end{bmatrix}\right]^{-1} \begin{bmatrix} l \\ l^* \end{bmatrix} + \frac{LR}{s^2} + UR \tag{E.1}$$

The displacement modal model expression (E.1) can be also expressed by (see section 2.8.3)

$$[H(\omega)] = [C]\left[s[I] - \left[A\right]\right]^{-1}\left[B\right] + \frac{LR}{s^2} + UR \tag{E.2}$$

In Laplace domain the differentiation is performed with s multiplication. Thus, the velocity FRF will be given by

$$s[H(\omega)] = s(C[s[I] - A]^{-1}B + \frac{[LR]}{s^2} + [UR]) \tag{E.3}$$

Since s is multiplied by matrices or vectors, the following expression is true.

$$s = (s[I] - A) + A \tag{E.4}$$

Substituting the relation (E.4) in equation (E.3)

$$s[H(\omega)] = ((s[I] - A) + A)(C[s[I] - A]^{-1}B) + ((s[I] - A) + A)(\frac{[LR]}{s^2} + [UR])$$

$$<=> sH(\omega) = CA(s[I] - A)^{-1}B + CB + s(\frac{[LR]}{s^2} + [UR])$$

The $[D]$ matrix of a velocity FRF will be a null matrix, therefore

$$CB = 0 \tag{E.5}$$

Thus, the velocity FRF will be given as follows

$$sH(\omega) = CA(s[I] - A)^{-1}B + s(\frac{[LR]}{s^2} + [UR]) \tag{E.6}$$

In order to obtain the accelerance FRF another s multiplication must be performed

$$s^2H(\omega) = ((s[I] - A) + A)(CA(s[I] - A)^{-1}B) + ((s[I] - A) + A)s(\frac{[LR]}{s^2} + [UR])$$

$$<=> s^2H(\omega) = CAA(s[I] - A)^{-1}B + CAB + s^2(\frac{[LR]}{s^2} + [UR])$$

$$<=> s^2H(\omega) = CAA(s[I] - A)^{-1}B + CAB + [LR] + s^2[UR] \tag{E.7}$$

Therefore, the acceleration state-space model will be given by

$$\begin{cases} \{\dot{x}(t)\} = [A]\{x(t)\} + [B]\{u(t)\} \\ \{\ddot{y}(t)\} = [CAA]\{x(t)\} + [CAB + LR]\{u(t)\} \end{cases} \tag{E.8}$$

Note that, the $[UR]$ matrix cannot be directly included in $[D]$ matrix, since it is dependent on frequency. Otherwise would be obtained a frequency dependent state-space model. The upper residuals will be taken into account by converting them into residual modes. The modal parameters of those residuals modes are then used together with the modal parameters of the in-band flexible modes to construct the $[A]$, $[B]$, $[C]$, and $[D]$ matrices of the acceleration state-space model.

Appendix F

Mechanical properties of the numerical mechanical systems

In this appendix will be presented the chosen mechanical properties for the analyzed numerical mechanical systems at chapter 3.

Table F.1: Mechanical Properties of Mechanical System nº 1

Mechanical Components	Property Value	Units
k_{a1}	4×10^7	Nm^{-1}
k_{b1}	5×10^6	Nm^{-1}
c_{a1}	40	Nsm^{-1}
c_{b1}	50	Nsm^{-1}
m_1	9	Kg
m_2	4	Kg
m_3	5	Kg
m_4	7	Kg

Table F.2: Mechanical Properties of Mechanical System nº 2

Mechanical Components	Property Value	Units
k_{a1}	500	Nm^{-1}
k_{a2}	450	Nm^{-1}
k_{m1}	100	Nm^{-1}
k_{m2}	100	Nm^{-1}
k_{p1}	100	Nm^{-1}
k_{p2}	150	Nm^{-1}
k_{p3}	5	Nm^{-1}
c_{a1}	50	Nsm^{-1}
c_{a2}	50	Nsm^{-1}
c_{m1}	20	Nsm^{-1}
c_{m2}	20	Nsm^{-1}
c_{p1}	50	Nsm^{-1}
c_{p2}	50	Nsm^{-1}
c_{p3}	10	Nsm^{-1}
m_{a1}	10	Kg
m_{f1}	1×10^{-6}	Kg
m_{f2}	1×10^{-6}	Kg
m_{a2}	3	Kg
m_{a3}	3	Kg
m_{f3}	1×10^{-6}	Kg
m_{f4}	1×10^{-6}	Kg
m_{p1}	5	Kg
m_{p2}	7	Kg
m_{f5}	1×10^{-6}	Kg
m_{f6}	1×10^{-6}	Kg
m_{p3}	10	Kg
m_{p4}	1	Kg

Table F.3: Mechanical Properties of Mechanical System nº 3

Mechanical Components	Property Value	Units
k_{a1}	4×10^{7}	Nm^{-1}
k_{a2}	3×10^{7}	Nm^{-1}
k_{b1}	4×10^{7}	Nm^{-1}
k_{b2}	3×10^{7}	Nm^{-1}
c_{a1}	40	Nsm^{-1}
c_{a2}	20	Nsm^{-1}
c_{b1}	40	Nsm^{-1}
c_{b2}	20	Nsm^{-1}
m_1	9	Kg
m_2	4	Kg
m_3	4	Kg
m_4	9	Kg

Table F.4: Mechanical Properties of Mechanical System nº 4

Mechanical Components	Property Value	Units
k_{a1}	4×10^7	Nm^{-1}
k_{a2}	3×10^7	Nm^{-1}
k_{b1}	4×10^7	Nm^{-1}
k_{b2}	3×10^7	Nm^{-1}
k_m	1×10^7	Nm^{-1}
c_{a1}	40	Nsm^{-1}
c_{a2}	20	Nsm^{-1}
c_{b1}	40	Nsm^{-1}
c_{b2}	20	Nsm^{-1}
c_m	20	Nsm^{-1}
m_1	9	Kg
m_2	4	Kg
m_3	4	Kg
m_4	9	Kg

Appendix G

Stabilization Diagram

In this appendix, will be presented a stabilization diagram in a frequency band between 3 Hz and 30 Hz. This stabilization diagram is similar to the obtained ones for the analyzed real substructures at chapter 4.

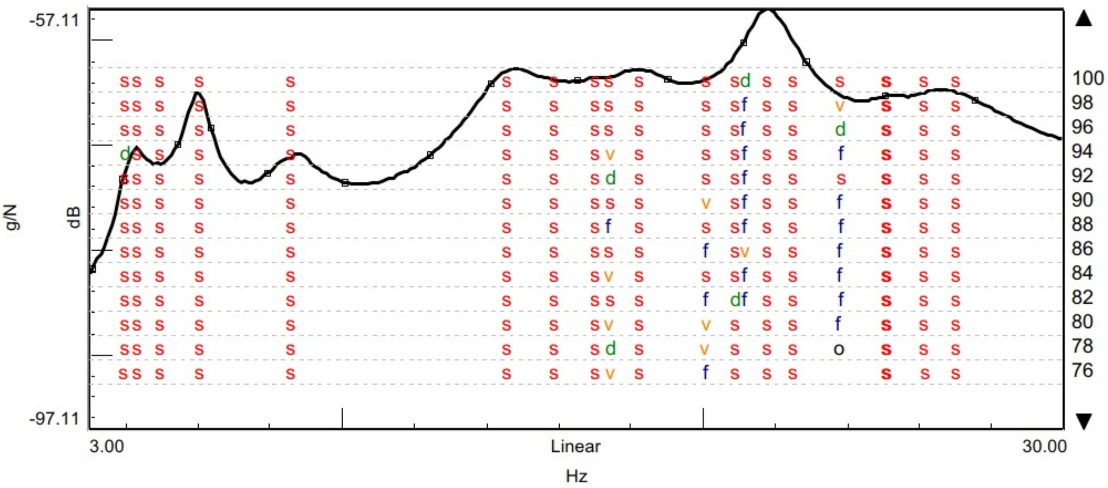

Figure G.1: Stabilization diagram [El-Kafafy et al., 2015]

Note that, the presented numbers in the right side vertical axis are correspondent to the used model order in each analysis (see section 2.8.1). It is also of importance to understand the meaning of each letter presented in the stabilization diagram.

- The o denotes the appearance of a new pole;
- The f denotes that the pole is stable in terms of frequency;
- The d denotes that the pole is stable in terms of damping and frequency;
- The v denotes that the pole is stable in terms of participation factors and frequency;
- The s denotes that the pole is stable in all the parameters, frequency, damping and participation factors.

Note that, a pole is stable in terms of a parameter if the variation of that parameter verify the correspondent established pre-set limit between two consecutive model orders (see section 2.8.1) [Siemens, 2019].